[Papers in Palaeontology, Vol. 7, Part 4, 2021, pp. 2141–2181]

NEW AND REVISED SMALL SHELLY FOSSIL RECORD FROM THE LOWER CAMBRIAN OF NORTHERN IRAN

by LÉA DEVAERE[1,2,*], DIETER KORN[2], ABBAS GHADERI[3,*], ULRICH STRUCK[2] *and* ALIREZA K. BAVANDPUR[4]

[1]Université de Lille, CNRS, UMR 8198 – Evo-Eco-Paleo, F-59000 Lille, France; lea_devaere@hotmail.fr
[2]Museum für Naturkunde Berlin, Leibniz Institut für Evolutions- und Biodiversitätsforschung, Invalidenstraße 43, 10115 Berlin, Germany; dieter.korn@mfn.berlin, ulrich.struck@mfn.berlin
[3]Department of Geology, Faculty of Sciences, Ferdowsi University of Mashhad, Azadi Square, Mashhad 9177948974, Iran; aghaderi@um.ac.ir
[4]Geological Survey of Iran, Meraj Avenue, Azadi Square, Tehran, Iran; alireza_karimi_b@yahoo.com
*Corresponding authors

Typescript received 11 September 2020; accepted in revised form 17 May 2021

Abstract: Small shelly fossils (SSFs) are highly informative of the 'Cambrian explosion'. Their palaeobiodiversity has been documented from lower Cambrian deposits worldwide but it remains elusive in areas such as Iran, despite this region occupying a critical position on the north-western Gondwana margin during the early Cambrian. This new study of the SSFs of the lower Cambrian of northern Iran provides a large new dataset from this understudied area. We revise the micropalaeontological signal of the Soltanieh Formation of the Alborz Mountains and introduce novel data from the Soltanieh and overlying Barut Formations of the Soltanieh Mountains. The new, solid taxonomic and stratigraphic SSF data enable us to distinguish two successive microfaunal assemblages. The first occurs in the Soltanieh Formation of the Soltanieh and Alborz Mountains and is dominated by anabaritids (*Anabarites trisulcatus*, *A.* ex gr. *trisulcatus*, *A. tristichus*, *A. dalirense* sp. nov., *Cambrotubulus decurvatus*) along with protoconodonts (*Protohertzina anabarica* and *P. unguliformis*), maikhanellids (*Maikhanella multa*, *Purella squamulosa* and *Purella* sp.), *Aetholicopalla adnata*, indeterminate cones and irregular tubes. The second assemblage, from the Barut Formation, is dominated by a diverse assemblage of molluscs (*Oelandiella korobkovi* and cap-shaped morphotypes). Siphogonuchitid sclerites also occur in both assemblages. The two SSF assemblages are characteristic of the Terreneuvian. Our dataset enables us to assess the sequence of faunal change of the Ediacaran–Cambrian transition; in contrast to the tube–sclerite–brachiopod succession presented in the literature, the Iranian fauna changes from one dominated by tubes and sclerites, to one dominated by molluscs and sclerites.

Key words: small shelly fossils, Cambrian, Iran, Terreneuvian, Alborz Mountains, micropalaeontology.

In recent decades, our knowledge of the 'Cambrian explosion' has benefited from studies of a large amount of fossil data, especially from the famous, exceptionally preserved biotas such as those of the Maotianshan Shale (South China; e.g. Hou *et al.* 2017) and of the Burgess Shale (Canada; e.g. Briggs *et al.* 1994), among others. The small shelly fossils (SSFs), a polyphyletic group of microfossils generally preserved in phosphate that thrived at the beginning of the Cambrian (during the so-called 'pre-trilobitic' Cambrian), can also largely contribute to our understanding of the explosion of biomineralizing animal life in the Cambrian, especially of its initial phase. Their palaeobiodiversity has been documented in early Cambrian deposits from all of the palaeocontinents and has proven to be of significant use for biostratigraphy (e.g. Devaere *et al.* 2019), palaeobiogeography (e.g. Yang *et al.* 2015), and phylogenetic (e.g. Shu *et al.* 2014) and palaeoecologic reconstructions (e.g. Budd & Jackson 2016).

In some critical areas, however, information on SSFs has remained elusive, although it is of major importance for the validation of their different uses. This is the case for Iran: early Cambrian SSFs were reported for the first time from the Soltanieh Formation of the Alborz Mountains by Hamdi (1989) and Hamdi *et al.* (1989), without any taxonomic descriptions. In Hamdi (1989), the palaeobiodiversity of SSFs is presented as a list of occurrences. Part of the listed taxa are illustrated and a composite stratigraphical column showing the stratigraphic range of some of the listed taxa is provided for the Soltanieh Formation at two localities of the Alborz Mountains. The two localities are called Dalir and Valiabad, from the name of the villages located close to the north–south road crossing the Alborz Mountains between Chalus and Tehran (the village of Dalir is located 40 km to the southwest of the town of Marzan-Abad, and Valiabad is located 30 km to the south of Marzan-Abad). The authors failed

doi: 10.1002/spp2.1391

to find SSFs at other localities (two sections in the Soltanieh Mountains and one at Hasanakdar, also along the Chalus road in the Alborz Mountains). Hamdi *et al.* (1989) presented the palaeobiodiversity of the SSFs of the Soltanieh Formation as a list of faunal and floral sequences with few illustrations, and part of their distribution is reported in a composite stratigraphical column for the Soltanieh Formation of the same two localities, although the column shows the first appearance datum points of the main early skeletal fossil taxa. Later, Hamdi (1995) published a report on the Precambrian–Cambrian deposits in Iran (in Persian), in which a biostratigraphic framework with five assemblage zones and a chronostratigraphic interpretation is proposed for the Soltanieh Formation based on the data from the previous publications. That work is accompanied by expanded illustrations of the small shelly fauna from Dalir and Valiabad. In addition to the SSFs of the two aforementioned sections, rare SSFs from the lower Cambrian of Yazd are also illustrated: molluscs and hyoliths from the Bonloukhi section, Bafq area and chancelloriids from the Chah-Shour section, Saghand area (Hamdi, 1995). A field meeting was then organized in 1996 by Hamdi for the International Geological Coordination Program (IGCP) 366, at which Neoproterozoic to Ordovician successions of the Alborz Mountains were visited, including the previously studied, SSF-yielding localities (Zhuravlev *et al.* 1996). After these studies in the 1990s, very few studies on SSFs were conducted in Iran. CiabeGhodsi *et al.* (2006) focused on the trace fossil *Trichophycus pedum* at the Soltanieh type section. They mention the presence of *Anabarites* sp. and *Protohertzina* sp. in the Soltanieh Formation at the type section but no specimen is illustrated. Tashayoee *et al.* (2012) listed and illustrated SSFs from the Soltanieh Formation at the Garmab section (village of Hasanakdar) of the Alborz Mountains and proposed two SSF assemblage zones. Both studies failed to provide a description and stratigraphic range for the identified taxa, which are essential information for any further biostratigraphic and palaeobiogeographic interpretations. Finally, Shahkarami *et al.* (2017*a*, *b*) focused on the ichnofossils of the Soltanieh Formation but synthesized the results on the SSFs from the previous studies for discussion. Despite the deficiencies of the previous studies, the figured material attests to the relative abundance, diversity and preservation of the SSFs from the critical Ediacaran–Cambrian transition.

This new study on the SSFs of northern Iran was therefore conducted to improve and enlarge on the promising data from this key area. The Soltanieh Formation of the Alborz Mountains is revised for its micropalaeontological content at the sections of Dalir and Valiabad. In addition, novel micropalaeontological studies are presented from the Soltanieh Mountains for the Soltanieh Formation, but also for the fossiliferous overlying Barut Formation. The aim of this new work is to provide solid SSF data (with taxonomy and stratigraphic extension) for further biostratigraphic and palaeobiogeographic interpretations. This substantial dataset enables us to: (1) identify distinct microfaunal assemblages; (2) provide a revised biochronostratigraphic interpretation of the succession; and (3) offer new considerations for the interpretation of the evolution of biodiversity in the framework of the Cambrian explosion.

GEOLOGICAL SETTING

This work focuses on the SSFs of the lower Cambrian of Iran, which outcrops best in the Soltanieh and Alborz Mountains in the northern part of the country (Fig. 1A). The Soltanieh Mountains, located to the south of the cities of Zanjan and Soltanieh, are a narrow mountain range located close to and south of the central Alborz Mountains and run in a north-west–south-east direction (Fig. 1B). The width of the Soltanieh Mountains ranges between 10 and 12 km and the length extends to more than 150 km. The range corresponds to an uplift of Mesozoic, Palaeozoic and Precambrian rocks produced by a fault zone aligned to the north-east border of the range (Fig. 1B, D, E; Stöcklin, 1968; Hassanzadeh *et al.* 2008; Ghadimi *et al.* 2012). This longitudinal fault zone is accompanied by cross-faults of various directions, producing a complicated mosaic pattern (Fig. 1B, D, E; Stöcklin *et al.* 1964, 1965; Hassanzadeh *et al.* 2008; Ghadimi *et al.* 2012). The Alborz Mountains are a sinuous, narrow (*c.* 120 km wide), east–west-trending mountain range that extends for 2000 km from eastern Turkey to Afghanistan along the southern margin of the Caspian Sea (Fig. 1B; Zanchi *et al.* 2006; Zandkarimi *et al.* 2016). It is a double-verging transpressional fold-and-thrust belt complex (Guest *et al.* 2006, and references therein; Etemad-Saeed *et al.* 2016; Etemad-Saeed & Najafi 2019). Oblique convergence is accommodated through a combination of left-lateral strike–slip and thrust faulting (Fig. 1C; Ballato *et al.* 2011). The Alborz, and most probably the Soltanieh Mountains, resulted from the Alpine orogeny, from the Late Triassic Cimmerian phase (resulting from the collision of the Central Iranian Block with Eurasia) to the post-Oligocene stage of intracontinental deformation (related to the collision between the Arabian and Eurasian plates) (Stöcklin *et al.* 1964, 1965; Stöcklin, 1968; Zanchi *et al.* 2009; Ballato *et al.* 2011; Zandkarimi *et al.* 2016; Etemad-Saeed *et al.* 2016, Madanipour *et al.* 2017; Etemad-Saeed & Najafi 2019).

During the Ediacaran–Cambrian transition, the Iranian blocks were originally part of a series of peri-Gondwanan terranes that bordered the north-western margin of

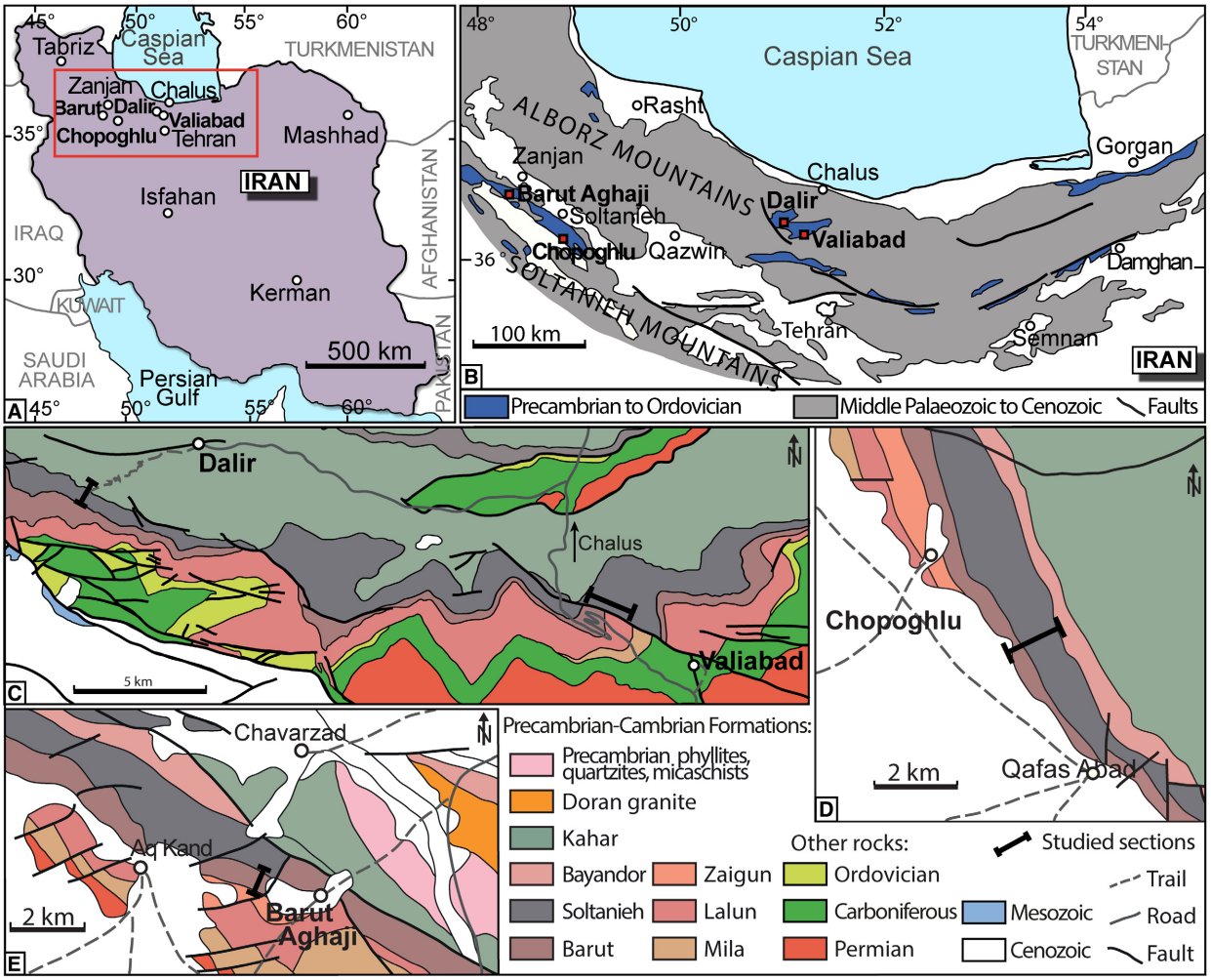

FIG. 1. Geological setting of the study area. A, map of Iran with the main cities marked and visited localities highlighted in bold; outlined area magnified in B. B, map of the Soltanieh and central Alborz Mountains; middle Palaeozoic to Cenozoic rocks in grey and Precambrian to Ordovician rocks in blue (modified from Stöcklin *et al.* 1964). C, geological map of part of the central Alborz Mountains with the location of the studied sections near Dalir and Valiabad (modified from Vahdati Daneshmand & Nadim 1999). D, geological map of part of the Soltanieh Mountains with the location of the studied section south-east of the village of Chopoghlu (modified from Stöcklin & Eftekharnezhad 1969). E, geological map of part of the Soltanieh Mountains with the location of the studied section near the village of Barut-Aghaji (modified from Stöcklin & Eftekharnezhad 1969).

Gondwana (the so-called Proto-Palaeotethyan margin *sensu* Lasemi 2001 and Proto-Tethyan margin *sensu* Stampfli & Borel 2002). This part of the peri-Gondwanan margin is interpreted either as a thermally subsiding passive margin of the Afro-Arabian platform that was formed after the late Proterozoic rifting of the north-western Gondwana supercontinent (Stöcklin, 1968; Berberian & King 1981; Husseini 1989; Talbot & Alavi 1996; Lasemi 2001, 2007, 2017) or alternatively as an active continental margin with Cadomian arc plutonism and volcanism resulting from the southwards subduction of the Proto-Tethys ocean along the northern margin of Gondwana (Ramezani & Tucker 2003; Hassanzadeh *et al.* 2008; Horton *et al.* 2008; Moghadam *et al.* 2015, 2016, 2017; Malek-Mahmoudi *et al.* 2017; Etemad-Saeed & Najafi 2019).

The lower Cambrian of the Soltanieh and Alborz Mountains, on which this study focuses, is recorded in the mixed carbonate–siliciclastic successions of the Soltanieh and Barut Formations. The Soltanieh Formation was defined by Stöcklin *et al.* (1964) from ridges east of the village of Chopoghlu (or Chopoqlu) in the Soltanieh Mountains, to the south of the town of Soltanieh (Fig. 1B). The Soltanieh Formation is 1160 m thick and is composed of three

members at the type locality, described by Stöcklin *et al.* (1964) from bottom to top as follows.

1. The lowest member is the Lower Dolomite Member, which is 123 m thick and consists of yellow, recrystallized, well-bedded dolostone with many black and white chert bands up to 50 cm thick.
2. The Chopoghlu Shale Member is 247 m thick and consists of dark green–grey argillaceous, siliceous and silty-micaceous slatey shales. In the uppermost part, blue–black, thin-platy, nodular, partly siliceous limestones and calcareous shales are interbedded within the shales.
3. The Upper Dolomite Member is very thick (790 m) and is composed of white to yellow, massive, recrystallized dolostone. Within the dolostone, two levels (5 m and 73 m) of green, micaceous, slatey shales are intercalated. In the uppermost part, dark grey, well-bedded dolostones and limestones with nodules of black chert are present.

The overlying Barut Formation was defined by Stöcklin *et al.* (1964) in hills north-west of the village of Barut-Aghaji in the Soltanieh Mountains. It corresponds to a 714-m-thick succession of alternating purple to green shales and sandstones and dark, laminated dolostones and limestones with chert nodules. The Soltanieh Formation was later recognized in the Alborz Mountains by Hamdi and Golshani in 1983 *in* Hamdi 1989. In the Alborz Mountains, Hamdi (1989) identified five members in the Soltanieh Formation at Dalir and Valiabad due to the presence of a thicker shale intercalation in the Upper Dolomite Member as defined by Stöcklin *et al.* (1964). Therefore, Hamdi (1989) described from bottom to top: (1) the Lower Dolomite Member (165 m thick); (2) the Lower Shale Member (120 m thick); (3) the Middle Dolomite Member (180 m thick); (4) the Upper Shale Member (90 m thick); and (5) the Upper Dolomite Member (580 m thick). The stratigraphic subdivisions of Stöcklin *et al.* (1964) and Hamdi (1989) have not been formally defined according to the International Stratigraphic Guide and such a procedure is beyond the scope of this paper. However, for practical purposes, this terminology is used in the rest of the paper, with the subdivisions of Stöcklin *et al.* (1964) and Hamdi (1989) used for the successions of the Soltanieh and Alborz Mountains, respectively.

In this study, the Soltanieh and Barut Formations were also investigated in the Soltanieh Mountains, around the type locality of the Soltanieh Formation (Fig. 1D) and of the Barut Formation (Fig. 1E). The type section of the Soltanieh Formation was visited and limestone levels sampled for SSFs but they did not yield any fossils. A second section was studied and sampled for SSFs (sample numbers starting with CH reported in Fig. 2) to the south-east of the type section, in a valley midway between the villages of Chopoghlu and Qafas Abad (coordinates of the start of the section N36.17998°; E48.92794°; Fig. 1D). Above the recognizable Bayandor Formation, we identified the Lower Dolomite Member, which is *c.* 100 m thick and consists of yellow, recrystallized, massive dolostone with numerous black and white chert bands (only the upper part is represented in Fig. 2). The Chopoghlu Shale Member is 108 m thick and dominated by shales (Fig. 2). In the lower part, limestone nodules and irregular beds are observed (Fig. 2). Massive, yellow, recrystallized dolostone constitutes most of the Upper Dolomite Member, which is 617 m thick (Fig. 2). Blue and finely laminated limestones are intercalated in the Upper Dolomite Member: a 22 m interval is present in the lowermost part and a 50 m interval at 136 m above the base of the member (Fig. 2). The Barut Formation overlies the Soltanieh Formation and its base corresponds to 24 m of blue, finely bedded limestones alternating with thin shale beds in the section south-east of the village of Chopoghlu (SE Chopoghlu section) (Fig. 2). The base of the Barut Formation was also studied and sampled for SSFs at the type locality, where it consists of finely bedded blue limestones interbedded with rare shales (Fig. 2; sample numbers starting with B).

The Soltanieh Formation was also studied at Dalir and Valiabad, the localities of Hamdi (1989, 1995) and Hamdi *et al.* (1989) (Fig. 1B, C). At Dalir (N36.31310°; E51.04605°), the succession is well exposed along the trail leading to an abandoned phosphate mine in the Upper Shale Member, and was studied from the base of the Lower Dolomite Member up to the lower part of the Upper Dolomite Member (only the fossiliferous interval is represented in Fig. 3, with sample numbers starting with D). The Lower Dolomite Member contains thick, massive, yellow dolostone and black cherts. The Chopoghlu Shale Member (delimited by the first and last occurrence of shale beds) is dominated by crumbly, grey, slatey shales in the lower part and centimetre-sized beds of cherty dolostone in the upper part. A 5-m-thick, dark limestone and 5-m-thick, yellow dolostone are intercalated in the upper part of the Chopoghlu Shale Member (Fig. 3). The Middle Dolomite Member consists of 67 m of massive, yellowish dolostone (Fig. 3). The Upper Shale Member is delimited by the first and last occurrence of shale beds. In its lower 35 m, alternations of thin beds of shales with dolostone and then phosphatic limestones are present (Fig. 3). The upper 68 m of the Upper Shale Member is dominated by dark shales (Fig. 3). The lowermost 8 m of the Upper Dolomite Member corresponds to thinly bedded, grey limestone (Fig. 3). The rest of the Upper Dolomite Member consists of massive, yellowish dolostone. At Valiabad (N36.27268°; E51.27462°), the succession is more difficult to study due to intense

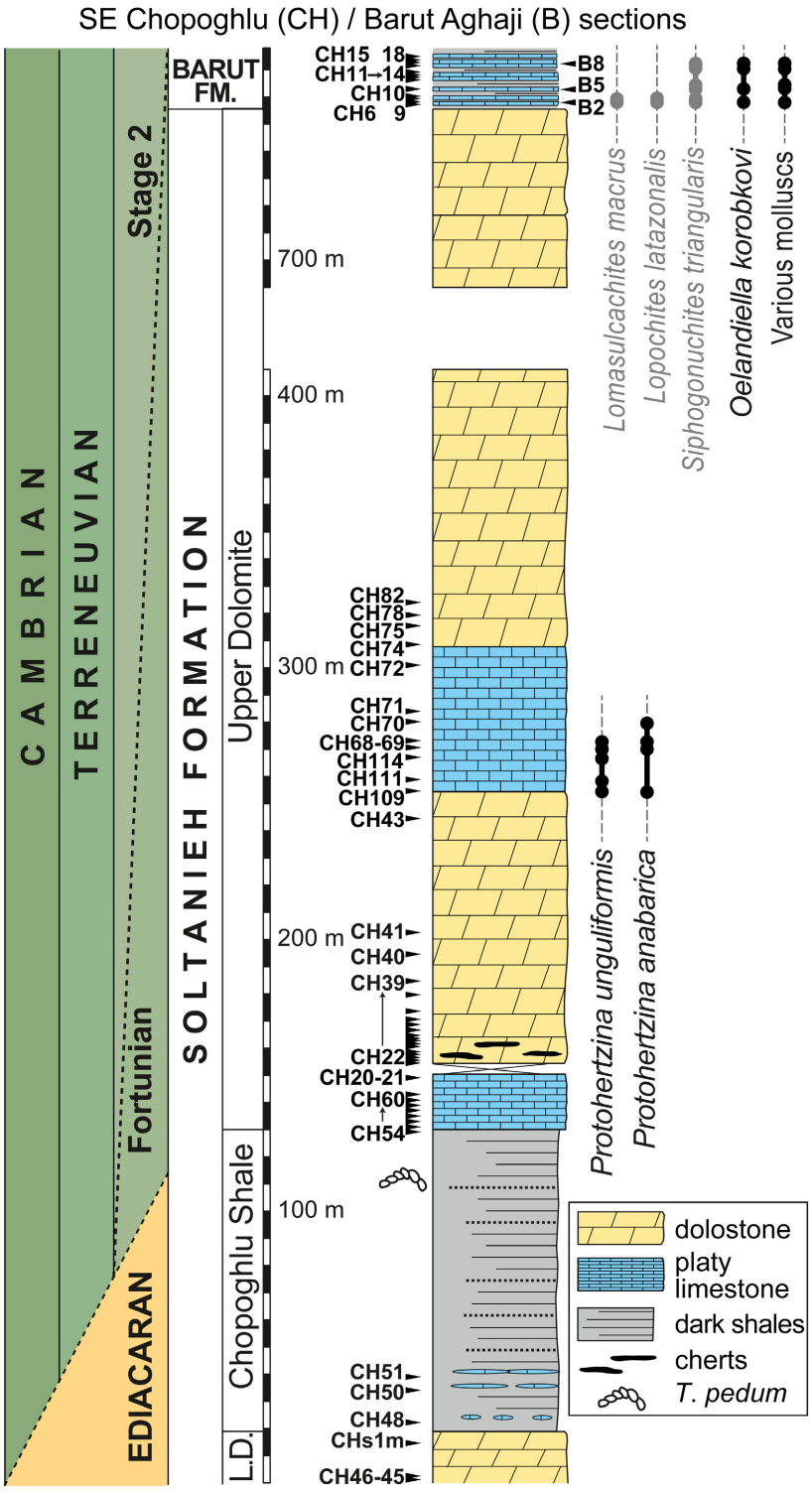

FIG. 2. Stratigraphic column and small shelly fossil (SSF) range through part of the Soltanieh and Barut Formations at the section south-east of the village of Chopoghlu (SE Chopoghlu) and at the Barut Aghaji section (stratigraphic subdivision terminology following Stöcklin *et al.* 1964), with chronostratigraphic interpretation. The position of the Ediacaran–Cambrian boundary is not resolved at this section based on SSF data from this study (oblique dashed line). Sample position is indicated by numbers: numbers starting with CH were collected at the SE Chopoghlu section and numbers starting with B were collected at the Barut section; their position is inferred by correlation in the stratigraphic column of the SE Chopoghlu section. The presence of *Treptichnus pedum* in the upper part of the Chopoghlu Shale Member is inferred from the report of the trace fossil by CiabeGhodsi *et al.* (2006) at the Chopoghlu type section. The lower part of the Lower Dolomite Member of the Soltanieh Formation and the upper part of the Barut Formation have been observed but are not represented due to an absence of SSFs. Occurrence data in black refer to species described in this work and occurrence data in grey refer to those that are currently unpublished. *Abbreviation*: LD, Lower Dolomite Member.

vegetation cover and the presence of a large fault along the trail where the best outcrops are present, therefore only part of it has been sampled and is represented in Fig. 4. We could observe the Lower Dolomite Member, which was largely dominated by cherts. The Chopoghlu Shale Member is dominated by shales in the lower part, while the upper part is more cherty. The Middle Dolomite Member consists of massive, yellow dolostone except for a few metres of cherts in the lowermost part (sample numbers starting with V reported in Fig. 4). The lower

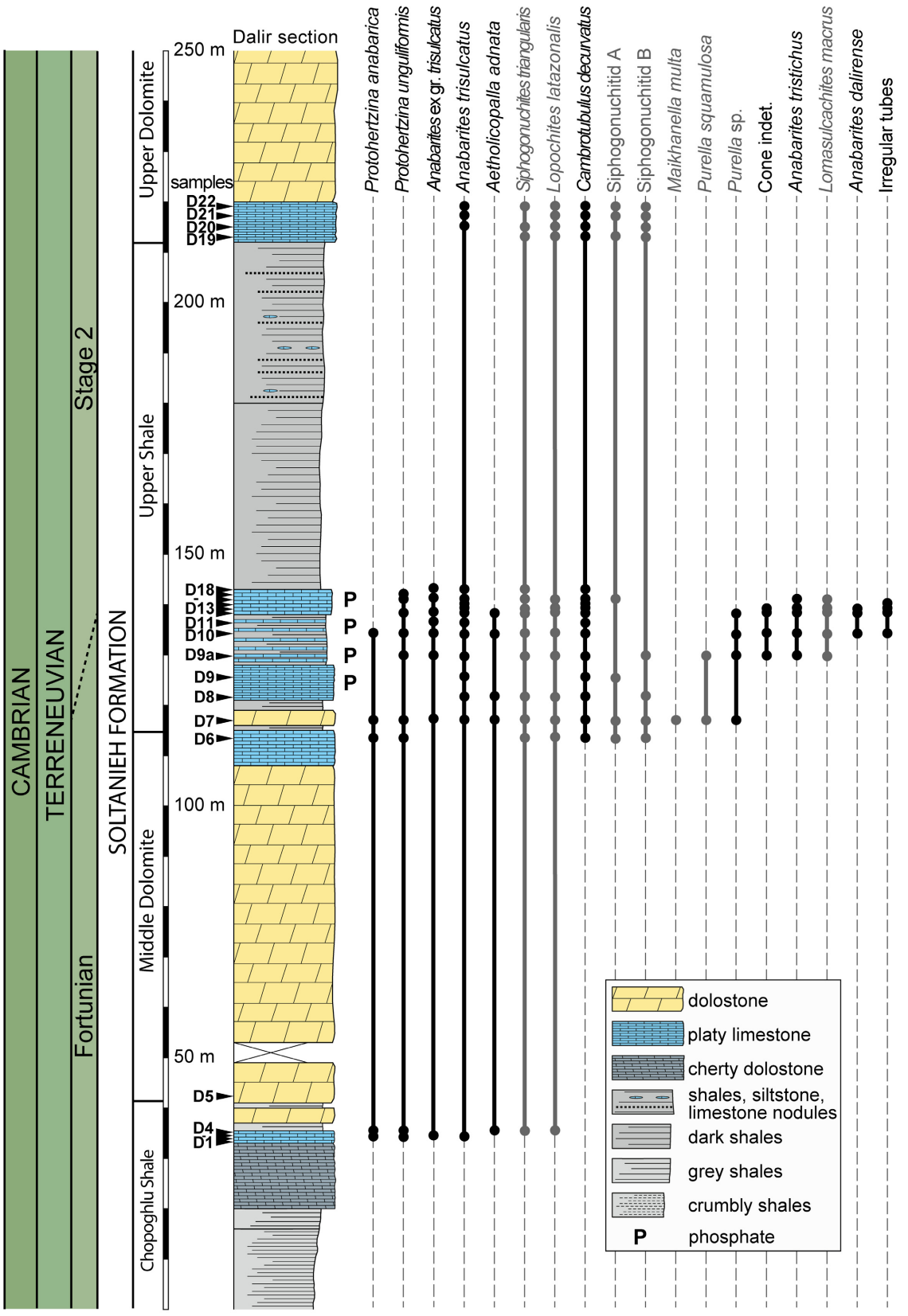
CAMBRIAN
TERRENEUVIAN
Fortunian
Stage 2
SOLTANIEH FORMATION
Chopoghlu Shale
Middle Dolomite
Upper Shale
Upper Dolomite
Dalir section
250 m
200 m
150 m
100 m
50 m
samples
D22
D21
D20
D19
D18
D13
D11
D10
D9a
D9
D8
D7
D6
D5
D4
D1
P
Protohertzina anabarica
Protohertzina unguliformis
Anabarites ex gr. trisulcatus
Anabarites trisulcatus
Aetholicopalla adnata
Siphogonuchites triangularis
Lopochites latazonalis
Cambrotubulus decurvatus
Siphogonuchitid A
Siphogonuchitid B
Maikhanella multa
Purella squamulosa
Purella sp.
Cone indet.
Anabarites tristichus
Lomasulcachites macrus
Anabarites dalirense
Irregular tubes
dolostone
platy limestone
cherty dolostone
shales, siltstone, limestone nodules
dark shales
grey shales
crumbly shales
phosphate

FIG. 3. Stratigraphic column and small shelly fossil (SSF) range of part of the Soltanieh Formation (stratigraphic subdivision terminology following Hamdi 1989) at the section south-west of the village of Dalir with chronostratigraphic interpretation. Sample position is indicated by numbers starting with D. The Lower Dolomite Member, the lower part of the Chopoghlu Shale Member and the upper part of the Upper Dolomite Member (*sensu* Hamdi 1989) of the Soltanieh were observed but are not represented here due to an absence of SSFs. Occurrence data in black refer to species described in this work and occurrence data in grey refer to those that are currently unpublished.

22 m of the Upper Shale Member contains thinly bedded, blue, phosphatic limestone beds alternating with dark shales (Fig. 4), and the upper part contains only dark shales. The contact between the Upper Shale Member and the Upper Dolomite Member was not observed due to intense vegetation cover. The Upper Dolomite Member produces abrupt cliffs, which makes access to the overlying Barut Formation too difficult in the two localities of the Alborz Mountains.

MATERIAL AND METHOD

In the Soltanieh Mountains 86 carbonate samples were collected from the SE Chopoghlu section and 8 at the Barut section exclusively for micropalaeontological studies (Fig. 2). Samples from the Alborz localities were also collected for micropalaeontological studies: 22 at the Dalir section (Fig. 3) and 17 at the Valiabad section (Fig. 4).

For micropalaeontological analyses, a minimum of 1 kg of each carbonate sample was processed in acid. For samples productive of SSFs, more material was processed (up to 2.5 kg). All the acid processing was performed at the Museum für Naturkunde Berlin (MfN). Samples were first broken into fragments and dissolved, either with *c.* 10% acetic acid when dealing with limestone or with *c.* 8% formic acid for the slightly dolomitic limestone. The acid-resistant residues were washed in water, wet-sifted (>50 μm), dried, and the microfossils manually picked from the dried residues under a stereomicroscope. The SSFs were stuck on stubs with carbon tape, coated with carbon and observed and imaged with a scanning electron microscope (JEOL-6610 LV) at the MfN. The described and figured material is housed in the collections of University Lille (USTL; Université des Sciences et Technologie de Lille) following the recommendation of the International Commission on Zoological Nomenclature.

RESULTS

This new study of the SSFs of the Soltanieh and Barut Formations of the Soltanieh and Alborz Mountains provides detailed, new and revised occurrences of SSFs in northern Iran. In this paper we excluded the siphogonuchitids and maikhanellids from the systematic section, although they are present in the successions along with the described taxa. Only their range is reported in the figures and is discussed (Figs 2–4). Another paper will focus on the systematic and detailed description of recovered siphogonuchitids and their phylogenetic implications.

In the Soltanieh Mountains, SSFs are relatively rare, and this is the first report of SSFs from this area. At the locality we studied, south-east of the village of Chopoghlu, SSFs first occur in the finely bedded, blue limestones of the lower middle part of the Upper Dolomite Member (*sensu* Stöcklin *et al.* 1964; Fig. 2). The SSFs of the Upper Dolomite Member in the Soltanieh Mountains are restricted to protoconodonts (*Protohertzina anabarica* Missarzhevsky, 1973 and *P. unguliformis* Missarzhevsky, 1973; Fig. 2). SSFs were then recovered in the Barut Formation at the SE Chopoghlu section and at the Barut type section (Fig. 2). They correspond to *Oelandiella korobkovi* Vostokova, 1962 and various other molluscs and siphogonuchitids (*Lomasulcachites macrus* Qian & Jiang *in* Jiang, 1980, *Lopochites latazonalis* Qian, 1977 and *Siphogonuchites triangularis* Qian, 1977).

In the Alborz Mountains, SSFs are well preserved, abundant and diversified. The lowest recoveries of SSFs are in the upper part of the Chopoghlu Shale Member at Dalir and in the lower part of the Upper Shale Member at Valiabad. At Dalir, 18 species are identified from the upper part of the Chopoghlu Shale Member to the lower part of the Upper Dolomite Member (*sensu* Hamdi 1989), and include (Fig. 3) protocondonts (*Protohertzina anabarica* and *P. unguliformis*), anabaritids (*Anabarites trisulcatus* Missarzhevsky *in* Voronova & Missarzhevsky, 1969, *A.* ex gr. *trisulcatus* Missarzhevsky *in* Voronova & Missarzhevsky, 1969, *A. tristichus* Missarzhevsky *in* Rozanov *et al.*, 1969, *A. dalirense* sp. nov., *Cambrotubulus decurvatus* Missarzhevsky *in* Rozanov *et al.*, 1969), *Aetholicopalla adnata* Conway Morris *in* Bengtson *et al.*, 1990, and indeterminate cones and irregular tubes, all of which are described in this paper. Siphogonuchitids (*Lomasulcachites macrus* Qian & Jiang *in* Jiang, 1980, *Lopochites latazonalis* Qian, 1977, *Siphogonuchites triangularis* Qian, 1977 and siphogonuchitid sp. A and B) and maikhanellids (*Maikhanella multa* Zhegallo *in* Voronin *et al.*, 1982, *Purella squamulosa* Qian & Bengtson, 1989 and *Purella* sp.) are also present and their stratigraphic ranges reported (Fig. 3), but they will be thoroughly described in another paper. At Valiabad, the same species are present but are

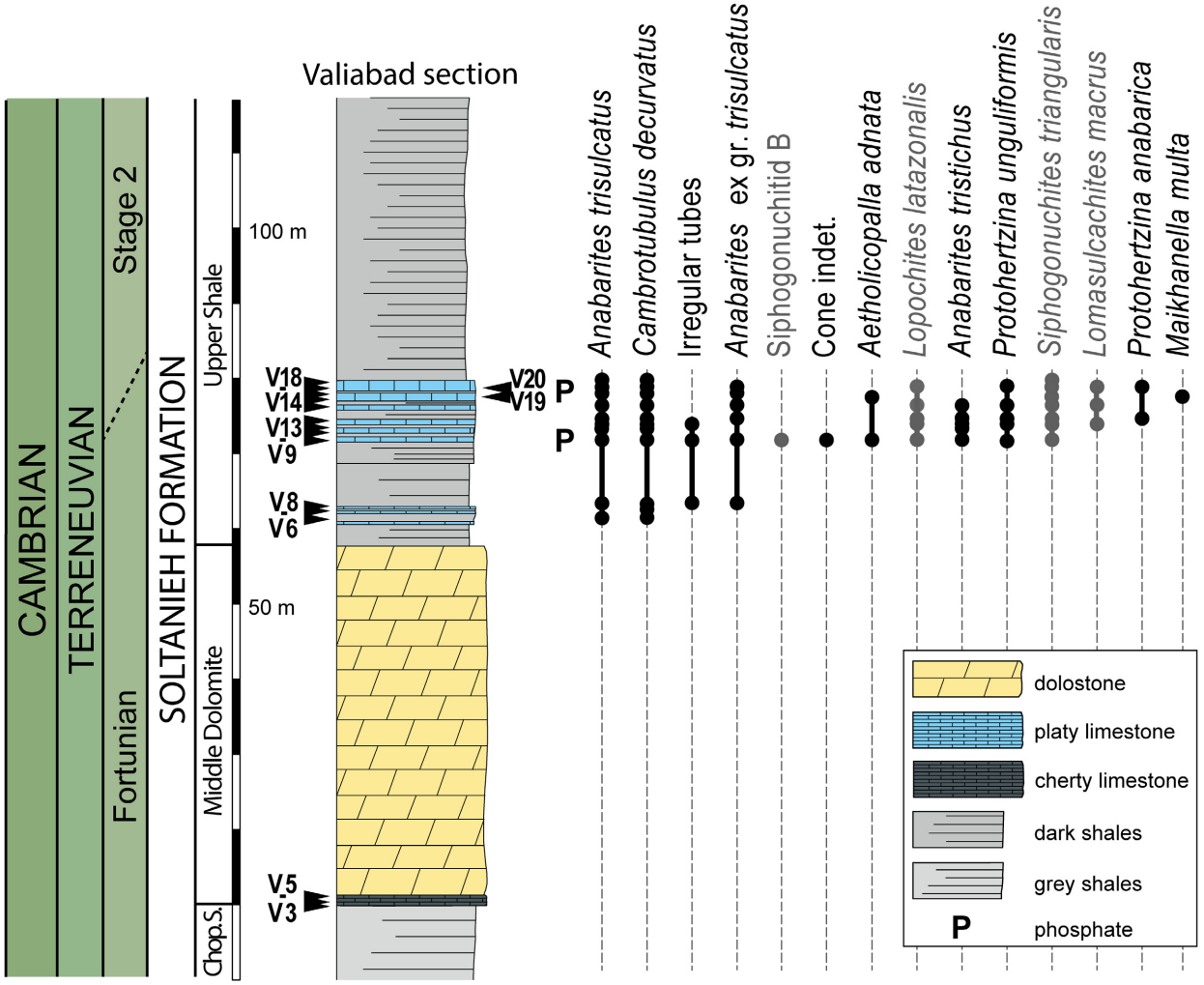

FIG. 4. Stratigraphic column and small shelly fossil (SSF) range of part of the Soltanieh Formation (stratigraphic subdivision terminology following Hamdi 1989) at the section north-west of the village of Valiabad with chronostratigraphic interpretation. Sample position is indicated by numbers starting with V. Occurrence data in black refer to species described in this work and occurrence data in grey refer to those that are currently unpublished.

found only in the Upper Shale Member, except for *Anabarites dalirense*, *Purella* sp. and siphogonuchitid sp. A, which are absent (Fig. 4). No macrofossils were detected in the field or in the samples at any of the studied localities, except for *Chuaria* Walcott, 1899 in the Chopoghlu Shale Member.

DISCUSSION

This work constitutes a comprehensive study of the SSFs from the lower Cambrian of northern Iran. It includes a revision of the taxonomy and stratigraphic extension of the SSFs of the Soltanieh Formation of the Alborz Mountains at Dalir and Valiabad (Figs 3,4), which were first described by Hamdi (1989, 1995) and Hamdi *et al.* (1989). It is extended by novel data on the SSFs of the Soltanieh and Barut Formations of the Soltanieh Mountains (Fig. 2). This substantial dataset enables us to discuss the following points.

SSF assemblages of the lower Cambrian of northern Iran

In order to take previous data into account for the identification of SSF assemblages from the Soltanieh and Barut Formations of the Soltanieh and Alborz Mountains, the taxonomic data from this study and from Hamdi (1989, 1995) and Hamdi *et al.* (1989) are compared, to enable the identification of a number of synonyms (Table 1). Some of the species (*Alborzinites iranensis*, *Cambroclavus fangxianensis*, *Dabashanites mirus*, *Hyolithellus vladimirovae*,

Hyolithellus sp., *Igorella*? *cyrtoliformis*, *Igorella* cf. *hamata*, *Obtusoconus longiconica*, *Obtusoconus rostriptutea*, *Palaeophirhabda complexa*, *Pelagiella lorenzi*, *Psammathopalas amphidos*, *Pseudovalitheca crassa*, *P. glabella*, *Purella tainzhushanensis*, *Rugatotheca typica* and *Thambetolepis dalirensis*) listed (but not figured) by Hamdi (1989, 1995) and Hamdi *et al.* (1989) have not been recovered in the present study despite detailed observations in the field, thorough sampling and careful processing. The figured specimens assigned by Hamdi (1995) to *Bemella simplex*, *Ginella savitzkii*, *Ginella orectes*, *Igorella vali-abadensis*, *Igorella mioribis* and *Yunnanopleura biformis* show few diagnostic characters and fall in the range of morphological variations of the specimens referred to as cap-shaped molluscs in the present study. Hamdi (1995) assigned broken specimens to the species *Coleolella reeta* and *Heraultipegma* sp. but his material is too fragmentary to permit identification. In addition to the figured specimens, Hamdi (1989) listed many other species of SSFs in the description of the stratigraphy and fauna of the Soltanieh Formation at Dalir and Valiabad. However, without illustration, assessment of their taxonomic validity is impossible.

With regard to the taxonomic assessment of Hamdi (1989, 1995) and Hamdi *et al.* (1989), discrepancies were noted between the stratigraphic extension in those studies and that of the species identified in our study. According to our data, the stratigraphic extension of the SSFs is restricted to the interval from the upper part of the Upper Shale Member to the lower part of the Barut Formation, whereas Hamdi (1989) and Hamdi *et al.* (1989) reported (without illustration) *Hyolithellus*? sp., *Igorella* sp., monoplacophora?, *Olivooides multisulcatus*, *Protohertzina* sp., ?*Sabellitides*, *Rugatotheca* sp., phosphatic tubes and figured *Archaeooides granulatus*, *Hyolithellus* cf. *filiformis*, *Rugatotheca typica*, and biglobular fossils (Hamdi, 1995) from the Lower Dolomite Member at Valiabad. Despite careful observation and sampling of the Lower Dolomite Member at Dalir and Valiabad and in the valley south-east of Chopoghlu, no microfossils were recovered from this member. Moreover, according to Hamdi (1989, 1995), molluscs (species of *Bemella*, *Igorella*, *Oelandiella*, *Obtusoconus*, *Protoconus*, *Purella*, *Scenella*, *Sinoconus*, *Xiadongoconus* etc. are listed but not figured) first occur in the upper part of the Upper Shale Member exclusively at Valiabad. Tashayoee *et al.* (2012) also figure a possible specimen of *Obtusoconus rostriptutea* from the Upper Dolomite Member at Garmab (Alborz Mountains). In our study, no molluscs were recovered from the upper Shale Member, or from the lower part of the Upper Dolomite Members, the limestones of which were thoroughly investigated at Dalir. The upper part of the Upper Shale Member and the lower part of the Upper Dolomite Member were not accessible at Valiabad due to thick vegetation cover. We recovered molluscs only from the Barut Formation in the Soltanieh Mountains. It is possible, according to Hamdi (1989, 1995) and Hamdi *et al.* (1989), that molluscs occur below the level suggested by our new data, the upper part of the Upper Shale Member, and that they were recorded only in limited areas (Valiabad and Garmab). However, at Valiabad, the section is located close to a fault (Fig. 1C). In this context, it is also possible that the samples of the mollusc assemblages in Hamdi (1989, 1995) and Hamdi *et al.* (1989) may actually come from the Barut Formation (or even from an overlying formation such as the Zaigun, Lalun or Mila Formations; Fig. 1C) and not from the Upper Shale Member.

Based on the stratigraphic range of all the SSFs identified in each section derived from this study (Figs 2–4), we suggest the identification of two microfaunal assemblages. The first assemblage corresponds to SSFs occurring in the entire Soltanieh Formation in the Soltanieh and Alborz Mountains. It is composed of protoconodonts (*Protohertzina anabarica* and *P. unguliformis*), anabaritids (*Anabarites trisulcatus*, *A.* ex gr. *trisulcatus*, *A. tristichus*, *A. dalirense*, *Cambrotubulus decurvatus*), maikhanellids (*Maikhanella multa*, *Purella squamulosa* and *Purella* sp.) and of *Aetholicopalla adnata*, indeterminate cones and irregular tubes. The biodiversity and abundance of this assemblage are dominated by tubes of anabaritids. The second assemblage is dominated, in diversity and abundance, by molluscs of the Barut Formation, which include *Oelandiella korobkovi* and various cap-shaped morphotypes. Along with the taxa of both assemblages there also occur siphogonuchitid sclerites of *Lomasulcachites macrus*, *Lopochites latazonalis*, *Siphogonuchites triangularis* and two morphotypes of unidentified siphogonuchitid species.

Interpretations of SSF assemblages and of the resulting chronostratigraphy should be considered with caution, considering recent advances in the identification of various factors affecting the SSF record. Indeed, SSF data are the result of acid extraction of microfossils from carbonate rocks. Therefore, the record of SSFs is strongly affected by the sampling procedure, given that only carbonate levels are targeted, leaving gaps in fossil data from the siliciclastic and dolomitic intervals. The extraction technique also introduces biases into the fossil record, given that originally calcareous shells are dissolved in the process (Jacquet *et al.* 2019). Phosphatization (replacement of the calcareous shell) and phosphogenesis (phosphatic coating or mould) are necessary for the recovery of the originally calcareous shells from acid-resistant residues, whereas originally siliceous and phosphatic shells are not affected (Jacquet *et al.* 2019). Phosphatization and phosphogenesis are the result of particular depositional and taphonomic processes outlined in Pruss *et al.* (2018

TABLE 1. Comparison of the taxonomy and stratigraphic distribution of the species identified in this study with data from Hamdi (1989, 1995) and Hamdi *et al.* (1989).

This study		Hamdi (1989, 1995), Hamdi *et al.* (1989)		
Species	Occurrence	Species	Figure	Occurrence
Anabarites trisulcatus	CSM + MDM + USM + UDM	*Anabarites trisulcatus*	Hamdi *et al.* (1989): fig. 3h Hamdi (1995): pl. 5, figs 1–6; pl. 10, figs 5–7	MDM + USM
Anabarites tristichus	USM	*Anabarites trisulcatus*	Hamdi (1989): pl. 4, figs 4–5, 7	MDM + USM
Protohertzina anabarica	CSM + MDM + USM	*Protohertzina anabarica*	Hamdi (1989): pl. 1, figs 3, 6–7	MDM + USM
		Protohertzina cf. *anabarica*	Hamdi (1995): pl. 5, figs 17, 18	USM
		Protohertzina robusta	Hamdi (1989): pl. 2, figs 4–8	MDM
Protohertzina unguliformis	CSM + MDM + USM	*Protohertzina unguliformis*	Hamdi (1989): pl. 1, figs 1, 2 Hamdi (1995): pl. 5, figs 7–10	MDM
		Protohertzina anabarica	Hamdi *et al.* (1989): fig. 3g	
		Protohertzina cf. *unguliformis*	Hamdi (1989): pl. 1, fig. 10; pl. 3, fig. 1	MDM
		Protohertzina cf. *siciformis*	Hamdi (1995): pl. 5, figs 11–13	MDM + USM
		Hastina sp.	Hamdi (1989): pl. 1, figs 4, 5	MDM
Cambrotubulus decurvatus	MDM + USM	*Cambrotubulus decurvatus*	Hamdi (1989): pl. 4, figs 1–3, 6 Hamdi *et al.* (1989): fig. 3e	MDM + USM
		Rugatotheca cf. *typica*	Hamdi (1995): pl. 5, fig. 14	MDM
		Conotheca subcurvata	Hamdi (1995): pl. 5, figs 15, 16	MDM + USM
Siphogonuchites triangularis	CSM + MDM + USM + UDM + BF	*Siphogonuchites triangularis*	Hamdi (1995): pl. 6, figs 5–9, 13; pl. 10, fig. 1	MDM + USM
		Siphogonuchites triangulatus	Hamdi (1989): pl. 3, fig. 7	USM
		Palaeosulcachites cf. *biformis*	Hamdi (1989): pl. 3, figs 5, 6	MDM + USM
Lopochites latazonalis	CSM + MDM + USM + UDM + BF	*Lopochites quadragonus*	Hamdi (1995): pl. 6, figs 14, 15	MDM
		Drepanochites dilatatus	Hamdi (1995): pl. 6, figs 10–12	MDM
		Quadrochites disjunctus	Hamdi (1995): pl. 8, figs 4, 5	MDM
		Lopochites cf. *latazonalis*	Hamdi (1995): pl. 10, fig. 2	MDM + USM
Lomasulcachites macrus	USM + BF	*Lomasulcavichites macrus*	Hamdi (1995): pl. 14, figs 2, 3	USM
Aetholicopalla adnata	CSM + MDM + USM	*Archaeooides granulatus*	Hamdi (1995): pl. 7, fig. 5	MDM + USM
Maikhanella multa	USM	*Lapidites emeishanensis*	Hamdi (1995): pl. 7, figs 1–3, 6–8	MDM
		Maikhanella cf. *multa*	Hamdi (1989): pl. 5, figs 2, 4	MDM
		Maikhanella multa	Hamdi *et al.* (1989): fig. 3d	
Oelandiella korobkovi	BF	*Latouchella* cf. *korobkovi*	Hamdi (1995): pl. 11, figs 1, 2, 8, 9, 12; pl. 16, figs 11, 12	USM + UDM
		Hubeispira nitida	Hamdi (1995): pl. 11, figs 3, 11	USM
		Latouchella maidipingensis	Hamdi (1995): pl. 11, figs 4–6, 7, 10; pl. 16, figs 7–10	USM + UDM
		Latouchella korobkovi	Hamdi (1989): pl. 6, figs 1, 2 Hamdi (1995): pl. 12, figs 3, 7, 9, 11, 12	USM
		Latouchella sp.	Hamdi (1989): pl. 6, figs 3, 4	USM
		Latouchella ex gr. *korobkovi*	Hamdi (1989): pl. 6, fig. 5	USM
		Archaeospira ornata	Hamdi (1995): pl. 12, figs 6, 8, 10	USM
		Archaeospira regularis	Hamdi (1995): pl. 14, figs 1, 2	USM
Irregular tube	USM	?*Aldanella* sp.	Hamdi *et al.* (1989): fig. 3b	n.a.
Indeterminate cones	USM	Indet. internal mould of flaring tube	Hamdi (1989): pl. 3, fig. 4	MDM

BF, Barut Formation; CSM, Chopoghlu Shale Member; MDM, Middle Dolomite Member; n.a., not applicable; UDM, Upper Dolomite Member of the Soltanieh Formation; USM, Upper Shale Member.

and references therein) and Freeman *et al.* (2019 and references therein), which therefore introduce a bias into the distribution of SSFs in sections. SSF distribution thus appears to be influenced by facies (e.g. Jacquet *et al.* 2019) and additionally by palaeoenvironmental conditions (e.g. bathymetry; Jacquet *et al.* 2019). The impact on regional biostratigraphy and the global correlation of shell mineralogy, extraction technique, palaeoenvironmental, depositional and taphonomic conditions associated with SSF data should thus be considered.

The SSF data from northern Iran presented in this paper, as are any traditional SSF data, are subject to the biases described above. Indeed, the SSFs were mostly extracted by acetic acid digestion from limestone levels. Limestone intervals were preferentially sampled from the mixed carbonate–siliciclastic succession of the Soltanieh and Barut Formations. However, it was possible to reduce the gaps in the SSF distribution in the siliciclastic intervals of the sections thanks to the presence of limestone intercalations within the shales, which were sampled, dissolved and picked for SSFs (Figs 2–4). Dolostones, which represent a considerable thickness of the Soltanieh Formation, are also unfavourable to the extraction of SSFs but efforts were made to sample the less dolomitic beds, which were dissolved with formic acid for SSF extraction (Figs 2–4). Acid extraction of SSFs also introduced a bias in the SSF distribution due to the mineralogy of their shells. The shells of the recovered anabaritids, maikhanellids, siphogonuchitids and *Aetholicopalla adnata* are interpreted as calcareous. These taxa are preserved as phosphatic replacement of the shells/tests (*Anabarites trisulcatus*, *Aetholicopalla adnata*), phosphatic internal coatings (*Anabarites tristichus*, *A. trisulcatus*, *A. dalirense*, *Cambrotubulus decurvatus*) and/or external coatings (*Aetholicopalla adnata*), and/or internal moulds (*Anabarites tristichus*, *A. trisulcatus*, *A.* ex gr. *trisulcatus*, *A. dalirense*, *Cambrotubulus decurvatus*, *Oelandiella korobkovi*, *Aetholicopalla adnata*). The original mineralogy of the shells of the indeterminate cones and irregular tubes also described in this study is not known, therefore the taphonomic impact on their record cannot be assessed with certainty, but they are preserved as internal moulds, which suggests a calcareous mineralogy. As stated by Jacquet *et al.* (2019), the occurrences of these calcareous taxa are strongly related to facies (i.e. depositional environment and preservation potential) and therefore to palaeoenvironmental conditions. In order to evaluate how lithological and taphonomic constraints influence the stratigraphic distribution of the SSFs in northern Iran, detailed microfacies and multivariate analyses associated with the micropalaeontological data presented in this paper will be integrated in a future study (following Jacquet *et al.* 2019). The only originally phosphatic elements from the described Iranian assemblages are the protoconodonts *Protohertzina anabarica* and *P. unguliformis*. According to Jacquet *et al.* (2019), given that the distribution of phosphatic taxa is more reliable than that of calcareous taxa, the range of *Protohertzina anabarica* and *P. unguliformis* in the Iranian sections should therefore be prioritized in biostratigraphic and correlation discussions.

Revision of biochronostratigraphic interpretations of the lower Cambrian of northern Iran

Most of the taxa identified in the Soltanieh and Barut Formations of northern Iran have a wide palaeogeographic distribution and a relatively well-described stratigraphic range that enable their use for biostratigraphic studies and chronostratigraphic interpretations of the sections. It appears that, from the composite stratigraphic range of globally distributed taxa (Fig. 5), the sampled and fossiliferous studied intervals of the Soltanieh and Barut Formations correspond to the Terreneuvian

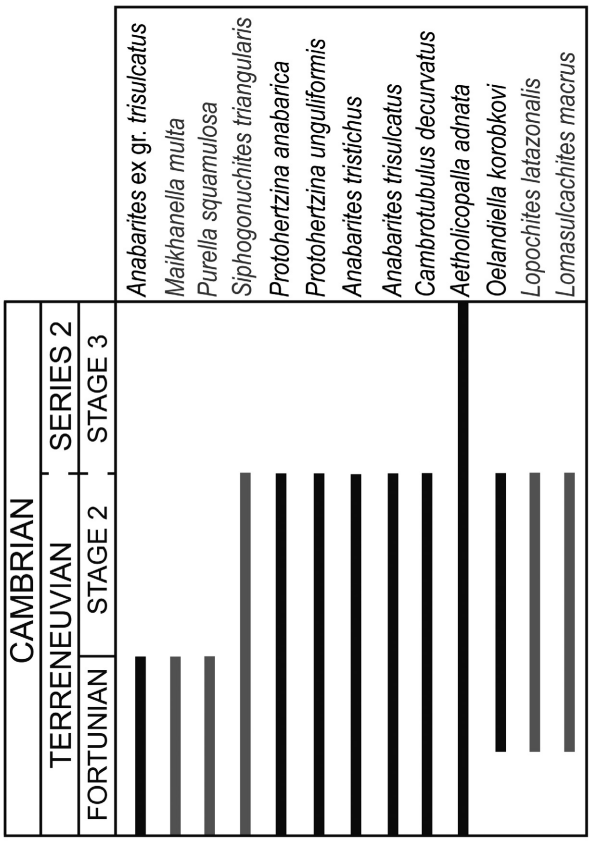

FIG. 5. Range of globally distributed taxa recorded in the Soltanieh and Barut Formations (see Table S1 for detailed references). Occurrence data in black refer to species described in this work and occurrence data in grey refer to those that are currently unpublished.

(Figs 2–4). Only one species (*Aetholicopalla adnata*) of the 12 biostratigraphically significant species has a stratigraphic range extending up to the Cambrian Stage 3 (Fig. 5). Only two formally identified species are restricted to the Fortunian: *Maikhanella multa* and *Purella squamulosa* (Fig. 5). Therefore, the upper limit of the Fortunian can be interpreted at or above the highest occurrence of those taxa. Hence, the transition from the Fortunian to the Cambrian Stage 2 is most probably located in the lower part of the Upper Shale Member, where the highest occurrences of *Maikhanella multa* and *Purella squamulosa* are reported at Dalir and Valiabad (Figs 3, 4). *Maikhanella multa* and *Purella squamulosa* were not recovered in the Soltanieh Mountains, therefore the position of the transition from the Fortunian to the Cambrian Stage 2 cannot be identified based on biostratigraphic data (Fig. 2), but can be inferred from lithological correlations with the record from the Alborz Mountains. No SSF restricted to the Cambrian Stage 3 has been recovered from the Soltanieh and Barut Formations of the Alborz and Soltanieh Mountains.

Our chronostratigraphic interpretation of the Soltanieh Formation of the Alborz Mountains differs from that of Hamdi (1989, 1995) and Hamdi *et al.* (1989), which was further promoted by Shahkarami *et al.* (2017*a*, *b*). They considered the upper part of the Soltanieh Formation to be Cambrian Stage 3. Such an interpretation is questionable due to several lines of evidence. A Cambrian Stage 3 age is deduced from the presence, in the Alborz Mountains exclusively, of *Pelagiella lorenzi* in the upper part of the Upper Shale Member, a fossil used as an index for the Cambrian Stage 3 in Siberia (see discussion in Devaere *et al.* 2013). However, the assignment of the specimens of Hamdi (1989, 1995) and Hamdi *et al.* (1989) to *Pelagiella lorenzi* is doubtful. Such an assignment has been challenged by Parkhaev & Kalova (2011), who considered the Iranian specimens to be synonyms of *Aldanella crassa*. Kouchinsky *et al.* (2017) related them to *A. crassa* too but also to *Pseudoyangtzespira selindeica*. We agree that the specimens should not be assigned to *Pelagiella*, which is characterized by a flat or slightly depressed spiral surface and a triangular to subtriangular apertural section, given that the Iranian specimens assigned to *P. lorenzi* are subplanispirally coiled and have an oval aperture (Hamdi 1995, pl. 16, figs 1–6). The Iranian specimens assigned to *P. lorenzi* therefore most probably correspond to specimens of *Oelandiella korobkovi* with a broken apertural margin. Otherwise, the other molluscs described by Hamdi (1989, 1995) and Hamdi *et al.* (1989) are not restricted to the Cambrian Stage 3 but have instead been reported in the Terreneuvian. Trilobites have been reported from the Soltanieh Formation, which suggests a Cambrian Stage 3 age (Hamdi 1989). However, the presence of *Eoredlichia* and *Wutingaspis* sp. in the Upper Shale Member was only informally mentioned by H. Salehi (*in* Hamdi 1989) and this find was not confirmed by Hamdi (1989, 1995) or Hamdi *et al.* (1989), and no trilobites were recovered in the present study.

Our new chronostratigraphic interpretation is more congruent, to some degree, with the one based solely on ichnostratigraphy by Shahkarami *et al.* (2017*a*, *b*), who identified four ichnozones. Ichnozone 1 spans the middle interval of the Chopoghlu Shale and is similar to the ichnofauna of the Ediacaran (Shahkarami *et al.* 2017*a*). However, due to the interpretations of Hamdi (1989, 1995) and Hamdi *et al.* (1989), which suggest that Fortunian SSFs occurred in the Lower Dolomite Member, and due to environmental settings associated with this ichnofauna in Iran, Shahkarami *et al.* (2017*a*) concluded that Ichnozone 1 is a distal expression of the Fortunian *Treptichnus pedum* Zone. Ichnozone 2 corresponds to the upper part of the Chopoghlu Shale Member; it the Middle Dolomite Member, and the lower part of the Upper Shale Member; it is defined by the first occurrence of *Treptichnus pedum*, and is regarded as Fortunian in age (Shahkarami *et al.* 2017*a*). Such an interpretation is congruent with the first occurrence of SSFs in the upper part of the Chopoghlu Shale at Dalir and in the lower part of the upper Dolomite (*sensu* Stöcklin *et al.* 1964; equivalent to the Middle Dolomite of Hamdi 1989) south-east of Chopoghlu, as shown in the present study. Ichnozone 3 represents the middle part of the Upper Shale Member and is interpreted as Fortunian to Cambrian Stage 2 (Shahkarami *et al.* 2017*a*), as suggested by the SSF distribution in the present study. Ichnozone 4, defined by the first occurrence of *Psammichnites gigas*, corresponds to the uppermost part of the Upper Shale Member and is regarded as Cambrian Stage 2–3 (Shahkarami *et al.* 2017*a*).

Contribution of the SSFs from northern Iran to our knowledge of the evolution of palaeobiodiversity during the Cambrian explosion

The identification of two distinct, successive microfaunal assemblages in the Terreneuvian successions of northern Iran can be compared with the few global and regional patterns of faunal changes during the pre-trilobitic Cambrian advanced in the literature. Maloof *et al.* (2010), Porter (2010) and Kouchinsky *et al.* (2012) presented sequences of first appearance of various clades of metazoans at the global scale, by considering biomineralization events; whereas Li *et al.* (2007) and Zhu *et al.* (2017) reconstructed early Cambrian metazoan fossil

sequential occurrences for south China from a biodiversity perspective, and Budd & Jackson (2016) presented global faunal sequences from an evolutionary perspective. The raw data on which these faunal sequences have been interpreted are, however, not detailed and it would be necessary to have access to the raw data to evaluate the interpretations. In each sequence, anabaritids and protoconodonts are part of the first faunal assemblage (protoconodonts are slightly delayed compared with anabaritids for Li *et al.* 2007, Maloof *et al.* 2010, Kouchinsky *et al.* 2012 and Zhu *et al.* 2017). They are accompanied by sclerites (grouped as the debated 'coeloscleritophorans') in Maloof *et al.* (2010) and Porter (2010), whereas sclerites appear later in south China according to Li *et al.* (2007). Other tubular organisms (hyolithelminths and the rather conical hyoliths) are directly associated with the assemblage of anabaritids, protoconodonts and sclerites according to Maloof *et al.* (2010) and Porter (2010), whereas they are slightly delayed according to Li *et al.* (2007), Kouchinsky *et al.* (2012) and Zhu *et al.* (2017). In the Maloof *et al.* (2010) study, molluscs appear later than anabaritids, protoconodonts, and sclerites. However, the first appearance of 'cap-shaped fossils' is reported simultaneously as protoconodonts and sclerites by Maloof *et al.* (2010), who include under this term possible univalved molluscs, but also sclerites of halkieriids or other 'coeloscleritophorans' and isolated valves of possible brachiopods. For Li *et al.* (2007), Porter (2010) and Kouchinsky *et al.* (2012), molluscs first occur simultaneously in the assemblage with anabaritids, protoconodonts and coeloscleritophorans, whereas they are reported as occurring later by Zhang *et al.* (2017). Budd & Jackson (2016) proposed a sequence of faunal change for the Ediacaran–Cambrian transition by grouping taxa under the informal term 'X world' according to the type of assemblage (Fig. 6). According to the authors, the terminal Ediacaran is characterized by problematic tubes best represented by *Cloudina*. Similarly, the basalmost part of the Cambrian is also dominated by an assemblage of tubes of uncertain affinities, notably of anabaritids and by protoconodonts of the genus *Protohertzina* and sponge spicules and ctenophores, which has been named 'tube world' (Budd & Jackson 2016). Then, various cap-shaped fossils including the 'scaly' shells *Purella* and *Maikhanella*, halkieriids and many other taxa dominate the upper half of the Fortunian in the 'sclerite world'. In Cambrian Stage 2, the assemblages are dominated by brachiopods ('brachiopod world') and hyolithids, and by archaeocyaths with associated fauna in reef settings (Budd & Jackson 2016). The Cambrian Stage 3 is marked by the appearance and rapid diversification of trilobites ('trilobite world'; Budd & Jackson 2016). This pattern is deduced from global data on the early Cambrian at the time of writing and is expected to change with additional information. Our work on the SSFs of northern Iran provides new data to review these faunal sequences. No terminal Ediacaran tubes were recovered in this study. From this work, it appears that most of the Fortunian of northern Iran records what we have described as the first microfaunal assemblage, which is dominated by tubes of anabaritids (*Anabarites* and *Cambrotubulus*) and the protoconodont *Protohertzina* (Fig. 6), along with a minority of maikhanellids (*Maikhanella* and *Purella*). This is relatively congruent with the interpretations of Li *et al.* (2007), Maloof *et al.* (2010), Porter (2010), Kouchinsky *et al.* (2012) and Zhang *et al.* (2017), although hyoliths and

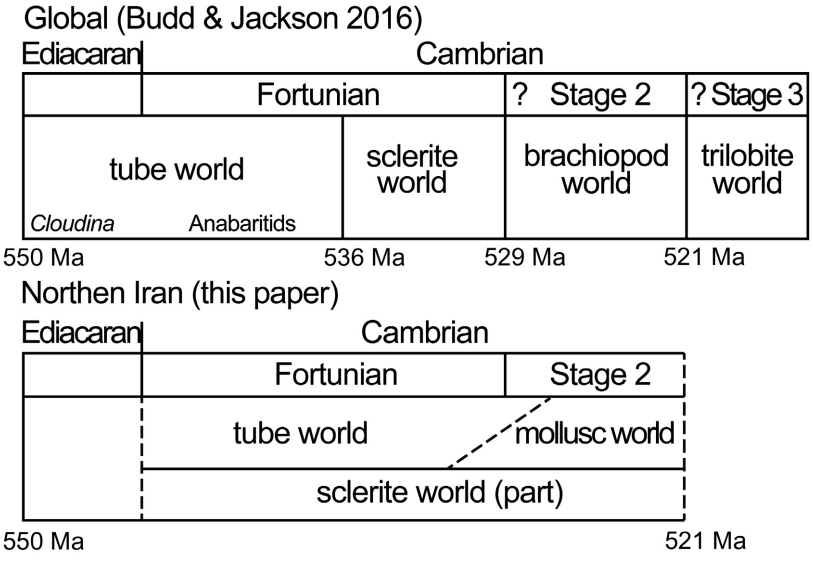

FIG. 6. Sequence of faunal change in the Cambrian based on Budd & Jackson (2016) (above) and this study of small shelly fossils (SSFs) from northern Iran (below).

hyolithelminths are missing from northern Iran. It corresponds to the tube world and part of the sclerite world of Budd & Jackson (2016). Our second assemblage, interpreted as Cambrian Stage 2, is dominated by molluscs in diversity and abundance, and is called the 'mollusc world' (Fig. 6). This sequence, with a delayed appearance of molluscs compared with the assemblage of anabaritids, protoconodonts and sclerites, is similar to the sequence described by Zhang *et al.* (2017) but differs from the interpretations of Li *et al.* (2007), Maloof *et al.* (2010) and Porter (2010), although data on the actual species that these authors consider as molluscs would be necessary for appraisal of the interpretation. The mollusc assemblage was not recognized by Budd & Jackson (2016). In Iran the siphogonuchitid sclerites also occur in both assemblages, therefore part of the sclerite world of Budd & Jackson (2016) occurs as a background signal during the entire Terreneuvian in northern Iran (Fig. 6). The discrepancies in the sequence of faunal changes for the pre-trilobitic Cambrian demonstrate the necessity to precisely identify the sequence of faunal changes by constructing taxonomically solid databases, first at the regional scale, so that datasets can then be compared between regions to identify a possible global signal, but such a work is beyond the scope of this study.

CONCLUSION

This work on the Soltanieh and Barut Formations of the Soltanieh and Alborz Mountains provides new and revised data on occurrences of SSFs from the lower Cambrian of northern Iran. One part of the study focuses on the novel report of SSFs from the Soltanieh and Barut Formations of the Soltanieh Mountains, and the other part consist of new data used for a revision of work previously conducted in the Soltanieh Formation of the Alborz Mountains for the taxonomy and stratigraphic range of the SSFs (Hamdi 1989, 1995; Hamdi *et al.* 1989). Regarding the results from the SSFs, two distinct microfaunal assemblages are identified in the successions. The first assemblage of SSFs occurs from the upper part of the Chopoghlu Shale Member to the lower part of the Upper Dolomite Member of the Soltanieh Formation in the Soltanieh and Alborz Mountains and is characterized by the dominant anabaritids (*Anabarites trisulcatus*, *A.* ex gr. *trisulcatus*, *A. tristichus*, *A. dalirense*, *Cambrotubulus decurvatus*), protoconodonts (*Protohertzina anabarica* and *P. unguliformis*), maikhanellids (*Maikhanella multa*, *Purella squamulosa* and *Purella* sp.), *Aetholicopalla adnata*, indeterminate cones and irregular tubes. The second assemblage, from the basal part of the Barut Formation, is dominated by molluscs in diversity and abundance (*Oelandiella korobkovi* and various cap-shaped morphotypes). Siphogonuchitid sclerites of *Lomasulcachites macrus*, *Lopochites latazonalis*, *Siphogonuchites triangularis* and two morphotypes of unidentified siphogonuchitid species also occur in both assemblages, and they will be thoroughly described and discussed in a later publication. The two SSF assemblages are characteristic of the Terreneuvian, therefore the interval between the upper part of the Chopoghlu Shale Member and the lower part of the Barut Formation is Terreneuvian in age. This interpretation is partly congruent with the ichnostratigraphy of Shahkarami *et al.* (2017*a*, *b*), which identifies the interval between the Lower Dolomite Member and the middle part of the Upper Shale Member as Fortunian, and the uppermost part of the Upper Shale Member as Cambrian Stage 2–3. In the present study, no SSFs occurring in the Cambrian Stage 3 have been recovered from the Soltanieh and overlying Barut Formations, therefore this result differs completely from the interpretation of Hamdi (1989, 1995) and Hamdi *et al.* (1989), who classified most of the Upper Dolomite Member as corresponding to the Cambrian Stage 3 based solely on the occurrence of one species, the assignment of which is doubtful. Our dataset on the Terreneuvian faunal evolution of northern Iran enables us to discuss the sequence of faunal change for the Ediacaran–Cambrian transition proposed by Li *et al.* (2007), Maloof *et al.* (2010), Porter (2010), Kouchinsky *et al.* (2012), Budd & Jackson (2016) and Zhang *et al.* (2017). The successive Terreneuvian tube, sclerite, and brachiopod worlds of Budd & Jackson (2016) are better represented in northern Iran by successive tube and mollusc worlds, both with a sclerite background.

Institutional abbreviation. USTL, Université de Sciences et Technologie de Lille, France.

SYSTEMATIC PALAEONTOLOGY

by Léa Devaere, Dieter Korn *and* Abbas Ghaderi

Phylum ?CHAETOGNATHA Leuckart, 1854

Class, Order & Family UNCERTAIN

Genus PROTOHERTZINA Missarzhevsky, 1973

Type species. Protohertzina anabarica Missarzhevsky, 1973; Fortunian, mouth of the Kotujkan River, Siberia, Russia.

Diagnosis. See Qian & Bengtson (1989).

Remarks. Part-based taxonomy is applied here for the identification of the spine-shaped phosphatic elements from the Soltanieh Formation. They are assigned to the genus *Protohertzina* because of the laterally slightly compressed spine-shape of the simple elements, which are characteristic for this genus.

Kouchinsky *et al.* (2017) restudied the topotype material of *P. anabarica*, in which the morphological variation led those authors to unify *P. anabarica*-type elements or *P. unguliformis*-type elements under the species *P. anabarica*. However, in the Iranian material, specimens assigned to *P. anabarica* and *P. unguliformis* described below are clearly different and are characterized by very distinct morphologies without any continuous morphological transition; this does not support an amalgamation of *P. anabarica*-type and *P. unguliformis*-type elements under the species *P. anabarica* in a context of part-based taxonomy. They might represent different elements from the same apparatus but it is not possible to confirm this in the absence of articulated apparatus and/or statistical analysis of the distribution of both morphological groups. Also, *P. anabarica* and *P. unguliformis* do not necessarily co-occur in all of the samples: they co-occur only in six samples, whereas *P. unguliformis* occurs alone in eight samples and *P. anabarica* in one sample. The two distinct morphological groups from the Alborz Mountains are therefore assigned to two different species.

Protohertzina anabarica Missarzhevsky, 1973
Figure 7A–J

1973 *Protohertzina anabarica* Missarzhevsky; pp 54–55, figs 1–3, pl. 9 figs 1, 2, 4, 6.
1977 *Protohertzina robusta* Qian; p. 268, pl. 2 figs 13–14.
1977 *Protohertzina anabarica* Missarzhevsky; Qian, p. 267–268, pl. 2 figs 7, 8, 11, 12.
1979 *Protohertzina anabarica* Missarzhevsky; Qian *et al.*, pl. 4 figs 3–4.
1980 *Protohertzina* cf. *anabarica*; Conway Morris & Fritz, fig. 3a–c.
1981 *Protohertzina anabarica* Missarzhevsky; Missarzhevsky & Mambetov, fig. 16.9.
1983 *Protohertzina anabarica* Missarzhevsky; Azmi, pl. 5 figs 1–2, 14, pl. 6 figs 1, 6, 8.
1983 *Protohertzina unguliformis* Missarzhevsky; Azmi, p. 384, pl. 5 figs 3, 4, 11–13.
1984 *Hastina quadrigoniata* Yang & He; p. 38–39, pl. 2 figs 4–5.
1984 *Protohertzina robusta* Qian; Chen, pl. 1 fig. 13.
1984 *Protohertzina anabarica* Missarzhevsky; Xing *et al.*, pl. 3 figs 24–25.
1984 *Protohertzina anabarica* Missarzhevsky; Xing *et al.*, pl. 14 figs 12–13.
?1984 *Protohertzina anabarica* Missarzhevsky; Luo *et al.*, pl. 7 figs 6, 6a.
1984 *Protohertzina dabashanensis* Yang & He; p. 41, pl. 2 figs 1–3.
1985 *Protohertzina anabarica* Missarzhevsky; Nowlan *et al.*, p. 245, fig. 8A–F.
?1985 *Protohertzina* sp. B; Nowlan *et al.*, p. 246, pl. 9.
1987 *Protohertzina anabarica* Missarzhevsky; Brasier & Singh, p. 333–334, figs 5.1–8, 14–16, 21–22, 24–25.
?1988 *Protohertzina unguliformis* Missarzhevsky; Mambetov, p. 152, fig. a.
1989 *Protohertzina anabarica* Missarzhevsky; Hamdi, pl. 1 figs 3, 6–7.
1989 *Protohertzina robusta* Qian; Hamdi, pl. 2 figs 4–8.
1989 *Protohertzina anabarica* Missarzhevsky; Qian, pp 212–213, pl. 47 figs 1–2, pl. 53 figs 1–5, pl. 86 figs 5, 6.
1989 *Protohertzina anabarica* Missarzhevsky; Qian & Bengtson, pp 68–69, fig. 40.
?1989 *Protohertzina anabarica* Missarzhevsky; Landing *et al.*, p. 765, fig. 7.2.
?1991 *Protohertzina anabarica* Missarzhevsky; Bhatt, fig. 4A.
1995 *Protohertzina* cf. *anabarica* Missarzhevsky; Hamdi, pl. 5 figs 17–18.
1996 *Protohertzina anabarica* Missarzhevsky; Esakova & Zhegallo, p. 99, pl. 4, fig. 1.
2004 *Protohertzina anabarica* Missarzhevsky; Azmi & Paul, fig. 3f.
2004 *Protohertzina anabarica* Missarzhevsky; Steiner *et al.*, fig. 3.8.
2006 *Protohertzina anabarica* Missarzhevsky; Pyle *et al.*, p. 316 figs 6.5–6.8.
2007 *Protohertzina anabarica* Missarzhevsky; Steiner *et al.*, fig. 4A.
?2014 *Protohertzina anabarica* Missarzhevsky; Guo *et al.*, figs 2g–h, $5n_1$–n_2.
2014*a* *Protohertzina anabarica* Missarzhevsky; Yang *et al.*, fig. 12A–B.
2016 *Protohertzina anabarica* Missarzhevsky; Yang *et al.*, fig. 7K.
2017 *Protohertzina unguliformis* Missarzhevsky; Kouchinsky *et al.*, p. 396–400, fig. 57H–J.

Diagnosis. See Qian & Bengtson (1989).

Material. 30 complete or broken elements including the figured specimens USTL3198-6, USTL3200-1 and USTL3223-7.

Preservation. Almost complete elements preserved as phosphatic walls with internal cavity partially filled with phosphatized material (Fig. 7A–F) or as phosphatized internal moulds broken at the base (Fig. 7G–J).

Description. The generally complete elements are robust, spine-shaped, bilaterally symmetrical (Fig. 7A, G, J) with a height between 1.465 and 2.635 mm. A moderate lateral compression and gentle (Fig. 7I) to strong (up to 56°; Fig. 7B) curvature occurs in the median plane (=plane of bilateral symmetry); the apical part has a slight curvature, while the maximum curvature can be seen at the base (Fig. 7B–E). The apex has a sharp angle of divergence of *c.* 9° (between 7° and 11°; Fig. 7A, G, J) and a circular cross-section. The base is flared with a semi-circular cross-section elongated in the plane perpendicular to the median plane (Fig. 7D). Apertural width (W, distance between the opposite lateral ridges at the aperture): *c.* 640 μm; apertural length (L, distance between the convex and planar sides at the aperture): *c.* 410 μm; W/L, *c.* 1.55. The cross-section of the elements is semi-circular due to the presence of two sides differentiated at one-third of the height below the apex: one rounded,

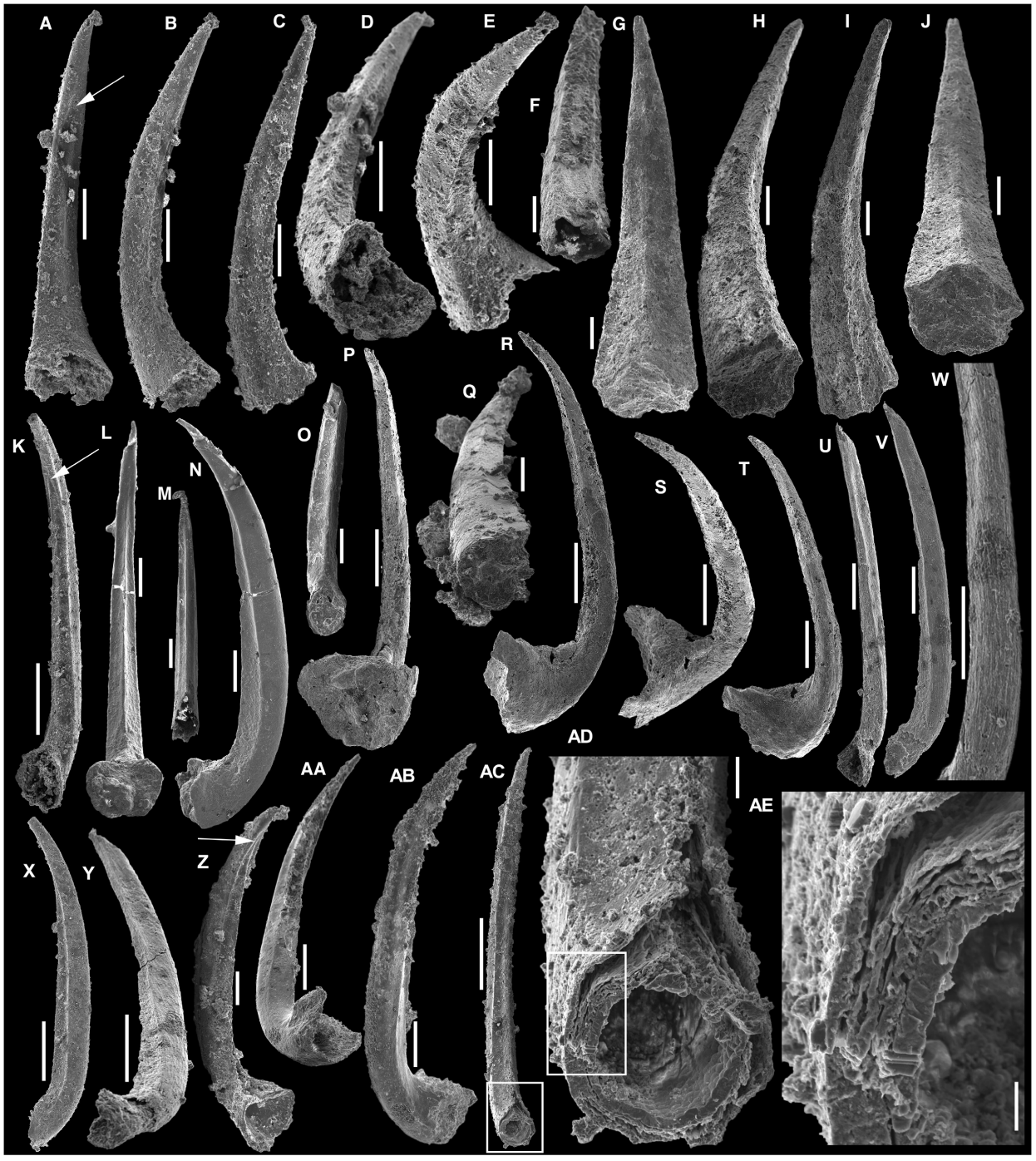

FIG. 7. *Protohertzina* Missarzhevsky, 1973, from the Soltanieh Formation of the Alborz and Soltanieh Mountains, Iran. A–J, *Protohertzina anabarica* Missarzhevsky, 1973: A–E, USTL3223-7; F, USTL3198-6; G–J, USTL3200-1. K–AE, *Protohertzina unguliformis* Missarzhevsky, 1973: K, X, USTL3224-5; L, N, USTL3202-1; M, USTL3201-10; O, USTL3211-4; Q, USTL3199-2; P, R–T, USTL3205-1; U–W, Y, USTL3222-2; Z, USTL3224-3; AA–AB, USTL3201-2; AC–AE, USTL3224-1. Scale bars represent: 200 μm (A–J, L–O, U–AB); 500 μm (K, P, R–T, AC); 100 μm (Q); 50 μm (AD); 20 μm (AE).

smooth, convex side is opposite one relatively planar side with a weakly defined median ridge. The two sides are separated by well-defined, prominent lateral ridges arranged at a right angle (Fig. 7B, D, E, I). Lateral ridges appear at the apex and are first marked by a triangular area (arrow in Fig. 7A). When the shell is preserved, its thickness is *c.* 35 μm (Fig. 7D).

Remarks. The Iranian specimens described here are assigned to *P. anabarica* because of the absence of a median keel and the absence of a lateral depression, both of which are typical of *P. yudomica* Demidenko, 2006. They differ from *P. biformis* Qian, 1989 and *P. dabashanensis* Yang & He, 1984 by the stronger lateral compression, and from *P. siciformis* Missarzhevsky, 1973 by the weaker lateral compression. The present specimens share most morphological characters with *P. unguliformis* Missarzhevsky, 1973. However, they can be separated from *P. unguliformis* by the weaker lateral compression, the well-defined, non-merging, prominent lateral ridges that separate the broader convex side from the planar sides, and by the more continuous transition between the adapical part and the base.

Distribution. Terreneuvian, Soltanieh Formation, Iran: samples D2, D4, D6, D7 and D10 of the Dalir section and samples V13 and V20 of the Valiabad section, Alborz Mountains; samples CH109, CH68, CH69 and CH70 of the SE Chopoghlu section, Soltanieh Mountains.

Protohertzina unguliformis Missarzhevsky, 1973
Figure 7K–AE

1973 *Protohertzina unguliformis* Missarzhevsky; p. 55, text-figs 4, 5, pl. 9 fig. 3.
1975 *Protohertzina unguliformis* Missarzhevsky; Matthews & Missarzhevsky, pl. 3, figs 5, 6.
1977 *Protohertzina unguliformis* Missarzhevsky; Bengtson, fig. 9.
1977 *Protohertzina anabarica* Missarzhevsky; Qian, p. 267–268, pl. 2 figs 9–10.
1979 *Protohertzina anabarica* Missarzhevsky; Qian *et al.*, pl. 4 figs 2, 5–6.
1982 *Emeidus primitivus* Chen; p. 258, pl. 1, fig. 35.
1983 *Protohertzina unguliformis* Missarzhevsky; Azmi, p. 384, pl. 5 figs 3, 4, 11–13.
1983 *Protohertzina unguliformis* Missarzhevsky; Azmi & Pancholi, p. 367, pl. 1 figs 9, 10, 13.
1983 *Protohertzina unguliformis* Missarzhevsky; Bengtson, p. 8, figs 1a–1e.
1983 *Hastina bialata* Yang *et al.*; pl. 2, figs 7–9.
1984 *Protohertzina unguliformis* Missarzhevsky; Qian & Yin, p. 112, pl. 5 figs 6, 7.
1984 *Protohertzina unguliformis* Missarzhevsky; Wang *et al.*, pl. 5 figs 4a, 4b.
1984 *Protohertzina anabarica* Missarzhevsky; Xing *et al.*, pl. 21 fig. 2, pl. 28 fig. 16.
1984 *Hastina bialata* Yang & He; p. 39, pl. 2 figs 14–21.
1985 *Protohertzina unguliformis* Missarzhevsky; Nowlan *et al.*, p. 245, fig. 8g–k.
1987 *Protohertzina anabarica* Missarzhevsky; Brasier & Singh, figs 5, 9, 10–13, 19–20, 23, 26–28.
1989 *Protohertzina unguliformis* Missarzhevsky; Hamdi, pl. 1 figs 1–2.
1989 *Protohertzina* cf. *unguliformis*; Hamdi, pl. 1 fig. 10, pl. 3 fig. 1.
1989 *Protohertzina* cf. *siciformis*; Hamdi, pl. 5 figs 11–13.
1989 *Hastina* sp.; Hamdi, pl. 1 figs 4–5.
1989 *Protohertzina anabarica* Missarzhevsky; Hamdi *et al.*, fig. 3g.
1989 *Protohertzina unguliformis* Missarzhevsky; Missarzhevsky, pl. 25 fig. 1.
1989 *Protohertzina unguliformis* Missarzhevsky; Qian, p. 213, pl. 53 figs 6–13, pl. 58 figs 8, 9.
1989 *Protohertzina unguliformis* Missarzhevsky; Qian & Bengtson, p. 69, text-figs 41, 42.
1995 *Protohertzina unguliformis* Missarzhevsky; Hamdi, pl. 5 figs 7–10.
1996 *Protohertzina unguliformis* Missarzhevsky; Esakova & Zhegallo, p. 100, pl. 4 figs 2, 3.
2004 *Protohertzina anabarica* Missarzhevsky; Azmi & Paul, fig. 3d, e.
2004 *Protohertzina unguliformis* Missarzhevsky; Qian *et al.*, fig. 1 F, K.
2004 *Protohertzina anabarica* Missarzhevsky; Steiner *et al.*, figs 3.11–12, 6.11, 8.11.
2007 *Protohertzina unguliformis* Missarzhevsky; Steiner *et al.*, fig. 4B.
2010 *Protohertzina unguliformis* Missarzhevsky; Parkhaev & Demidenko, p. 927, pl. 29 figs 2, 3.
2012 *Protohertzina unguliformis* Missarzhevsky; Tashayoee *et al.*, pl. 1, fig. 7.
?2012 *Protohertzina siciformis* Missarzhevsky; Tashayoee *et al.*, pl. 2, fig. 4.
2014 *Protohertzina anabarica* Missarzhevsky; Guo *et al.*, figs 2d–f, 5p.
2014*a* *Protohertzina anabarica* Missarzhevsky; Yang *et al.*, fig. 12C.
2014*b* *Protohertzina anabarica* Missarzhevsky; Yang *et al.*, fig. 2O–P.
2016 *Protohertzina unguliformis* Missarzhevsky; Budd & Jackson, fig. 6a.
2016 *Protohertzina anabarica* Missarzhevsky; Yang *et al.*, fig. 7I–J.
2017 *Protohertzina unguliformis* Missarzhevsky; Kouchinsky *et al.*, pp 396–400, fig. 57A–G, K.

Diagnosis. See Qian & Bengtson (1989).

Material. 215 complete or fragmentary elements including the figured specimens USTL3199-2 and USTL3201-2, 3201-10, 3202-1, 3205-1, 3211-4 and USTL3222-2, 3224-1, 3224-3, 3224-5.

Preservation. The elements are almost complete and preserved as phosphatic walls with an internal cavity that is partially filled with phosphatized material (Fig. 7K, M, U–AE) or as phosphatized internal moulds (Fig. 7L, N–T).

Description. The spine-shaped, bilaterally symmetrical elements (Fig. 7L, P, AC) range in height from 1.565 to 3.645 mm. They are slender with strong lateral compression and strongly curved in the median plane (up to 90°; Fig. 7N, R, T, V, X–AB). Apical part with moderate curvature, maximum curvature at the base. Sharp apex with angle of divergence of *c.* 3° with a range from 1.6° to 6° (Fig. 7L, P, AC) and a circular cross-section. Flared base with nearly heart-shaped cross-section elongated in the plane perpendicular to the median plane (Fig. 7L, P, Z, AA). Apertural width, *c.* 485 μm; apertural length, *c.* 410 μm; W/L, *c.* 1.18. The shape of the cross-section of the abapical part of the element is due to presence of two sides differentiated very shortly after the apex

(Fig. 7O, Q, AC, AD): one rounded, convex side with a faint median ridge (Fig. 7T, AB) opposite one subdivided by a prominent median ridge into two planar to concave surfaces (Fig. 7L, M, O, P, AC). The two sides are separated by well-defined lateral ridges (Fig. 7N, R, U, V, X–AC) that appear around the apex and are first marked by a triangular area (arrow in Fig. 7K, Z). The wall of thickness *c.* 30 μm is, when preserved, composed of multiple layers of 2–11 μm in thickness (Fig. 7AC–AE). The external surface of the wall layers is composed of longitudinally oriented fibres (Fig. 7V–W).

Remarks. The Iranian specimens are assigned to *Protohertzina unguliformis* because of the absence of a median keel and a lateral depression, which are characteristic of *P. yudomica* Demidenko, 2006. They differ in the degree of lateral compression from *P. biformis* Qian, 1989 and *P. dabashanensis* Yang & He, 1984 (stronger compression) as well as from *P. siciformis* Missarzhevsky, 1973 (weaker compression). The specimens from Iran are morphologically most similar to *P. anabarica* (for separating characters, see discussion for this species above).

Distribution. Terreneuvian, Soltanieh Formation, Iran: samples D2, D4, D6, D7, D9a, D10, D13, D16 and D17 of the Dalir section and samples V9, V12, V13, V14 and V17 of the Valiabad section, Alborz Mountains; samples CH109, CH111, CH114, CH68 and CH69 of the SE Chopoghlu section, Soltanieh Mountains.

Phylum ?CNIDARIA Hatschek, 1888
Class & order UNCERTAIN
Family ANABARITIDAE Missarzhevsky, 1974
Genus ANABARITES Missarzhevsky *in* Voronova & Missarzhevsky, 1969

Type species. Anabarites trisulcatus Missarzhevsky *in* Voronova & Missarzhevsky, 1969; Fortunian, mouth of the Kotujkan River, Anabar Uplift, Siberia, Russia.

Diagnosis. See Kouchinsky *et al.* (2009).

Anabarites tristichus Missarzhevsky *in* Rozanov *et al.*, 1969
Figure 8

1965 *Hyolithellus* sp. Sysoev, p. 13, fig. 2.
1967 *Anabarites tristichus* Missarzhevsky; p. 20 [*nomen nudum*].
1969 *Anabarites tristichus* Missarzhevsky; Rozanov *et al.*, pp 156–157, pl. 8 figs 1, 14, 19.
1975 *Jakutiochrea tristicha* (Missarzhevsky); Val'kov, pl. 13 fig. 9.
1975 *Anabarites tristichus* Missarzhevsky; Matthews & Missarzhevsky, pl. 2 fig. 8.
1982 *Jakutiochrea* sp.; Val'kov, p. 78–79, pl. 13 fig. 20.
1982 *Jakutiochrea tristicha* (Missarzhevsky); Val'kov, pl. 13 figs 17–19.
1983 *Anabarites tristichus* Missarzhevsky; Sokolov & Zhuravleva, p. 160, pl. 51 fig. 2.
1984 *Anabarites gracilis* Chen; p. 62, pl. 1 fig. 9.
1987 *Jakutiochrea solita* Val'kov; pp 111–112, pl. 14 figs 1–5.
1987 *Jakutiochrea lenta* Val'kov; p. 114, pl. 14 figs 7–8.
?1987 *Jakutiochrea portentosa* Val'kov; p. 113, pl. 14 fig. 6.
1989 *Anabarites trisulcatus* Missarzhevsky; Brasier, pl. 7.4 fig. 9.
1989 *Anabarites trisulcatus* Missarzhevsky; Hamdi, pl. 4, figs 4–5, 7
1989 *Anabarites tristichus* Missarzhevsky; Khomentovsky & Karlova, p. 56, pl. 6 fig. 4.
1989 *Jacutiochrea tristicha* (Missarzhevsky); Missarzhevsky, pl. 13 figs 3, 16–17.
2002 *Jacutiochrea tristicha* (Missarzhevsky); Kouchinsky & Bengtson, figs 2–5.
2009 *Anabarites tristichus* Missarzhevsky; Kouchinsky *et al.*, pp 273–274, figs 26–28.
2012 *Jakutiochrea lenta* Mokova &Valko; Tashayoee *et al.*, pl. 1 fig. 6.
2017 *Anabarites tristichus* Missarzhevsky; Kouchinsky *et al.*, pp 420, fig. 76A–C, F.

Diagnosis. See Kouchinsky *et al.* (2009).

Material. 39 specimens including the figured material USTL3206-6, 3207-2, 3211-5, 3213-2, 3216-5 and USTL3220-7, 3220-8, 3224-2, 3225-10.

Preservation. The tubes are preserved as a thin phosphatic internal coating (*c.* 22 μm in thickness) partially or completely filled with phosphatic material (Fig. 8L–N, T, AC, AF) or as multiple-layered, thick phosphatic internal coating with individual layers from 3 to 46 μm in thickness for a total thickness of up to *c.* 58 μm, but without internal filling (Fig. 8C, D, H, I, L, Q, Z, AA). Internal surface of internal coating made of contiguous spherical phosphatic structures (Fig. 8O, AA). Simple, coarse internal phosphatic mould may also be present (Fig. 8A, E, K, Y, AG, AH). Different preservations may possibly be combined in the same specimen (Fig. 8A–E, H, I).

Description. The fragmentary tubes are open at both ends and have a length of between 0.995 and 4.360 mm, and are slightly (Fig. 8W, X, AC–AE) to relatively strongly (Fig. 8F, J–L, U, Y, AG, AH) irregularly helically curved. The cross-section is distinctly trilobate along the entire length and gives the specimens a triradial symmetry (Fig. 8A, D, E, H, L–N, Q, Y–AA, AC, AF). The diameter of the cross-section increases slowly and gradually towards the aperture (angle of divergence *c.* 2.50°). The apertural diameter varies between *c.* 190 and *c.* 470 μm. The trilobate cross-section is caused by equidistant longitudinal depressions (Fig. 8A–G, J–M, Q–T, V–Z, AC–AH) that vary from circular (diameter *c.* 20 μm; Fig. 8G, P, U) to elongated notches (length up to *c.* 60 μm; Fig. 8AB, AH, AI) that run along the length of the tube in a groove. The distance between notches ranges from 115 to 215 μm. Transverse striations on the external surface of

internal coatings and moulds are smooth, irregular, fine and packed (Fig. 8AB), or thick and distant (Fig. 8A–E), or absent (Fig. 8G, J–L, V–Z, AC–AG).

Remarks. The Iranian specimens have the typical triradial symmetry of *Anabarites* and are assigned to *A. tristichus* because of the presence of three chains of notches. These are situated in the grooves that separate the lobes and are only found in this species. Notches are also diagnostic of *Anabarites valkovi* (Bokova *in* Bokova & Vasil'eva, 1990), but in that species they are aligned longitudinally in the middle part of the three lobes, rather than in the grooves separating the lobes as in *A. tristichus*.

Distribution. Terreneuvian, Soltanieh Formation, Iran: samples D9a, D10, D13, D14 and D16 of the Dalir section and samples V9, V11, V12, V13 and V14 of the Valiabad section, Alborz Mountains.

Anabarites trisulcatus Missarzhevsky *in* Voronova & Missarzhevsky, 1969
Figure 9

1967 *Anabarites trisulcatus* Missarzhevsky; 20 [*nomen nudum*].
1969 *Anabarites trisulcatus* Missarzhevsky; Voronova & Missarzhevsky, p. 209, pl. 1 figs 8–9.
1969 *Anabarites trisulcatus* Missarzhevsky; Rozanov *et al.*, p. 156, pl. 8 fig. 10.
?1970 *Anabarites trisulcatus* Missarzhevsky; Val'kov & Sysoev, p. 97, pl. 1 figs 3–5.
1975 *Anabarites trisulcatus* Missarzhevsky; Matthews & Missarzhevsky, pl. 2 figs 4, 16.
?1975 *Anabarites trisulcatus* Missarzhevsky; Val'kov, pl. 13 figs 3–5.
?1977 *Anabarites rotundum* Qian; p. 260, pl. 1 figs 11–12.
1977 *Anabarites trisulcatus* Qian; p. 259, pl. 1 figs 9–10,18–19.
1978 *Anabarites trisulcatus* Missarzhevsky; Qian, p.15, pl. 3 figs 2–3, 12–13, pl. 4 figs 1–2.
1978 *Anabarites obliquasulcatus* Qian; p. 16, pl. 3 figs 6–8.
1978 *Anabarites sulcoconvex* Qian; p. 16, pl. 3 figs 9–10.
?1978 *Anabarites undulatus* Qian; pp 16–17, pl. 3 fig. 11.
1979 *Anabarites trisulcatus* Missarzhevsky; Qian *et al.*, pl. 2 figs 6–7.
?1981 *Anabarites signatus* Missarzhevsky & Mambetov; p. 73, pl. 3 figs 11, 17, 18.
1982 *Anabarites trisulcatus* Missarzhevsky; Val'kov, p. 74, pl. 11 figs 15–17.
1982 *Anabarites trisulcatus* Missarzhevsky; Luo *et al.*, p. 171, pl. 14 figs 7,9.
1982 *Anabarites primitivus* Qian & Jiang; Luo *et al.*, p. 172, pl. 14 fig. 10.
?1982 *Anabarites grandis* Val'kov; pp 74–75, pl. 11 fig. 18.
?1984 *Anabarites trisulcatus* Missarzhevsky; Chen, p. 54, pl. 1 fig. 18.
?1984 *Anabarites* cf. *trisulcatus*; Chen, pp 54–55, pl. 1 figs 19–20.
1985 *Anabarites trisulcatus* Missarzhevsky; Nowlan *et al.*, p. 242, fig. 6.
?1989 *Anabarites rotundus* Qian; Conway Morris & Chen, pp 620–628, figs 6–9, 12a, b.
?1989 *Anabarites sulcatus* (Bokova); Qian, p. 146, pl. 23, figs 10–15.
1989 *Anabarites sulcoconvex* Qian; Qian, p. 147, pl. 23 figs 3–9.
1989 *Anabarites tenuistriatus* Qian; p. 145, pl. 23 figs 1–2.
?1989 *Anabarites trisulcatus* Missarzhevsky; Qian, p. 147, pl. 23, figs 16–19, pl. 24 figs 1–4.
1989 *Anabarites trisulcatus* Missarzhevsky; Qian & Bengtson, pp 125–127, fig. 84.
1989 *Anabarites trisulcatus* Missarzhevsky; Conway Morris & Chen, pp 628–629, fig. 12c–k.
1989 *Anabarites trisulcatus* Missarzhevsky; Missarzhevsky, pl. 13 fig. 19, pl. 14 figs 1, 3–4.
1989 *Anabarites trisulcatus* Missarzhevsky; Hamdi *et al.*, fig. 3h.
1991 *Anabarites trisulcatus* Missarzhevsky; Khomentovsky & Karlova, pl. 1 fig. 2.
1991 *Anabarites valkovi* Fedorov; Khomentovsky & Karlova, pl. 1 fig. 1.
1995 *Anabarites trisulcatus* Missarzhevsky; Hamdi, pl. 5 figs 1–6, pl. 10 figs 5–7.
2002 *Anabarites trisulcatus* Missarzhevsky; Qian *et al.*, text-fig. 4.15–16.
2004 *Anabarites trisulcatus* Missarzhevsky; Steiner *et al.*, fig. 3.14.
2004 *Anabarites trisulcatus* form *sulcoconvex*; Steiner *et al.*, fig. 3.15.
2004 *Anabarites trisulcatus* form *obliquasulcatus*; Steiner *et al.*, fig. 3.16.
2005 *Anabarites* Missarzhevsky; Chen & Peng, figs 3, 4.
2005 *Anabarites rotundus* Qian; Feng, fig. 2A, B.
2005 *Anabarites trisulcatus* Missarzhevsky; Feng, fig. 2C, D.
?2005 *Anabarites* sp.; Feng, fig. 2E–H.
2006 *Anabarites trisulcatus* Missarzhevsky; Pyle *et al.*, p. 815 fig. 6.1–4.
2007 *Anabarites trisulcatus* Missarzhevsky; Steiner *et al.*, fig. 2D, E, F, I.
2009 *Anabarites trisulcatus* Missarzhevsky; Kouchinsky *et al.*, pp 255–258, figs 6, 7A–E, 11A–V, 12D.
2010 *Anabarites trisulcatus* Missarzhevsky; Rozanov *et al.*, p. 85, pl. 53 figs 6, 7.
2012 *Anabarites lutus* Val'kov & Sysoev; Tashayoee *et al.*, pl. 1 fig. 5.
2012 *Anabarites tripartitus* Missarzhevsky *in* Rozanov *et al.*; Tashayoee *et al.*, pl. 2 fig. 3.
2014 *Anabarites trisulcatus* Missarzhevsky; Guo *et al.*, figs 2i–j, 4o–p.
2015 *Anabarites trisulcatus* Missarzhevsky; Kouchinsky *et al.*, p. 499, fig. 69A, E.
2017 *Anabarites trisulcatus* Missarzhevsky; Kouchinsky *et al.*, pp 417–419, fig. 74A–F, H, I, K.

Diagnosis. See Kouchinsky *et al.* (2009).

Material. Several thousands of complete and fragmentary specimens including the figured material USTL3203-1, 3204-4,

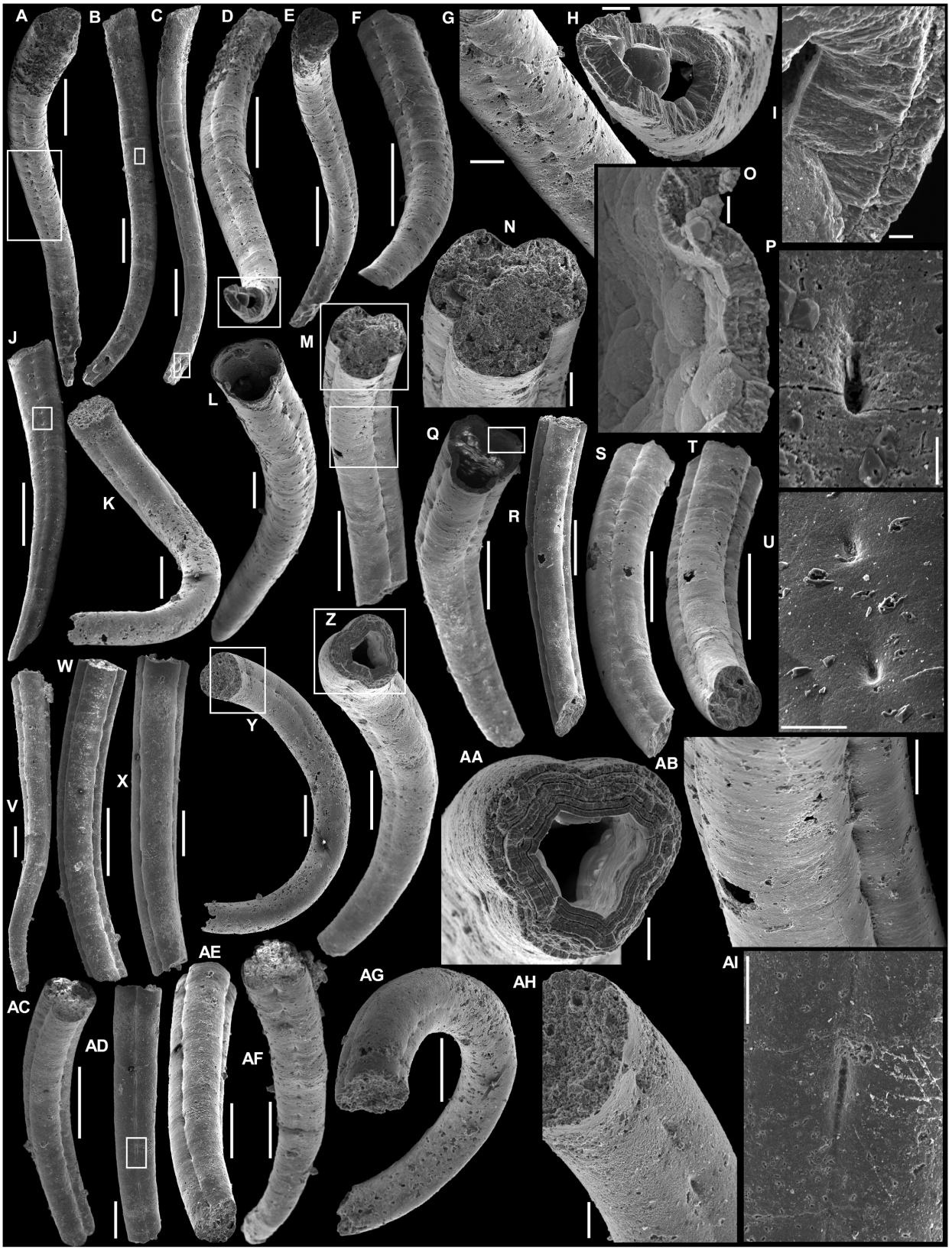
A
B
C
D
E
F
G
H
I
J
K
L
M
N
O
P
Q
R
S
T
U
V
W
X
Y
Z
AA
AB
AC
AD
AE
AF
AG
AH
AI

FIG. 8. *Anabarites tristichus* Missarzhevsky *in* Rozanov *et al.*, 1969, from the Soltanieh Formation at Dalir and Valiabad, Alborz Mountains, Iran. A–E, G–I, P, USTL3206-6: A, lateral view, outline area magnified in G to show notches in the longitudinal depression; B, lateral view, outlined area magnified in P to show detail of notch; C, lateral view, outlined area magnified in I to show microstructure of internal coating; D, adapical view, outlined area magnified in H to show cross-section of internal coating; E, lateral view. F, J, L, U, USTL3207-2: F, adapical view; J, lateral view, outlined area magnified in U to show notches in the longitudinal depression; L, apertural view. M, N, R–T, AB, USTL3213-2: M, apertural view, upper outlined area magnified in N to show the trilobate apertural cross-section, and lower outlined area magnified in AB to show details of a lobe and longitudinal depression with notches; R–S, lateral views; T, adapical view. O, Q, USTL3225-10: Q, apertural view, outlined area magnified in O to show details of the internal coating. K, Y, AG, AH, USTL3224-2: K, lateral view; Y, apertural view, outlined area magnified in AH; AG upper view. V, AF, USTL3220-8: V, lateral; AF, apertural view. W, AC, USTL3220-7: W, lateral; AC, apertural view. X, AD, AE, AI, USTL3216-5: X, lateral view; AD, lateral view, outlined area magnified in AI; AE, adapical view. Z, AA, USTL3211-5: Z, apertural view, outlined area magnified in AA to show the multi-layered internal coating. Scale bars represent: 500 μm (A–F, J, M, R–T, W, AC); 100 μm (G, N, AB); 50 μm (H, U, AA, AH, AI); 10 μm (I, O); 200 μm (K, L, Q, V, X–Z, AD–AG); 20 μm (P).

3205-4, 3207-9, 3209-8, 3210-1, 3212-2, 3212-8, 3213-5, 3214-5, 3215-6, and USTL3221-7, 3222-3, 3223-5.

Preservation. The tubes are preserved as coarse phosphatic internal moulds with a fine outer surface reproducing the internal surface of the tube in detail (Fig. 9A–H, I–K, O–S) or with thin phosphatic internal coating of a thickness between 4 and 44 μm (Fig. 9X–AJ). Rare specimens are preserved with thin internal coating and coarse phosphatic material made of botryoidal amalgamation of coccoidal pseudomorphs within the internal cavity (Fig. 9T, X–AB, AF–AH). One specimen possesses a coarse phosphatic replacement of the wall (Fig. 9L, M).

Description. Complete and fragmented tubes are open at both ends (originally or by fragmentation) with a length of between 0.765 and 5.325 mm. The tubes are relatively straight (Fig. 9B, C, E, F), undulating (Fig. 9A, D, I, L, M, R, S), curved (Fig. 9J, K, O–Q) or strongly helically curved (Fig. 9AC–AE, AJ). When the apex is preserved, it is always open, with a circular cross-section (Fig. 9G, V, W); longitudinal furrows, grooves or depressions are absent at the apical part (Fig. 9A, B, G, H, Q, R, V, W). In one specimen, the apical part is angled from the abapical part of the tube (Fig. 9H, J, K), otherwise progressive transition occurs from the apical to the abapical part of the tube with a rapid increase in diameter (Fig. 9G, V, W). The cross-section of the abapical part of the tube is slightly trilobate along the entire length, giving the specimens a triradial symmetry (Fig. 9C, F, J, Q, S, U). The apertural diameter varies between *c.* 155 and *c.* 963 μm. The diameter of the cross-section increases slightly and gradually towards the aperture (angle of divergence, *c.* 4°). The trilobate cross-section is caused by equidistant shallow, wide and not well-delimited longitudinal depressions (Fig. 9A–E, I–P, R–T, X, Z, AC–AI). Transverse striations may occur on the external surface of internal coatings and moulds; they are irregular, indistinct, coarse and distant (Fig. 9I, N, S, AC, AI), and often absent (Fig. 9A–E, J, K, O–R, T, AC–AE, AJ).

Remarks. The specimens from the Alborz Mountains have the typical triradial symmetry of *Anabarites*, and are assigned to *A. trisulcatus* because they possess the slowly expanding general shape of the tubes, showing three rounded lobes separated by shallow grooves or depressions. The few and barely visible imprints of transverse striations on the internal moulds/coatings do not show a clear curvature towards the aperture in the grooves. However, this character is highly variable in specimens of *A. trisulcatus* (e.g. Kouchinsky *et al.* 2009, figs 6, 7) and is not diagnostic of the species. The coarse phosphatic material in the internal cavity, which consists of a botryoidal amalgamation of coccoidal pseudomorphs, is similar to the preserved digestive tracts of hyoliths (e.g. Devaere *et al.* 2014). However, the preservation in the Iranian anabaritid specimens is too coarse to enable any conclusions to be reached regarding the nature of the structure.

Distribution. Terreneuvian, Soltanieh Formation, Iran: samples D2, D7, D8, D9, D9a, D10, D11, D13, D14, D15, D16, D18, D20, D21 and D22 of the Dalir section and samples V6, V8, V9, V11, V12, V13, V14, V16, V17, V18, V19 and V20 of the Valiabad section, both Alborz Mountains.

Anabarites ex gr. *trisulcatus* Missarzhevsky *in* Voronova & Missarzhevsky, 1969
Figure 10

Material. Complete and fragmented specimens including the figured material USTL3203-2, 3203-7, 3209-2, 3216-8 and USTL3217-3, 3219-1.

Preservation. The tubes are preserved as a phosphatic internal mould with a delicate outer surface reproducing the internal surface of the tube in detail (Fig. 10C, M–N).

Description. Fragmented tubes open at both ends with a length of between 1.315 and 5.335 mm. The tubes are relatively straight (Fig. 10A, I), or slightly curved (Fig. 10H–L) to strongly helically curved (Fig. 10B, D–F). The cross-section is slightly trilobate along the entire length, giving the specimens a triradial symmetry (Fig. 10C, E, H–J, L). Diameter of cross-section slightly and gradually increases towards the aperture (angle of divergence, *c.* 5.5°). Apertural diameter varies between *c.* 287 and *c.* 820 μm. Trilobate cross-section caused by equidistant, shallow, sharp and narrow longitudinal furrows (Fig. 10). Transverse striations on the external surface of internal moulds fine, regular and close (Fig. 10C, M, N) but absent on most specimens (Fig. 10A, B, D–L, O).

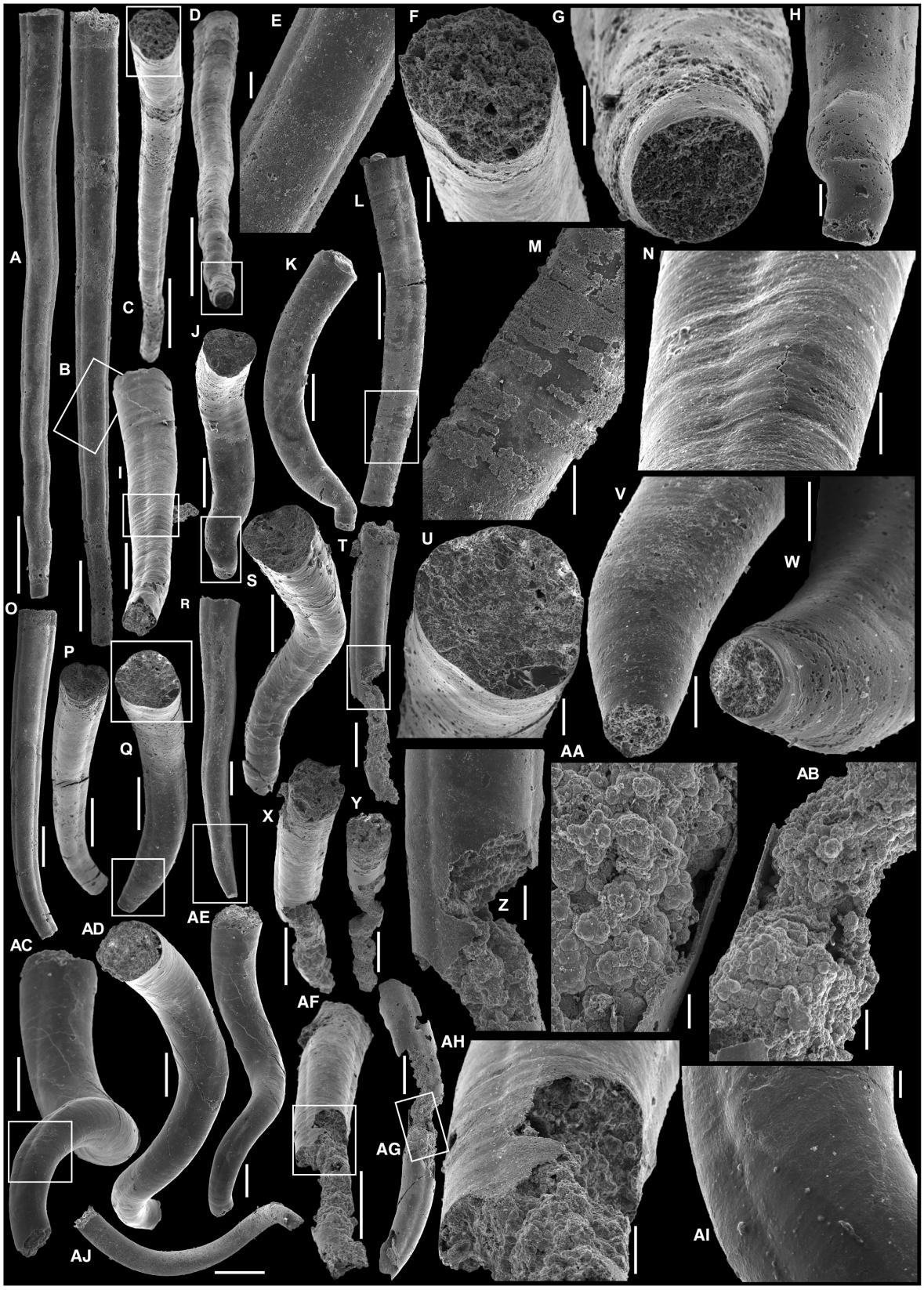
A
B
C
D
E
F
G
H
I
J
K
L
M
N
O
P
Q
R
S
T
U
V
W
X
Y
Z
AA
AB
AC
AD
AE
AF
AG
AH
AI
AJ

FIG. 9. *Anabarites trisulcatus* Missarzhevsky *in* Voronova & Missarzhevsky, 1969, from the Soltanieh Formation at Dalir and Valiabad, Alborz Mountains, Iran. A, D, G, USTL3212-2: A, lateral view; D, adapical view, outlined area magnified in G to show details of the circular apical cross-section. B, C, E, F, USTL3223-5: B, lateral view, outlined area magnified in E to show lobe and longitudinal depressions; C, apertural view, outlined area magnified in F to show the trilobate apertural cross-section. H, J, K, USTL3209-8: J, apertural view, outlined area magnified in H to show detail of the apex; K, lateral view. I, N, USTL3204-4: I, adapical view, outlined area magnified in N to show transverse striations on external surface of internal coating. L, M, USTL3210-1: L, lateral view, outlined area magnified in M to show phosphatic replacement of tube wall. O, P, USTL3205-4: O, lateral; P, apertural view. Q, U, W, USTL3212-8: Q, apertural view, upper outlined area magnified in U to show the apertural cross-section, and lower outlined area magnified in W to show the circular apical end. R, V, USTL3214-5: R, lateral view, outlined area magnified in V to show detail of the apex. S, USTL3207-9 in apertural view. T, X, Z, AF, AH, USTL3222-3: T, lateral view, outlined area magnified in Z to show phosphatic internal coating and unidentified structure within the internal cavity; X, apertural view; AF, adapical view, outlined area magnified in AH to show coarse internal phosphatic material. Y, USTL3215-6 in apertural view with unidentified phosphatic structure within the internal cavity. AA–AB, AG, USTL3213-5: AA, coarse internal phosphatic material; AG, lateral view, outlined area magnified in AB to show coarse internal phosphatic material. AC–AE, AI, USTL3203-1: AC, adapical view, outlined area magnified in AI to show transverse striations and longitudinal depression; AD, apertural view; AE, lateral view. AJ, USTL3221-7 in lateral view. Scale bars represent: 500 μm (A–D, O, P, T, X, Y, AF, AG, AJ); 50 μm (E, G, H, N, U–W, AA, AI); 100 μm (F, Z, AB, AH); 200 μm (I–K, M, Q–S, AC–AE); 1 mm (L).

Remarks. The Iranian specimens show the typical triradial symmetry of *Anabarites*, and are assigned to *Anabarites* ex gr. *trisulcatus* following Kouchinsky *et al.* (2009). They possess the slowly expanding general shape of *A. trisulcatus*, with the three rounded lobes separated by longitudinal structures. The specimens described above have only some affinities with *A. trisulcatus* given that the structures separating the lobes are very distinct shallow, sharp and narrow furrows and clearly differ from the shallow but wide and not well-delimited depressions typical of *A. trisulcatus*. However, this variation may fall within the limits of the species; the notation 'ex gr.' is used to indicate that the specimens described here might belong to an unresolved species complex as suggested by Kouchinsky *et al.* (2009). The Iranian specimens are similar to *Anabarites* ex gr. *trisulcatus* form 1 of Kouchinsky *et al.* (2009).

Distribution. Terreneuvian, Soltanieh Formation, Iran: samples D2, D7, D9a, D10, D11, D13, D14, D16 and D18 of the Dalir section and samples V8, V9, V13, V14, V16 and V19 of the Valiabad section, Alborz Mountains.

Anabarites dalirense sp. nov.
Figure 11

LSID. urn:lsid:zoobank.org:act:17D9727B-0781-40FA-902A-64EC6EE5A901

Derivation of name. Named after the village of Dalir, which is on the access road to the section.

Holotype. Specimen USTL3213-1, Fig. 11A–E; phosphatic internal coating; Soltanieh Formation, Dalir Section located along the trail to the phosphate mine above the village of Dalir, Alborz Mountains, Iran.

Material. 9 specimens including the figured material USTL3211-7, 3213-1, 3214-8 and 3215-3.

Diagnosis. Species of *Anabarites* with a strongly curved tube forming a ring with a wide central gap. Internal moulds and coatings expressing three slightly rounded lobes separated by shallow, sharp and narrow longitudinal furrows. Low, irregular transverse plications on the external surface of internal coatings and moulds.

Preservation. The tubes are preserved as a thick internal coating that consists of an assemblage of phosphatic spheres (Fig. 11A, E, I) and/or as a coarse phosphatic internal mould with a fine outer surface (Fig. 11F–H, J–P); both preservation modes reproduce the internal surface of the tube in detail.

Description. Fragmentary tubes are open at both ends; they are strongly curved to form a half to a complete ring. Complete rings correspond to a curvature at 360° of the tube in one plan (Fig. 11A–K), with two overlapping extremities (Fig. 11A, E, F–H, J, K). Coiling of the tube is loose and forms a wide central gap with a diameter of between 530 and 665 μm (Fig. 11A, F). Incomplete rings correspond to the breakage of a tube (Fig. 11D) or to a strongly helically curved tube (Fig. 11L–O). The length of tube ranges from 1.870 to 2.345 mm. Apical and apertural extremities are never preserved but the cross-section at one extremity has a smaller diameter than at the other (Fig. 11J, L). The cross-section is oval (Fig. 11J) to slightly trilobate along the entire length and gives the specimens a triradial symmetry (Fig. 11D, L). Three equidistant shallow, sharp and narrow longitudinal furrows are present along the entire length of the tube (Fig. 11A–D, F–H, J–P). Low, irregular transverse plications are visible on the external surface of internal coatings and moulds (Fig. 11C, F–H, P).

Remarks. The triradial symmetry is produced by three furrows that separate the three lobes of the tube; this assigns the specimens to the genus *Anabarites* with certainty. The strong curvature of the tube, forming a loose ring, has never been reported for another species in the genus, and hence a new species is introduced here. Except for the ring shape, other

FIG. 10. *Anabarites* ex gr. *trisulcatus* Missarzhevsky *in* Voronova & Missarzhevsky, 1969, from the Soltanieh Formation at Dalir and Valiabad, Alborz Mountains, Iran. A, I, O, USTL3203-2: A, lateral view, outlined area magnified in O to show sharp longitudinal furrow; I, apertural view. B, D–F, USTL3217-3: B, D, lateral; E, apertural; F, upper view. G, L, USTL3209-2: G, lateral; L, apertural view. H, USTL3216-8 in apertural view. C, M–N, USTL3219-1: C, apertural view, lower outlined area magnified in M, and upper outlined area magnified in N to show transverse striations and longitudinal furrow. J–K, USTL3203-7: J, apertural; K, lateral view. Scale bars represent: 500 μm (A, G, I, L); 200 μm (B, D–F, H, J, K); 1 mm (C); 100 μm (M); 50 μm (N); 20 μm (O).

important characters of the specimens and especially the shallow, sharp and narrow longitudinal furrows are similar to that of *Anabarites* ex gr. *trisulcatus*. Some specimens from Iran assigned to *A*. ex gr. *trisulcatus* have a strong helical curvature (Fig. 10D–F) that tends towards the configuration of *A. dalirense*. This could correspond to variations in the same species. In the absence of the complete sequence of gradual morphological variations, they are considered separate herein. Some other taxa organized as tubes that are curved to form a ring that can be compared to *A. dalirense* are *Spirellus groenlandicus* Peel, 1988, which differs by the presence of multiple superimposed whorls; and *Obruchevella* Reitlinger, 1948, which differs in the helical twisting of whorls of an organic-walled microfossil.

Distribution. Terreneuvian, Soltanieh Formation, Iran: samples D10, D13 and D14 of the Dalir section, Alborz Mountains.

Genus CAMBROTUBULUS Missarzhevsky *in* Rozanov *et al.*, 1969

Type species. Cambrotubulus decurvatus Missarzhevsky *in* Rozanov *et al.*, 1969, Terreneuvian, mouth of the Ary-Mas-Yuryakh Creek, Kotuj River, Siberia, Russia.

Diagnosis. See Kouchinsky *et al.* (2009).

Cambrotubulus decurvatus Missarzhevsky *in* Rozanov *et al.*, 1969

Figure 12

1967 *Cambrotubulus decurvatus* Missarzhevsky; p. 20 [*nomen nudum*].

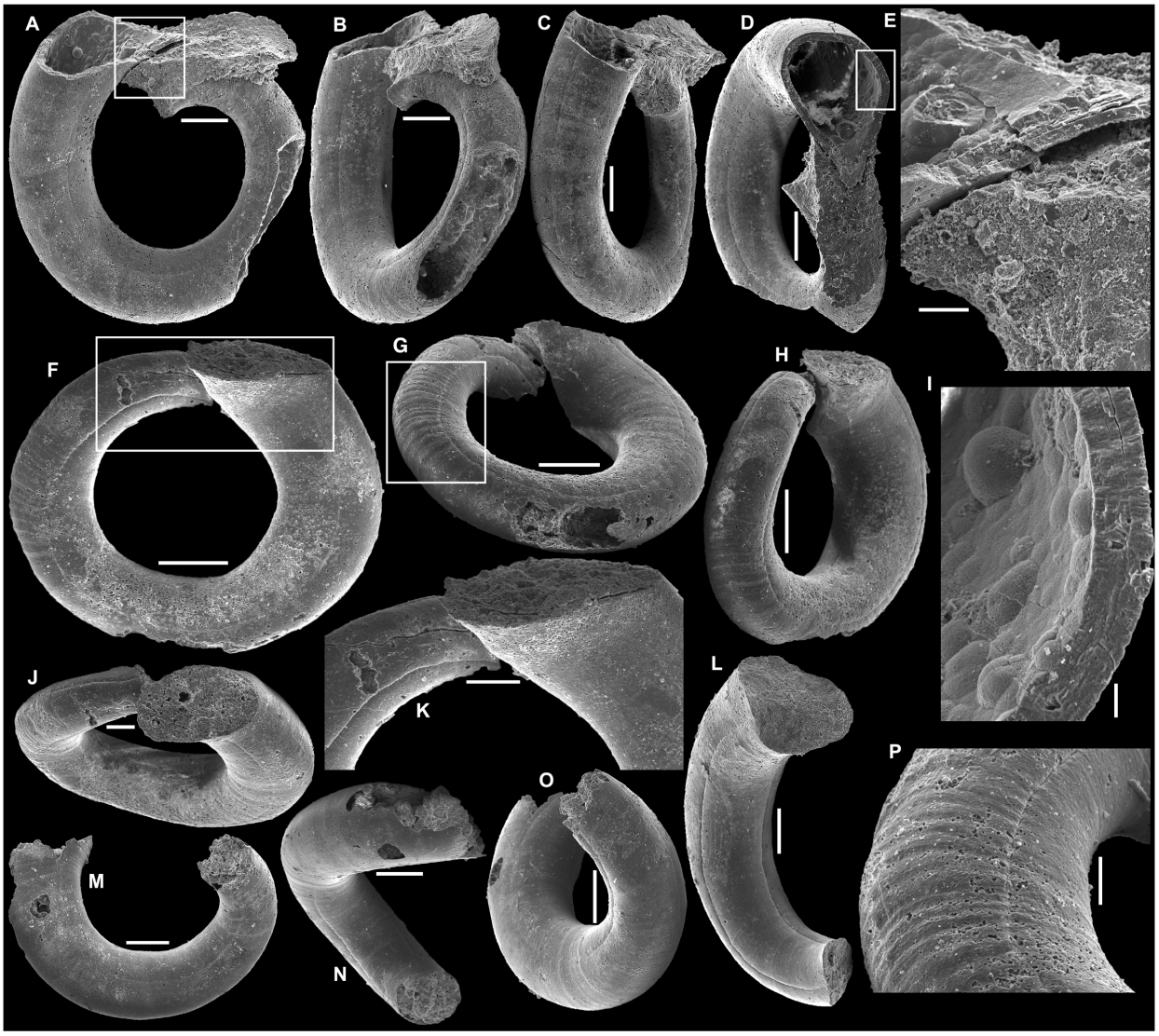

FIG. 11. *Anabarites dalirense* sp. nov. from the Soltanieh Formation at Dalir, Alborz Mountains, Iran. A–E, I, USTL3213-1: A, lateral view, outlined area magnified in E to show detail of internal coating and gap; B–C, lateral views; D, view of the openings, outlined area magnified in I to show detail of internal coating. F–H, J–K, P, USTL3214-8: F, lateral view, outlined area magnified in K to show overlap; G, oblique lateral view, outlined area magnified in P to show transverse folds; H, oblique lateral view; J, view of openings. L, USTLUSTL3211-7 in apertural view. M–O, USTL3215-3: M, lateral; N–O, oblique lateral views. Scale bars represent: 200 μm (A–D, F–H, L–O); 50 μm (E, P); 20 μm (I); 100 μm (J, K).

?1968 *Platysolenites sibirica* Val'kov; pp 116–117, figs 2–5.
1969 *Cambrotubulus decurvatus* Missarzhevsky; Rozanov *et al.*, p. 160, pl. 7 figs 5–7, 10.
1975 *Cambrotubulus decurvatus* Missarzhevsky; Matthews & Missarzhevsky, pl. 2 fig. 6.
?1975 *Cambrotubulus sibiricus* (Val'kov); Val'kov, pl. 14 figs 2–5.
1979 *Cambrotubulus decurvatus* Missarzhevsky; Qian *et al.*, p. 217, pl. 2 figs 13–16.
1982 *Cambrotubulus decurvatus* Missarzhevsky; Val'kov, p. 72, pl. 11 figs 1–12.
?1982 *Cambrotubulus sibiricus* (Val'kov); Val'kov, pp 72–73.
1983 *Cambrotubulus decurvatus* Missarzhevsky; Sokolov & Zhuravleva, p. 160, pl. 51 figs 3–4.
1984 *Cambrotubulus decurvatus* Missarzhevsky; Chen, p. 56, pl. 1 fig. 2.
?1987 *Cambrotubulus plicativus* Val'kov; pp 110–111, pl. 13 figs 19–21.
1989 *Cambrotubulus decurvatus* Missarzhevsky; pl. 13 figs 9–10.
1989 *Cambrotubulus conicus* Missarzhevsky; pl. 12 fig. 7.

1989 *Cambrotubulus decurvatus* Missarzhevsky; Hamdi, pl. 4, figs 1–3, 6.
1989 *Cambrotubulus decurvatus* Missarzhevsky; Hamdi *et al.*, fig. 3e.
1990 *Cambrotubulus crassus* Fedorov; Pel'man *et al.*, p. 25, pl. 2 fig. 1.
1995 *Rugatotheca* cf. *typica*; Hamdi, pl. 5 fig. 14.
1995 *Conotheca subcurvata* Yu; Hamdi, pl. 5 figs 15–16.
1996 *Cambrotubulus decurvatus* Missarzhevsky; Esakova & Zhegallo, p. 95, pl. 3 figs 12–16.
2002 *Cambrotubulus conicus* Missarzhevsky; Kouchinsky & Bengtson, fig. 8A–D.
2009 *Cambrotubulus* ex gr. *decurvatus*; Kouchinsky *et al.*, p. 286, figs 12B, 14M, 42–44.
2010 *Cambrotubulus decurvatus* Missarzhevsky; Rozanov *et al.*, p. 85, pl. 53 fig. 8.
2012 *Conotheca subcurvata* Yu; Tashayoee *et al.*, pl. 1 fig. 4.
2012 *Cambrotubulus*; Tashayoee *et al.*, pl. 2 fig. 5.
2017 *Cambrotubulus decurvatus* Missarzhevsky; Kouchinsky *et al.*, p. 425, fig. 79D–J, P.

Diagnosis. See Kouchinsky *et al.* (2009).

Material. Several thousand complete and fragmentary specimens including the figured material USTL3204-2, 3206-1, 3207-5, 3207-11, 3208-2, 3209-3, 3209-9, 3211-3, 3212-9, 3212-10, 3214-3, 3214-9, 3215-5, 3216-6, 3217-1, 3220-5, 3221-4, 3225-5, 3224-9 and 3227-8.

Preservation. The complete or fragmentary tubes are preserved in two modes: (1) as coarse phosphatic internal moulds with outer surface reproducing the internal surface of the tube in detail (Fig. 12A–S, U, AA–AK); or (2) as an internal coating consisting of an assemblage of phosphatic spheres (thickness of coating between 4.7 and 43.46 μm; Fig. 12A, T, V–X). Rare specimens are preserved with coarse phosphatic material made of a botryoidal amalgamation of coccoidal pseudomorphs within the internal cavity (Fig. 12W–Y); others are preserved with phosphatic filamentous structures on the surface of the internal mould (Fig. 12J–K).

Description. The tubes are open at both ends (originally or by fragmentation) with highly variable length, between 0.868 and 6.408 mm (see variation of size in the top right frame; Fig. 12A–I). The tubes are straight (Fig. 12C, L, P, AB, AD) and slightly to strongly undulating (Fig. 12A, B, D–F, R, U, AC, AE) to curved (Fig. 12G–I, W, AA, AG). Cross-section circular along the length of the tubes, as visible in the circular apical cross-section (Fig. 12O, S, Z, AF, AI) and in the circular apertural cross-section (Fig. 12N, R, T, AG). Diameter of cross-section slightly and gradually increasing towards the aperture (angle of divergence, *c.* 7.83°). The apertural diameter varies between *c.* 177 and *c.* 1024 μm. When preserved, the tapered apex is always open (Fig. 12O, Q, S, Z, AA, AF, AH–AJ). The transition from the apical to the abapical part is either continuous and progressive (Fig. 12Z, AH), continuous with a marked change in the angle of divergence (Fig. 12R, S, U) or discontinuous with a narrow furrow (Fig. 12O–Q, AA, AH, AI). Irregularly distant, transverse structures of different types, fine to coarse plications (Fig. 12A, O, AF) or fine striations (Fig. 12L–N, Z, AA, AJ, AK).

Remarks. In the absence of the apical part and operculum, it is sometimes difficult to differentiate *Cambrotubulus* from *Conotheca* (Kouchinsky *et al.*, 2009). However, many specimens recovered from Iran are preserved with the apical part, which is strongly tapered and always open, and no operculum has been recovered despite the recovery of several thousands of tubes. These characters are typical of *Cambrotubulus* and the specimens are therefore assigned to this genus. The specimens are assigned to the species *C. decurvatus*, which is interpreted to be the only valid species in the genus. *Conotheca conicus* Missarzhevsky, 1989, *C. crassus* Fedorov *in* Pel'man *et al.*, 1990, *C. plicativus* Val'kov, 1987 and *C. sibiricus* (Val'kov, 1968) are regarded as synonyms of *C. decurvatus*. *Conotheca corniformis* Elicki, 1994 cannot be assigned with certainty to the genus *Cambrotubulus* because the apical end is not known. As for some of the Iranian specimens of *Anabarites trisulcatus*, some specimens of *Cambrotubulus decurvatus* exhibit an unidentified phosphatic structure in the internal cavity. The phosphatic filaments present on the surface of internal moulds are interpreted as internal moulds of traces of the activity of endolithic microborers within the now-gone tube walls.

Distribution. Terreneuvian, Soltanieh Formation, Iran: samples D6, D7, D8, D9, D9a, D10, D11, D13, D14, D15, D16, D18, D19, D20, D21 and D22 of the Dalir section, and samples V6, V7, V8, V9, V11, V12, V13, V14, V16, V17, V18, V19 and V20 of the Valiabad section, both Alborz Mountains.

FIG. 12. *Cambrotubulus decurvatus* Missarzhevsky *in* Rozanov *et al.*, 1969, from the Soltanieh Formation at Dalir and Valiabad, Alborz Mountains, Iran. A, USTL3206-1. B, USTL3207-5. C, USTL3208-2. D, USTL3224-9. E, R–S, U, USTL3227-8: E; lateral view; R, apertural view; U, lateral view, outlined area magnified in S to show the apical end. F, USTL3204-2. G, AJ–AK, USTL3212-10: G, lateral view; AJ, apical view, outlined area magnified in AK to show transverse striations. H, O–Q, AI, USTL3212-9: H, lateral view; O, apical view, outlined area magnified in AI to show the circular cross-section of open end; P, lateral view, outlined area magnified in Q to show the apical part separated from the abapical area by a furrow. I, USTL3209-9. J–K, USTL3207-11: J, lateral view, outlined area magnified in K to show phosphatic filaments. L–N, USTL3221-4: L, lateral view, outlined area magnified in M to show the distant and fine transverse striations; N, apertural view. T, V, USTL3209-3: T, apertural view, outlined area magnified in V to show detail of the thick internal coating. W–X, USTL3220-5: W, lateral view, outlined area magnified in X to show the unidentified phosphatic internal structure. Y, USTL3214-3. Z–AA, AG, USTL3214-9: AA lateral view, outlined area magnified in Z to show apical part; AG, oblique apertural view. AB, USTL3217-1. AC, USTL3215-5. AD, AH, USTL3216-6: AD, lateral view, outlined area magnified in AH to show apical part. AE, USTL3211-3; AF, USTL3225-5. Scale bars represent: 500 μm (A–I, W, Y, AE); 200 μm (J, L, N, R, T, U, AC, AD, AF); 50 μm (K, M, Q, Z, AH); 20 μm (S, V, AI, AK); 100 μm (O, P, AA, AG, AJ); 10 μm (X); 1 mm (AB).


A
B
C
D
E
F
G
H
I
J
K
L
M
N
O
P
Q
R
S
T
U
V
W
X
Y
Z
AA
AB
AC
AD
AE
AF
AG
AH
AI
AJ
AK

Phylum MOLLUSCA Cuvier, 1797
Class HELCIONELLOIDA Peel, 1991
Order HELCIONELLIDA Geyer, 1994
Family HELCIONELLIDAE Wenz, 1938
Genus OELANDIELLA Vostokova, 1962

Type species. Oelandiella korobkovi Vostokova, 1962, Cambrian Stage 2, Kotuj River, East Krasnoyarsk Region, Siberia, Russia.

Diagnosis. See Gubanov & Peel (1999).

Oelandiella korobkovi Vostokova, 1962
Figure 13

1962 *Oelandiella korobkovi* Vostokova; p. 52, pl. 1 figs 1–4.
1962 *Oelandiella sibirica* Vostokova; p. 52, pl. 1 figs 5–7.
1969 *Latouchella korobkovi* (Vostokova); Rozanov *et al.*, p. 142, pl. 3 figs 4a, 7, 11, 12, 19, 20, pl. 4 fig. 17.
1979 *Anabarella emeiensis* Yu *in* Lu, pl. 3, fig. 15 [*nomen nudem*].
1979 *Latouchella raricostata* Yu *in* Lu, pl. 3 figs 4–9.
1979 *Archaeospira imbricata* Yu, p. 255, pl. 3 figs 24–27.
1979 *Archaeospira ornata* Yu, p. 255, pl. 4 figs 14–17.
1979 *Latouchella* cf. *memorabilis*; Yu, p. 252, pl. 3 fig. 20.
1979 *Yangtzespira exima* Yu, p. 255, pl. 4 figs 18–21.
1980 *Archaeospira ornata* Yu; Zhao *et al.*, p. 51.
1980 *Archaeospira ornata* Yu; Yin *et al.*, p. 156, pl. 13 figs 9, 10.
1980 *Archaeospira* sp.; Yin *et al.*, p. 156, pl. 13 figs 17, 18.
1980 *Bemella jacutica* (Missarzhevsky *in* Rozanov & Missarzhevsky); Yin *et al.*, p. 156, pl. 13 figs 4, 5.
1980 *Igorella* cf. *ungulata*; Jiang, pl. 3 fig. 8.
1980 *Latouchella korobkovi* (Vostokova); Jiang, p. 122, pl. 3 fig. 1a–c.
1980 *Latouchella korobkovi* (Vostokova); Missarzhevsky, pl. 6 figs 2, 3, 5a.
1980 *Latouchella korobkovi* (Vostokova); Yin *et al.*, p. 156, pl. 13 fig. 8 (cf. *korobkova* [sic]).
1980 *Latouchella songlingpoensis* Chen & Zhang, p. 195, pl. 1 figs 39, 46.
1980 *Maidipingoconus maidipingensis* (Yu); Yin *et al.*, p. 155, pl. 14 figs 1–3, 10, 11.
1980 *Yangtzespira regularis* Jiang; p. 120, pl. 3 fig. 2.
1980 *Yangtzespira regularis* Jiang; Luo *et al.*, p. 99, pl. 1 fig. 24.
1980 *Yunnanospira multiribis* Jiang; p. 120, pl. 3 fig. 3.
1980 *Yunnanospira multiribis* Jiang; Luo *et al.*, pl. 1 fig. 27.
1981 *Huanglingella polycostata* Chen *et al.*, p. 37, pl. 1 fig. 19.
1981 *Hubeispira nitida* Yu; p. 534, pl. I figs 14–19.
1981 *Yangtzespira xindianensis* Yu; p. 553, pl. 1 figs 11–13.
1982 *Igorella ungulata* Missarzhevsky *in* Rozanov *et al.*; Luo *et al.*, p. 191, pl. 20 fig. 4.
1982 *Latouchella korobkovi* (Vostokova); Luo *et al.*, p. 190, pl. 19 figs 8, 9.
1982 *Latouchella korobkovi* (Vostokova); Voronin *et al.*, p. 43, pl. 1 fig. 1.
1982 *Latouchella minuta* Zhegallo *in* Voronin *et al.*; p. 44, pl. 1 fig. 4.
1982 *Latouchella sibirica* (Vostokova); Voronin *et al.*, p. 44, pl. 1 fig. 2.
1982 *Yangtzespira exima* Yu; Luo *et al.*, p. 189, pl. 19 fig. 14.
1982 *Yangtzespira regularis* Jiang; He & Yang, pl. 3 figs 10–12.
1982 *Yangtzespira regularis* Jiang; Luo *et al.*, p. 189, pl. 19 fig. 10.
1982 *Yunnanospira multiribis* Jiang; Luo *et al.*, p. 189, pl. 19 fig. 13.
1983 *Latouchella korobkovi* (Vostokova); Zhegallo *in* Sokolov & Zhuravleva, p. 99, pl. 33 fig. 9.
1984 *Archaeospira ornata* Yu; Xing *et al.*, pl. 5 fig. 13.
1984 *Archaeospira ornata* Yu; Yu, p. 30, pl. 2 fig. 12.
1984 *Archaeospira* sp.; Chen, p. 58, pl. 1 fig. 14.
1984 *Maidipingoconus maidipingensis* (Yu); Chen, p. 58, pl. 1 fig. 14.
1984 *Gibbaspira acutumbonalis* He; p. 27, pl. 2 figs 1–4.
1984 *Uncinaspira pristina* He; p. 25, pl. 2 figs 16, 17.
1984 *Uncinaspira ruidocostata* He; p. 25, pl. 2 figs 10–13.
1984 *Yangtzespira exima* Yu; Luo *et al.*, pl. 10 fig. 1.
1984 *Yangtzespira exima* Yu; Yu, p. 28, pl. 2 figs 10, 11.
1984 *Yangtzespira multicostata* He *in* Xing *et al.*; pl. 13 figs 8, 9.
1984 *Yangtzespira regularis* Jiang; Xing *et al.*, pl. 10 fig. 13.
1984 *Yunnanospira multiribis* Jiang; Luo *et al.*, pl. 10 fig. 2.
1984 *Yunnanospira multiribis* Jiang; Xing *et al.*, pl. 10 fig. 20.
1987*a* *Archaeospira*? sp.; Yu, pl. 44 figs 1–2, pl. 45 figs 1–6.
1987*a* *Yangtzespira exima* Yu; Yu, pl. 5 figs 11–13, pl. 4 figs 6–8.
1987*b* *Archaeospira imbricata* Yu; Yu, p. 196, pl. 43 figs 7–10, pl. 46 figs 4–6, pl. 48 figs 2, 3, 5–8, pl. 49 figs 6–9, pl. 54 figs 4–6.
1987*b* *Archaeospira ornata* Yu; Yu, p. 194, text-figs 29a–29c, 57, pl. 43 figs 4–6, pl. 48 figs 1, 4, 9, pl. 49 figs 1–5, 10–12, pl. 50 figs 1–9, pl. 51 figs 1–7, pl. 53 figs 5–7, pl. 54 figs 1–3, pl. 58 fig. 9.
1987*b* *Archaeospira* sp.; Yu, p. 198, pl. 40 figs 1, 2, 5, 6, 10, 11, pl. 46 figs 9–11, pl. 47 figs 8, 9, pl. 53 figs 8, 9, pl. 54 figs 7–12.
1987*b* *Hubeispira nitida* Yu; Yu, p. 206, pl. 55 figs 1–7, pl. 56 figs 5–8.
1987*b* *Latouchella* cf. *korobkovi*; Yu, p. 185, pl. 39 figs 1–6, pl. 43 figs 1–3, pl. 46 figs 1–3, 7, 8, pl. 47 figs 3–7.
1987*b* *Yangtzespira exima* Yu; Yu, p. 211, text-figs 22, 29d, 29e, 64, pl. 47 figs 1, 2, pl. 53 figs 1–4, pl. 57 figs 1–8, pl. 58 figs 1–8, pl. 59 figs 1–7.
1987 *Latouchella vetula* Val'kov, pl. 1 fig. 1.
1988 *Latouchella angusta* (Cobbold); Kerber, p. 171, pl. 7 figs 7–10, 14–15, 17.
1988 *Yangtzespira exima* Yu; Yu, figs 8–10.
1989 *Archaeospira* cf. *ornata*; Qian & Bengtson, p. 116, fig. 74.
1989 *Archaeospira* cf. *songlingpoensis*; Qian & Bengtson, p. 116, text-fig. 75.
1989 *Archaeospira ornata* Yu; Qian & Bengtson, p. 112, text-figs 72, 73.

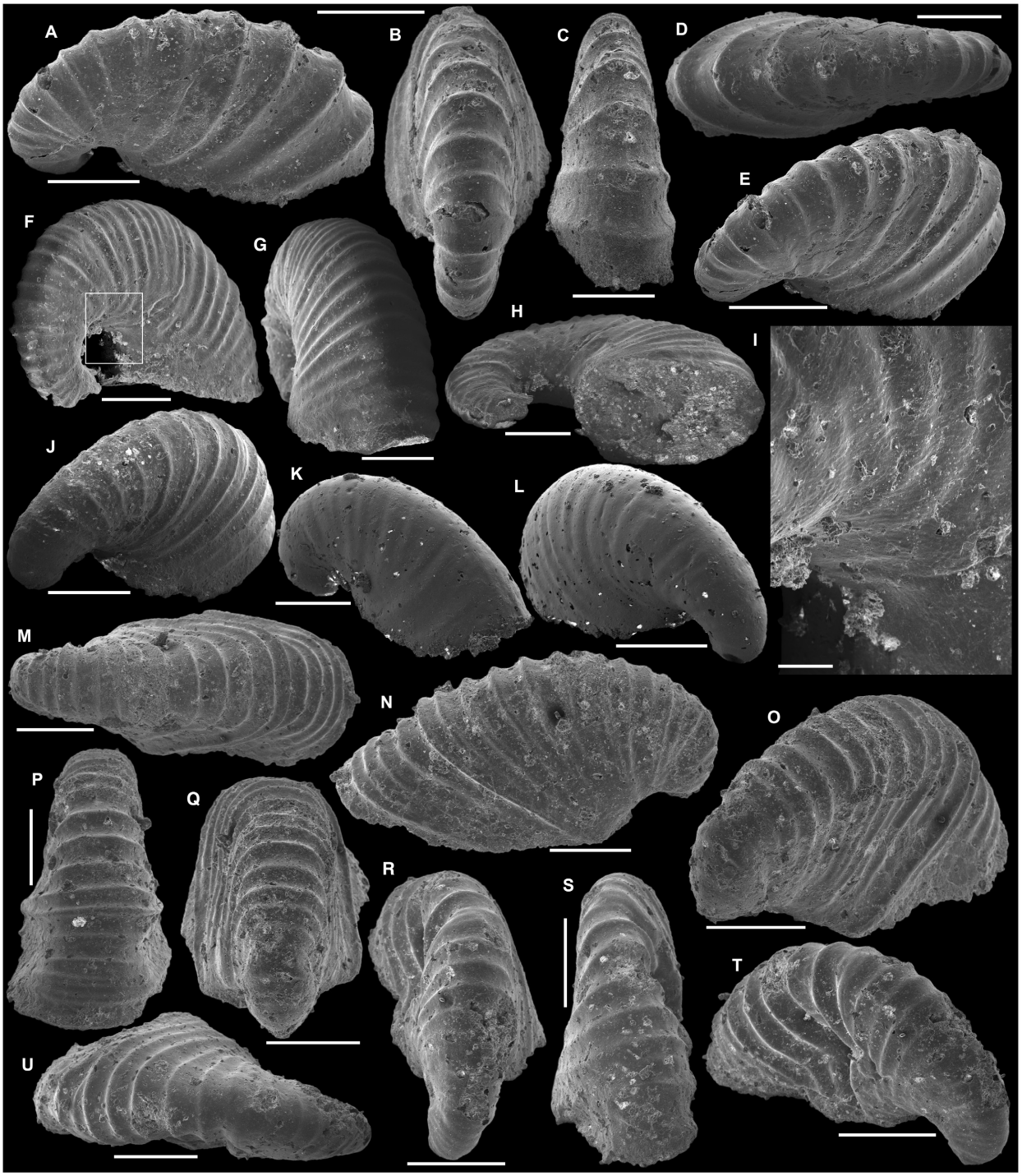

FIG. 13. *Oelandiella korobkovi* Vostokova, 1962, from the Barut Formation at Barut Aghaji and Chopoghlu, Soltanieh Mountains, Iran. A–E, USTL3230-6: A, lateral; B, posterior; C, anterior; D, upper; E, oblique lateral view. F–I, USTL3228-3: F, oblique lateral view, outlined area magnified in I to show polygonal imprints at the umbilicum; G, oblique anterior view; H, lower view. J, USTL3229-3 in oblique posterior view. K–L, USTL3229-9; K, oblique anterior; L, oblique posterior view. M–Q, USTL3230-9: M, upper; N, lateral; O, oblique lateral; P, anterior; Q, posterior view. R–U, USTL3230-3: R, posterior; S, anterior; T, oblique lateral; U, upper view. Scale bars represent: 500 μm (A–H, J–U); 100 μm (I).

1989 *Archaeospira* sp.; Khomentovsky & Karlova, p. 49, pl. 4 figs 1, 2.
1989 *Latouchella korobkovi* (Vostokova); Khomentovsky & Karlova, p. 48, pl. 3 fig. 6.
1989 *Latouchella korobkovi* (Vostokova); Hamdi, pl. 6 figs 1–2.
1989 *Latouchella* sp.; Hamdi, pl. 6 figs 3–4.
1989 *Latouchella* ex. gr. *korobkovi*; Hamdi, pl. 6 fig. 5.
1989 *Latouchella korobkovi* (Vostokova); Hamdi *et al.*, fig. 3a.
1989 *Latouchella maidipingensis*; Khomentovsky & Karlova, p. 49, pl. 3 fig. 8.
1989 *Yangtzespira regularis* Jiang; Khomentovsky & Karlova, p. 50, pl. 3 fig. 9.
1990 *Archaeospira ornata* Yu; Pel'man *et al.*, pl. 1 fig. 10.
1990 *Latouchella korobkovi* (Vostokova); Pel'man *et al.*, pl. 1 figs 20, 22, 27.
1990 *Igorella ungulata* Missarzhevsky *in* Rozanov *et al.*; Pel'man *et al.*, pl. 1 fig. 13.
1990 *Archaeospira ornata* Yu; Yu, pl. 8 figs 4–11.
1990 *Yangtzespira exima* Yu; Yu, p. 146, text-fig. 5, pl. 9 figs 1–10.
1991 *Latouchella korobkovi* (Vostokova); Dzik, figs 7e, 7f.
1994 *Latouchella korobkovi* (Vostokova); Luo *et al.*, pl. 2 fig. 2.
1994 *Yangtzespira regularis* Jiang; Luo *et al.*, pl. 2 fig. 1.
1995 *Archaeospira ornata* Yu; Hamdi, pl. 12 figs 6, 8, 10.
1995 *Archaeospira regularis* (Jiang); Hamdi, pl. 15 figs 1, 2.
1995 *Latouchella korobkovi* (Vostokova); Hamdi, pl. 11 figs 1, 2, 8, 9, 12 (cf. *korobkovi*), pl. 12 figs 3, 7, 9, 11, 12, pl. 16 figs 11, 12.
1995 *Latouchella maidipingensis* (Yu); Hamdi, pl. 11 figs 4–7.
1996 *Latouchella korobkovi* (Vostokova); Esakova & Zhegallo, p. 176, pl. 21 fig. 6.
1996 *Latouchella magnifica* Zhegallo *in* Esakova & Zhegallo, p. 179, pl. 21 fig. 7.
1996 *Latouchella minuta* Zhegallo *in* Voronin *et al.*; Esakova & Zhegallo, p. 179, pl. 21 fig. 4.
1996 *Latouchella numerosa* Zhegallo *in* Esakova & Zhegallo, p. 177, pl. 21 fig. 5.
1996 *Latouchella sibirica*; Esakova & Zhegallo, p. 176, pl. 21 fig. 3.
1998 *Latouchella korobkovi*; Vasil'eva, p. 80, pl. 6 figs 21, 23.
1998 *Latouchella sibirica* (Vostokova); Vasil'eva, p. 80, pl. 6 fig. 24.
1996 *Oelandiella korobkovi* Vostokova; Gubanov & Peel, p. 217, text-figs 4, 5, 6A–6D, 7.
1996 *Oelandiella sibirica* Vostokova; Gubanov & Peel, p. 217, text-fig. 6E–F.
2000 *Latouchella korobkovi* (Vostokova); Gubanov & Peel, figs 2a, 2b.
2003 *Archaeospira ornata* Yu; Feng & Sun, p. 27, text-fig. 6.
2003 *Oelandiella korobkovi* Vostokova; Demidenko *et al.*, figs 3a–3c.
2004 *Oelandiella korobkovi* Vostokova; Parkhaev, pl. 2 fig. 1.
2005 *Latouchella korobkovi* (Vostokova); Parkhaev, pl. 4 figs 2, 3, 5–8.
2006 *Latouchella korobkovi* (Vostokova); Demidenko & Parkhaev, text-figs 5d, 5e.
2008 *Latouchella korobkovi* (Vostokova); Parkhaev, text-figs 3.14C, 3.14D.
2010 *Latouchella korobkovi* (Vostokova); Parkhaev & Demidenko, pp 1054–1058, pl. 72 figs 1–16.
2010 *Latouchella korobkovi* (Vostokova); Rozanov *et al.*, p. 63, pl. 31 figs 1–9.
2013 *Oelandiella korobkovi* Vostokova; Devaere *et al.*, pp 7–12, fig. 4.
2014*a* *Oelandiella korobkovi* Vostokova; Yang *et al.*, fig. 18C–D.
2017 *Oelandiella korobkovi* Vostokova; Kouchinsky *et al.*, pp 331–333, figs 6, 7A–C, E, 8A, B.

Material. A few hundred broken to complete internal moulds including the figured specimens USTL3228-3, 3229-3, 3229-9, 3230-3, 3230-6 and 3230-9.

Preservation. Specimens are preserved as internal moulds.

Description. The univalve conchs are laterally compressed and coiled into half a whorl (Fig. 13N, O, T) to almost a complete whorl (Fig. 13A, F, L). The conch length ranges from 1.511 to 2.776 mm, the width from 0.413 to 1.128 mm and the height from 0.607 to 1.398 mm. The coiling is mainly planispiral with a slight asymmetric component (Fig. 13B, D, M, P–S, U); the apex is in the broad axis of bilateral symmetry (Fig. 13B, D, H, M, Q, R, U). Expansion of conchs rapid with a large aperture (from 0.739 to 1.869 mm), elongated along the anteroposterior axis (Fig. 13H). Lateral fields straight (Fig. 13P, Q) to slightly concave (Fig. 13B, C, G, L), affected by deformation in some specimens (Fig. 13M, O–T). External surface of internal moulds with comarginal ribs that always cross the dorsum in the best-preserved specimens (Fig. 13A–E, G, M–U) but slightly faded in the dorsal area in the worn specimens (Fig. 13K). Ribs fading toward the umbilicum (Fig. 13A, E, F, H, N, O, T). Maximum distance between ribs is 157–422 μm. High variability in number and distance between ribs (compare Fig. 13A and Fig. 13F). Specimens densely ribbed due to presence of intermediate ribs rapidly disappearing toward the umbilicum and flanked by two primary ribs (Fig. 13F, G, J). Ribs roughly triangular in transverse section, rounded (Fig. 13F–J) to sharp (Fig. 13A–E, M–U) depending on the preservation. Polygonal imprints present on the surface of internal moulds near the umbilicum (Fig. 13I).

Remarks. The specimens from Iran are assigned to the genus *Oelandiella* due to their typical coiling and the presence of ribs crossing the dorsum. *Oelandiella angusta* (Cobbold, 1935) and *O. vetula* (Val'kov, 1987) are probably junior synonyms of *O. korobkovi*; they differ only in the expression and number of ribs, which is interpreted as intraspecific by Devaere *et al.* (2013). *Oelandiella selindeica* (Bokova, 1990) is tightly coiled exclusively and clearly dextrally, whereas the present specimens are subsymmetrical. *Oelandiella memorabilis* (Missarzhevsky *in* Rozanov *et al.*, 1969) clearly differs from the Iranian specimens in the presence of an antispiral sinus on the ribs.

Distribution. Terreneuvian, Barut Formation, Iran: samples B5 and B8 of the Barut Aghaji section and samples CH7 and CH12 of the SE Chopoghlu section, Soltanieh Mountains.

CAP-SHAPED MOLLUSCS

Various internal moulds of univalved, cap-shaped molluscs were recovered from the limestone beds at the base of the Barut Formation in the sections of Barut Aghaji (samples B5 and B8) and of the valley south-east of Chopoghlu (sample CH10, CH12). All of them possess an apex overhanging the apertural margin (Fig. 14A, B, E, G, J, M, N). The first morphotype (Fig. 14A–D) is higher than wide and as long as high, laterally compressed and coiled for less than half a whorl (Fig. 14C, D). It has irregular folds that extend from one lateral field to the other, crossing the dorsum (Fig. 14C, D). The specimens are superficially similar to *Oelandiella korobkovi* but clearly differ in the coiling and ornaments: *Oelandiella korobkovi* is more tightly coiled than this first morphotype and has strong co-marginal ribs always crossing the dorsum, whereas in the first morphotype of cap-shaped molluscs, the co-marginal folds are faint and irregular. The second and third morphotypes are low (height smaller than width and length; Fig. 14E–J, M, N). The second morphotype is wide (Fig. 14E, H) whereas the third morphotype is similar to some specimens of *Bemella* Missarzhevsky *in* Rozanov *et al.*, 1969: it is slightly compressed laterally (Fig. 14J, K, M) and possesses polygonal imprints at the apertural margin and on the dorsum (Fig. 14L, O).

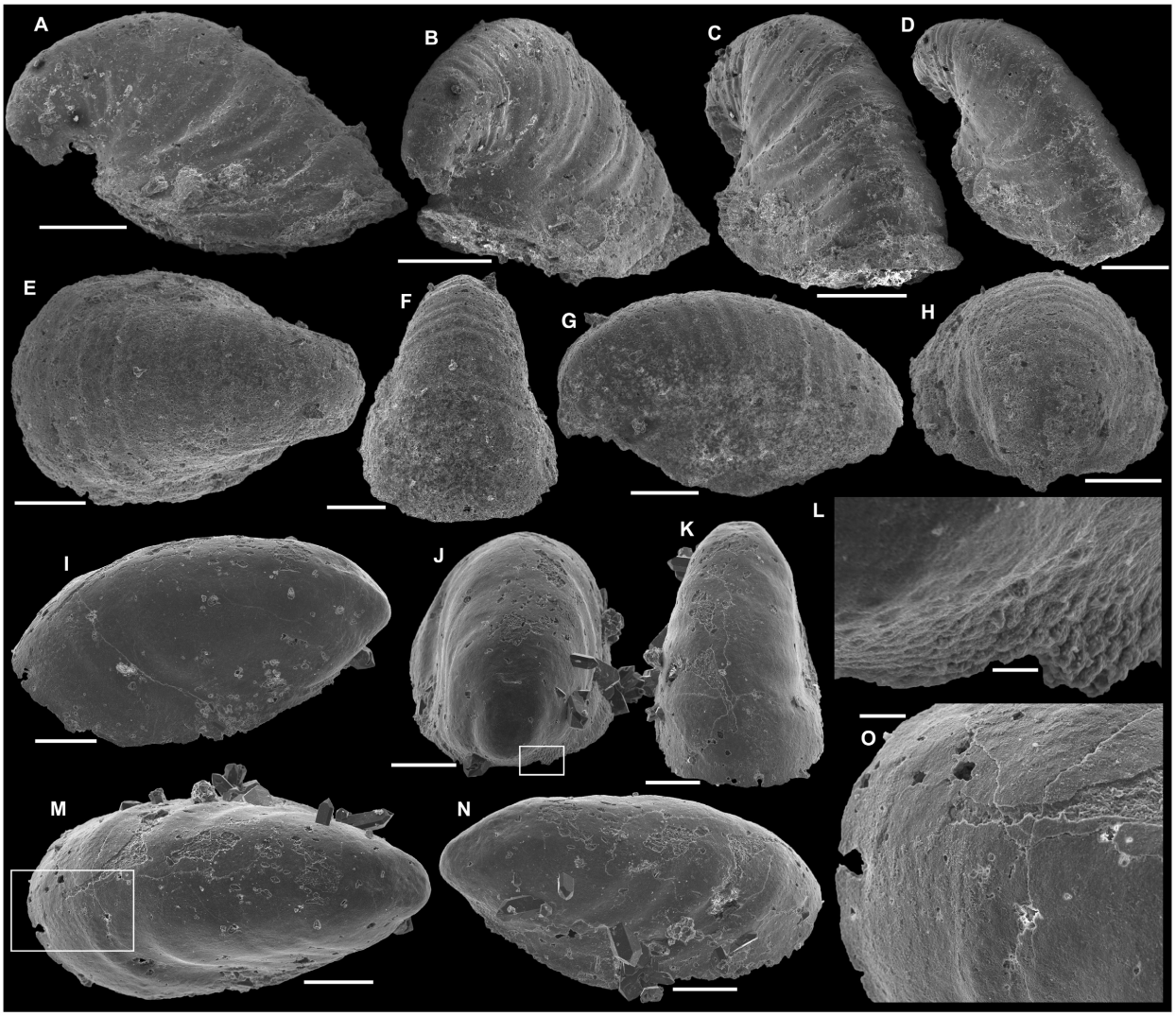

FIG. 14. Various cap-shaped molluscs from the Barut Formation at Barut Aghaji and Chopoghlu, Soltanieh Mountains, Iran. A–D, USTL3230-5: A, lateral; B, oblique posterior; C, oblique anterior; D, oblique upper view. E–H, USTL3230-7: E, upper; F, anterior; G, lateral; H, posterior view. I–O, USTL3197-7: I, lateral view; J, posterior view, outlined area magnified in L to show polygonal imprints under the apex; K, anterior view; M, upper view, outlined area magnified in O to show polygonal imprints on the surface of the internal mould; N, lateral view. Scale bars represent: 500 μm (A–D); 200 μm (E–K, M, N); 20 μm (L); 50 μm (O).

Phylum, Class, Order & Family UNCERTAIN
Genus AETHOLICOPALLA Conway Morris *in* Bengtson *et al.*, 1990

Type species. *Aetholicopalla adnata* Conway Morris *in* Bengtson *et al.*, 1990, Cambrian Stage 3, Curramulka, Yorke Peninsula, Stansbury Basin, Australia.

Diagnosis. See Bengtson *et al.* (1990).

Aetholicopalla adnata Conway Morris *in* Bengtson *et al.*, 1990
Figure 15

1988 *Archaeooides granulatus* Qian; Kerber, p. 189, pl. 11 figs 13–20.
1990 *Aetholicopalla adnata* Conway Morris *in* Bengtson *et al.*, p. 338, figs 213–216.
1992 *Archaeooides granulatus* Qian; Elicki & Schneider, pl. 16 figs 8, 9.
1998 *Aetholicopalla adnata* Conway Morris; Elicki, p. 58, pl. 1 figs 6–9, pl. 2.
2001 *Aetholicopalla adnata* Conway Morris; Demidenko *in* Gravestock *et al.*, pl. 12 figs 7–8.
2004 *Aetholicopalla adnata* Conway Morris; Wrona, p. 51, fig. 26D, E.
2009 *Aetholicopalla adnata* Conway Morris; Topper *et al.*, p. 219, figs 6S–U.
2010 *Archaeooides granulatus* Qian; Rozanov *et al.*, p. 87, pl. 54 fig. 6.
2013 *Aetholicopalla adnata* Conway Morris; Devaere *et al.*, p. 66, figs 25.1–23.
?2014*a* *Aetholicopalla adnata* Conway Morris; Yang *et al.*, fig. 13P.
2015 *Aetholicopalla adnata* Conway Morris; Kouchinsky *et al.*, fig. 73A.
2015 *Aetholicopalla adnata* Conway Morris; Yang *et al.*, fig. 7U.
2017 *Archaeooides granulatus* Qian; Kouchinsky *et al.*, fig. 82G.

Diagnosis. See Bengtson *et al.* (1990).

Material. 46 complete to broken phosphatic specimens including the figured material USTL3209-1, 3212-1 and 3226-5.

Preservation. The specimens are preserved as phosphate replacement of the test with pyrite overgrowth (Fig. 15A–F) or as internal mould (Fig. 15J) with partial external coating (Fig. 15G–I).

Description. The test is spherical (Fig. 15G–J) to ellipsoidal in shape (Fig. 15A–F; average flattening of 0.85) and 0.596–1.489 mm

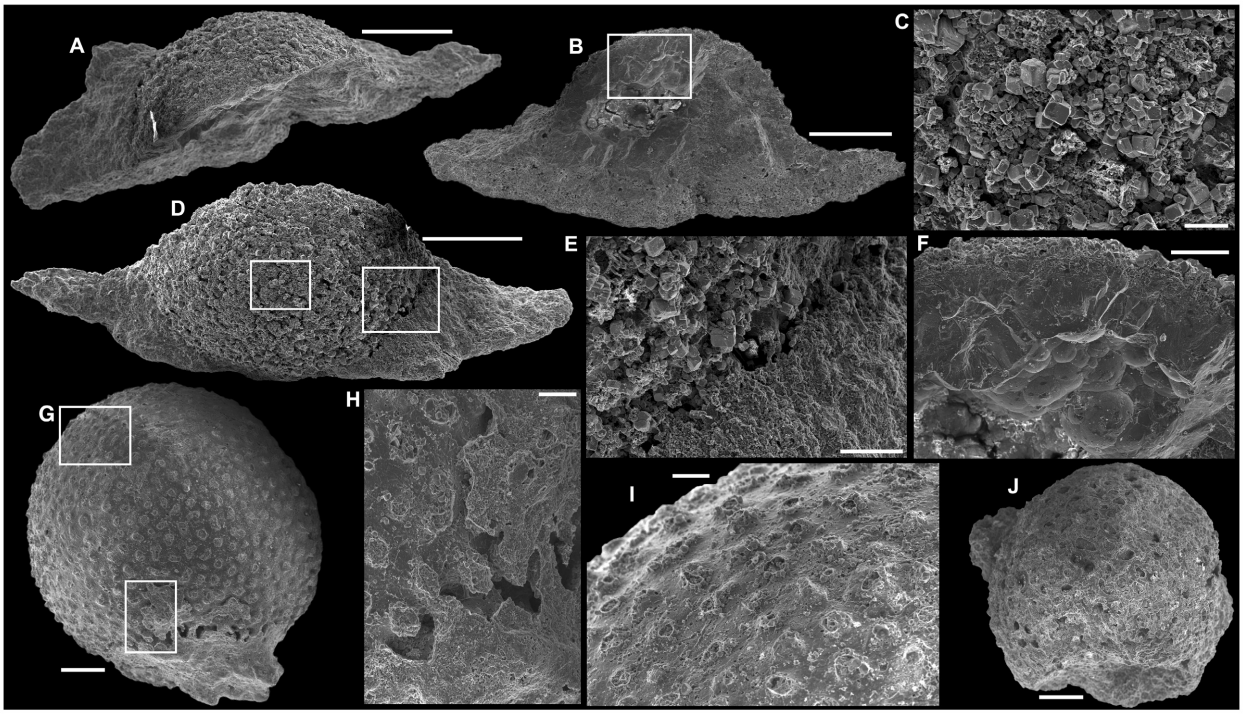

FIG. 15. *Aetholicopalla adnata* Conway Morris *in* Bengtson *et al.*, 1990 from the Soltanieh Formation at Dalir and Valiabad, Alborz Mountains, Iran. A–F, USTL3209-1: A, upper view; B, view of cross-section, outlined area magnified in F to show microstructure; D, lateral view, left outlined area magnified in C to show the external surface with pyrite crystals, and right outlined area magnified in E to show the contact between the microfossil and substrate. G–I, USTL3212-1: G, lateral view, lower outlined area magnified in H and upper outlined area magnified in I. J, USTL3226-5. Scale bars represent: 500 μm (A, B, D); 50 μm (C, H, I); 100 μm (E, F); 200 μm (G, J).

in diameter. Most specimens show a differentiated attachment area, which is either isolated (Fig. 15J) or still attached to the encrusted substrate (Fig. 15A, B, D, E, G, H). The attachment surface can be completely flat, but also convex or concave. The surface of the internal moulds is covered with slightly projecting tubes or pillars when filled with phosphatic material (Fig. 15G–I) up to 25 μm in height. The pillars are connected to a continuous external coating (Fig. 15G, H), whereas the tubes are connected to the external coating and appear as holes on the external surface (Fig. 15J). In one specimen, the test is completely replaced by a thick, recrystallized layer of phosphate (Fig. 15B, F) and pyrite crystals that are present on the outer surface of this thick layer (Fig. 15C–E). The internal surface of the thick layer is irregular and constituted of joined phosphatic rounded structures (Fig. 15B, F). The internal cavity is hollow (Fig. 15B, F).

Remarks. The specimens from Iran are assigned to the genus *Aetholicopalla* and particularly to the single species *Aetholicopalla adnata*, because of tubes or pillars and attachment surfaces that differentiate it from the comparable genus *Archaeooides* Qian, 1977.

Distribution. Terreneuvian, Soltanieh Formation, Iran: samples D4, D7, D8, D10 and D13 of the Dalir section and samples V9 and V19 of the Valiabad section, Alborz Mountains.

INDET. CONES

Figure 16

Indeterminate conical microfossils (32 specimens) are present in the interval of the Soltanieh Formation corresponding to the Fortunian (samples D9a, D10, D13 and D14 of the Dalir section and sample V9 of the Valiabad section). They are robust, conical, phosphatized internal moulds (Fig. 16) with a height range from 1.694 to 2.940 mm. They exhibit a moderate lateral compression and gentle curvature in the plane of bilateral symmetry (Fig. 16G, H, L–N). The apex is sharp (Fig. 16J) with an oval to circular cross-section (Fig. 16E, H). A ridge, located under the apex, connects it to the aperture and sharply separates the two lateral sides of the cone (Fig. 16C, H, L). The angle of divergence is wide at the base and ranges between 51° and 84° (Fig. 16C, D, I, O). The basal part has an irregular margin caused by a breakage (Fig. 16A–D, F–I, K–O). The cross-section of the aperture is teardrop-shaped, with a length between 0.890 and 1.448 mm and a width between 0.396 and 0.930 mm (Fig. 16F, G, M). The surface of the internal mould is smooth (Fig. 16).

Many Early Cambrian conical objects with indeterminate affinities were described and can be compared with the Iranian indeterminate cones. Some are ornamented cones, such as *Zhijinites* Qian, 1978 and *Stoibostrombus* Conway Morris & Bengtson *in* Bengtson *et al.*, 1990, and some are problematic cones as described by Kouchinsky *et al.* (2015, fig. 45). Their preservation with phosphatic walls is different from the preservation of

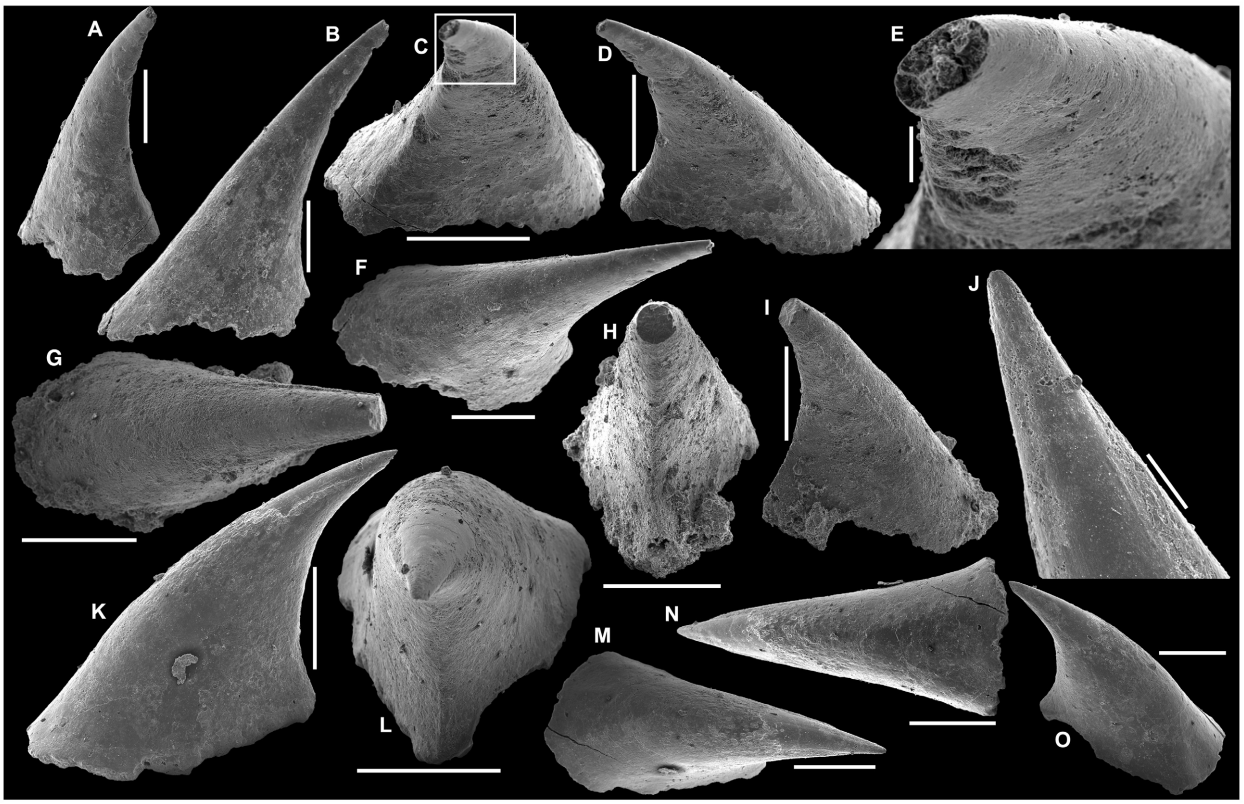

FIG. 16. Indeterminate cones from the Soltanieh Formation at Dalir and Valiabad, Alborz Mountains, Iran. A–F, USTL3214-6. G–I, USTL3220-3. J–O, USTL3212-7. Scale bars represent: 500 μm (A–D, F–I, K–O); 50 μm (E); 100 μm (J).

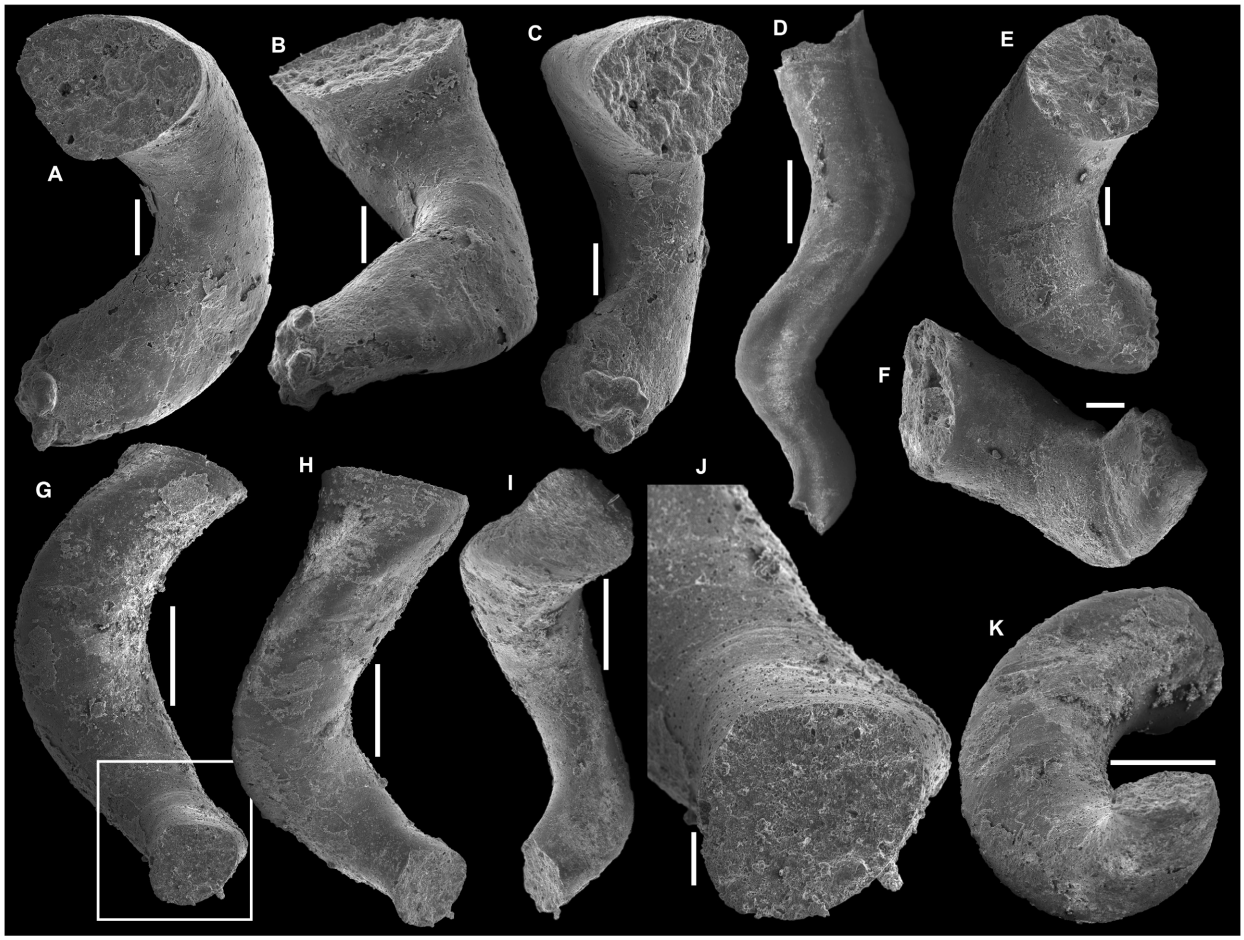

FIG. 17. Irregular tubes from the Soltanieh Formation at Dalir and Valiabad, Alborz Mountains, Iran. A–C, USTL3211-1. D, USTL3218-1. E–F, USTL3214-4. G–K, USTL3221-1. Scale bars represent: 200 μm (A–C, E–F); 1 mm (D); 500 μm (G–I, K); 100 μm (J).

Iranian specimens as internal moulds, making direct comparison difficult. *Archaeopetasus* Conway Morris & Bengtson *in* Bengtson *et al.*, 1990 and *Fomitchella* Missarzhevsky *in* Rozanov *et al.*, 1969 are more flared at the base, less laterally compressed and lack the subapical ridge visible in the Iranian specimens. The problematic cones from Iran can also be compared to protoconodont elements, especially of *Mongolodus* Missarzhevsky, 1977, although the latter are much more compressed laterally.

INDET. IRREGULAR TUBES
Figure 17

Indeterminate irregular tubes (37 specimens) come from samples D10, D13, D14 and D16 of the Dalir section and samples V8, V9 and V12 of the Valiabad section. They correspond to phosphatic internal moulds of tubes open at both ends; their length ranges from 2.020 to 6.822 mm (Fig. 17). The tubes are helically curved and twisted (Fig. 17B–D, F–K). The cross-section is rounded triangular along the length in the shortest specimens (Fig. 17A, C, G, J) and subcircular in the longest specimens (Fig. 17E). The diameter of the cross-section increases towards the aperture, where the angle of divergence reaches *c.* 18°. The apertural diameter ranges between 0.580 and 1.352 mm. The tubes are organized into three low convex to flat surfaces separated by rounded ridges (Fig. 17B, G–I). This causes the rounded triangular shape of the cross-section, which is reminiscent of that of *Anabarites*. However, in the irregular tubes, the circular cross-section occurs in the largest specimens and is thus opposite in *Anabarites*.

Acknowledgements. The authors warmly thank the staff of the MfN for assistance in producing the data for the paper, especially Markus Brinkmann for sawing the samples, Elisabeth Wittstock for carefully picking SSFs and Kirsten Born for guidance on the use of the SEM. Christian B. Skovsted (Natural History Museum of Stockholm) and an anonymous reviewer provided valuable advice and corrections that significantly improved the manuscript. LD benefited from a postdoctoral research fellowship of the Alexander von Humboldt Foundation. Open Access funding enabled and organized by Projekt DEAL.

DATA ARCHIVING STATEMENT

This published work and the nomenclatural act it contains, have been registered in ZooBank: http://zoobank.org/References/3768F94F-70F8-4C86-95AA-2B7667A1C024

Editor. Javier Álvaro

SUPPORTING INFORMATION

Additional Supporting Information may be found online in the supporting information tab for this article (https://doi.org/10.1002/spp2.1391):

Table S1. Global stratigraphic and geographic range of species identified in 'New and revised small shelly fossil record from the lower Cambrian of northern Iran'.

REFERENCES

AZMI, R. J. 1983. Microfauna and age of the Lower Tal Phosphorite of Mussoorie Syncline, Garhwal Lesser Himalaya, India. *Himalayan Geology*, **11**, 373–409.

—— and PANCHOLI, V. P. 1983. Early Cambrian (Tommotian) conodonts and other shelly microfauna from the upper Krol of Mussoorie Syncline, Garhwal Lesser Himalaya with remarks on the Precambrian–Cambrian boundary. *Himalayan Geology*, **11**, 360–372.

—— and PAUL, S. K. 2004. Discovery of Precambrian–Cambrian boundary protoconodonts from the Gangolihat Dolomite of Inner Kumaun Lesser Himalaya: implication on age and correlation. *Current Science*, **86**, 1653–1660.

BALLATO, P., UBA, C. E., LANDGRAF, A., STRECKER, M. R., SUDO, M., STOCKLI, D. F., FRIEDRICH, A. and TABATABAEI, S. H. 2011. Arabia–Eurasia continental collision: insights from late Tertiary foreland-basin evolution in the Alborz Mountains, northern Iran. *Geological Society of America Bulletin*, **123**, 106–131.

BENGTSON, S. 1977. *Aspects of problematic fossils in the early Palaeozoic*. Unpublished PhD thesis, University of Uppsala, Uppsala, Sweden, 71 pp.

—— 1983. The early history of the *Conodonta*. *Fossil & Strata*, **15**, 5–19.

—— CONWAY MORRIS, S., COOPER, B. J., JELL, P. A. and RUNNEGAR, B. N. 1990. Early Cambrian fossils from South Australia. *Memoirs of the Association of Australasian Palaeontologists*, **9**, 1–364.

BERBERIAN, M. and KING, G. C. P. 1981. Towards a paleogeography and tectonic evolution of Iran. *Canadian Journal of Earth Sciences*, **18**, 210–265.

BHATT, D. K. 1991. The Precambrian–Cambrian transition interval in Himalaya with special reference to small shelly fossils: a review of current status of work. *Journal of the Palaeontological Society of lndia*, **36**, 109–120.

BOKOVA, A. P. 1990. New lower Cambrian gastropods from the Siberian platform. *Paleontological Journal*, **24**, 134–136.

—— and VASIL'EVA, N. I. 1990. Some new species of skeletal problematics from the Lower Cambrian of the Olenyok uplift. Proceedings of the Institute of Geology and Geophysics, Siberian Branch of the USSR Academy of Sciences. Nauka USSR, Moscow, 159 pp. [in Russian]

BRASIER, M. D. 1989. Towards a biostratigraphy of the earliest skeletal biotas. 117–165. *In* COWIE, J. W. and BRASIER, M. D. (eds) *The Precambrian–Cambrian boundary*. Clarendon Press, Oxford.

—— and SINGH, P. 1987. Microfossils and Precambrian–Cambrian boundary stratigraphy at Maldeota, Lesser Himalaya. *Geological Magazine*, **124**, 323–345.

BRIGGS, D. E. G., ERWIN, D. H. and COLLIER, F. J. 1994. *The fossils of the Burgess Shale*. Smithsonian Institution Press, 238 pp.

BUDD, G. E. and JACKSON, I. S. C. 2016. Ecological innovations in the Cambrian and the origins of the crown group phyla. *Philosophical Transactions of the Royal Society B*, **371**, 20150287.

CHEN, M. 1982. The new knowledge of the fossil assemblages from Maidiping section, Emei County, Sichuan with reference to the Sinian–Cambrian boundary. *Scientia Geologica Sinica*, **3**, 253–262. [in Chinese, English summary]

CHEN, P. 1984. Discovery of Lower Cambrian small shelly fossils from Jijiapo, Yichang, West Hubei and its significance. *Professional Papers of Stratigraphy & Palaeontology*, **13**, 49–66.

CHEN, J. Y. and PENG, Q. Q. 2005. An Early Cambrian problematic organism (*Anabarites*) and its possible affinity. *Acta Palaeontologica Sinica*, **44**, 57–65. [in Chinese]

CHEN, Y. and ZHANG, S. 1980. Small shelly fossils from the early Lower Cambrian, Sonlingpo, eastern Yangtze Gorges. *Geological Review*, **26**, 190–197. [in Chinese]

CHEN, M., CHEN, Y. and ZHANG, S. 1981. The small shelly fossil assemblage in the limestone of the uppermost part of the Dengying Formation at Songlingpo, Yichang. *Journal of the Wuhan College of Geology, Earth Science*, **1**, 32–41. [in Chinese]

CIABEGHODSI, A. A., HAMDI, B., ABDI, M. H. and SADEGHI, A. 2006. Systematic and taphonomic study of Trichophycus pedum at the Soltanieh type section in SE of Zanjan. *Geosciences, Geological Survey of Iran*, **16**, 116–123. [in Persian]

COBBOLD, E. S. 1935. Lower Cambrian from Herault, France. *The Annals & Magazine of Natural History*, **16**, 25–48.

CONWAY MORRIS, S. and FRITZ, W. A. 1980. Shelly microfossils near the Precambrian–Cambrian boundary, Mackenzie Mountains, northwestern Canada. *Nature*, **286**, 381–384.

—— and CHEN, M. 1989. Lower Cambrian anabaritids from South China. *Geological Magazine*, **126**, 615–632.

CUVIER, G. 1797. *Tableau élémentaire de l'histoire naturelle des animaux*. Baudoin, Paris.

DEMIDENKO, Y. E. 2006. New Cambrian lobopods and chaetognaths of the Siberian Platform. *Paleontological Journal*, **40**, 234–243.

—— ZHEGALLO, E. A., PARKHAEV, P. Y. and SHUVALOVA, Y. V. 2003. Age of phosphorites from the Khubsugul Basin (Mongolia). *Doklady Earth Sciences*, **389**, 317–321.

DEVAERE, L., CLAUSEN, S., STEINER, M., ÁLVARO, J. J. and VACHARD, D. 2013. Chronostratigraphic and palaeogeographic significance of an early Cambrian microfauna from the Heraultia Limestone, northern Montagne Noire, France. *Palaeontologia Electronica*, **16** (2), 17A.

—— —— ALVARO, J. J., PEEL, J. S. and VACHARD, D. 2014. Terreneuvian orthothecid (Hyolitha) digestive tracts from Northern Montagne Noire, France; taphonomic, ontogenetic and phylogenetic implications. *PLoS One*, **9**, e88583.

—— —— SOSA-LEON, P. J., PALAFOX-REYES, J. J., BUITRON-SÁNCHEZ, B. E. and VACHARD, D. 2019. Early Cambrian small shelly fossils from northwest Mexico: biostratigraphic implications for Laurentia. *Palaeontologia Electronica*, **22** (2), 41A.

DZIK, J. 1991. Is fossil evidence consistent with traditional views of the early metazoan phylogeny? 47–56. *In* SIMONETTA, A. and CONWAY MORRIS, S. (eds) *The early evolution of Metazoa and the significance of problematic taxa*. Cambridge University Press.

ELICKI, O. 1994. Lower Cambrian carbonates from eastern Germany: palaeontology, stratigraphy and palaeogeography. *Neues Jahrbuch für Geologie und Paläontologie, Abhandlungen*, **191**, 69–93.

—— 1998. First report of Halkieria and enigmatic globular fossils from the central European Marianian (Lower Cambrian, Görlitz syncline, Germany). *Revista Española de Paleontología*, **no. extraordinario, Homenaje al Prof. Gonzalo Vidal**, 51–64.

—— and SCHNEIDER, J. 1992. Lower Cambrian (Atdabanian/Botomian) shallow-marine carbonates of the Görlitz Synclinorium (Saxony/Germany). *Facies*, **26**, 55–66.

ESAKOVA, N. V. and ZHEGALLO, E. A. 1996. Biostratigraphy and fauna of the Lower Cambrian of Mongolia. 1–216. *In* ROZANOV, A. Y. (ed.) *Proceedings of the Joint Soviet–Mongolian Paleontological Expedition* **46**. [in Russian]

ETEMAD-SAEED, N. and NAJAFI, M. 2019. Provenance and geochemical variations across the Ediacaran–Cambrian transition in the Soltanieh Formation, Alborz Mountains, Iran. *Geological Magazine*, **156**, 1157–1174.

—— HOSSEINI-BARZI, M., ADABI, M. H., MILLER, N. R., SADEGHI, A., HOUSHMANDZADEH, A. and STOCKLI, D. F. 2016. Evidence for ca. 560 Ma Ediacaran glaciation in the Kahar formation, central Alborz Mountains, northern Iran. *Gondwana Research*, **31**, 164–183.

FENG, M. 2005. Comparison of the Early Cambrian *Anabarites* between Ningqiang area, Shaanxi, and Chaohu area, Anhui. *Acta Micropalaeontologica Sinica*, **22**, 412–416.

FENG, W. M. and SUN, W. G. 2003. Phosphate replicated and replaced microstructure of molluscan shells from the earliest Cambrian of China. *Acta Palaeontologica Polonica*, **48**, 21–30.

FREEMAN, R. F., DATTILO, B. F. and BRETT, C. E. 2019. An integrated stratinomic model for the genesis and concentration of "small shelly fossil"-style phosphatic microsteinkerns in not-so-exceptional conditions. *Palaeogeography, Palaeoclimatology, Palaeoecology*, **535**, 109344.

GEYER, G. 1994. Middle Cambrian mollusks from Idaho and early conchiferan evolution. *New York State Museum Bulletin*, **481**, 69–86.

GHADIMI, A., IZADYAR, J., AZIMI, S., MOUSAVIZADEH, M. and ERAM, M. 2012. Metamorphism of late Neoproterozoic–early Cambrian schists in southwest of Zanjan from the Soltanieh Belt in northwest of Iran. *Journal of Sciences, Islamic Republic of Iran*, **23**, 147–161.

GRAVESTOCK, I., ALEXANDER, E. M., DEMIDENKO, Y. E., ESAKOVA, N. V., HOLMER, L. E., JAGO, J. B., LIN, T. M., MELNIKOVA, L., PARKHAEV, P. Y., ROZANOV, A. Y., USHATINSKAYA, G. T., ZANG, W. L., ZHEGALLO, E. A. and ZHURAVELV, A. Y. 2001. The Cambrian biostratigraphy of the Stansbury basin, South Australia. *Russian Academy of Sciences, Transactions of the Palaeontological Institute*, **282**, 1–344.

GUBANOV, A. P. and PEEL, J. S. 1999. *Oelandiella*, the earliest Cambrian helcionelloid mollusc from Siberia. *Palaeontology*, **42**, 211–222.

—— —— 2000. Cambrian monoplacophoran molluscs (Class Helcionelloida). *American Malacological Bulletin*, **15**, 139–145.

GUEST, B., STOCKLI, D. F., GROVE, M., AXEN, G. J., LAM, P. S. and HASSANZADEH, J. 2006. Thermal histories from the central Alborz Mountains, northern Iran: implications for the spatial and temporal distribution of deformation in northern Iran. *Geological Society of America Bulletin*, **118**, 1507–1521.

GUO, J., LI, Y. and LI, G. 2014. Small shelly fossils from the early Cambrian Yanjiahe Formation, Yichang, Hubei, China. *Gondwana Research*, **25**, 999–1007.

HAMDI, B. 1989. Stratigraphy and palaeontology of the late Precambrian to early Cambrian in the Alborz Mountains, Northern Iran. *Geological Survey of Iran Report*, **59**, 1–35.

—— 1995. *Precambrian, Cambrian sedimentary rocks in Iran*. Geological Survey of Iran, Treatise on the Geology of Iran, **20**, 353 pp. [in Persian]

—— BRASIER, M. D. and ZHIWEN, J. 1989. Earliest skeletal fossils from Precambrian–Cambrian boundary strata, Elburz Mountains, Iran. *Geological Magazine*, **126**, 283–289.

HASSANZADEH, J., STOCKLI, D. F., HORTON, B. K., AXEN, G. J., STOCKLI, L. D., GROVE, M., SCHMITT, A. K. and WALKER, J. D. 2008. U–Pb zircon geochronology of late Neoproterozoic–early Cambrian granitoids in Iran: implications for paleogeography, magmatism, and exhumation history of Iranian basement. *Tectonophysics*, **451**, 71–96.

HATSCHEK, B. 1888. *Lehrbuch der Zoologie*. G. Fischer, Jena, 144 p.

HE, T. G. 1984. Discovery of *Lapworthella bella* assemblage from Lower Cambrian Meishucun Stage in Niuniuzhai, Leibo county, Sichuan province. *Professional Papers of Stratigraphy & Paleontology*, **13**, 23–34. [in Chinese]

—— and YANG, X. H. 1982. Lower Cambrian Meishucun Stage of the western Yangtze stratigraphic region and its small shelly fossils. *Bulletin of the Chengdu Institute of Geological & Mineral Research*, **3**, 69–95. [in Chinese]

HORTON, B. K., HASSANZADEH, J., STOCKLI, D. F., AXEN, G. J., GILLIS, R. J., GUEST, B., AMINI, A. H.,

FAKHARI, M., ZAMANZADEH, S. M. and GROVE, M. 2008. Detrital zircon provenance of Neoproterozoic to Cenozoic deposits in Iran: implications for chronostratigraphy and collisional tectonics. *Tectonophysics*, **451**, 97–122.

HOU, X. G., SIVETER, D. J., SIVETER, D. J., ALDRIDGE, R. J., CONG, P. Y., GABBOTT, S. E., MA, X. Y., PURNELL, M. A. and WILLIAMS, M. 2017. *The Cambrian Fossils of Chengjiang, China: The flowering of early animal life*. Second edition. Wiley-Blackwell, 328 pp.

HUSSEINI, M. I. 1989. Tectonic and deposition model of late Precambrian–Cambrian Arabian and adjoining plates. *AAPG Bulletin*, **73**, 1117–1131.

JACQUET, S. M., BETTS, M. J., HUNTLEY, J. W. and BROCK, G. A. 2019. Facies, phosphate, and fossil preservation potential across a Lower Cambrian carbonate shelf, Arrowie Basin, South Australia. *Palaeogeography, Palaeoclimatology, Palaeoecology*, **533**, 109200.

JIANG, Z. 1980. The Meishucun Stage and fauna of the Jinning County, Yunnan. *Bulletin of the Chinese Academy of Geological Science*, Series I, **2**, 75–92. [in Chinese, English summary]

KERBER, M. 1988. Mikrofossilien aus Unterkambrischen Gesteinen der Montagne Noire, Frankreich. *Palaeontographica Abteilung A*, **202**, 127–203.

KHOMENTOVSKY, V. V. and KARLOVA, G. A. 1989. *Late Precambrian and early Palaeozoic Siberia: Current questions in stratigraphy*. Institute of Geology and Geophysics, Siberian Branch of the USSR Academy of Sciences, Nauka USSR, Novosibirsk. [in Russian]

—— —— 1991. *Late Precambrian and early Palaeozoic of Siberia. Siberian platform and its margin*. Institute of Geology & Geophysics, Siberian Branch of the USSR Academy of Sciences, Nauka, Novosibirsk. [in Russian]

KOUCHINSKY, A. and BENGTSON, S. 2002. The tube wall of Cambrian anabaritids. *Acta Palaeontologica Polonica*, **47**, 431–444.

—— —— CLAUSEN, S. and VENDRASCO, M. J. 2015. An early Cambrian fauna of skeletal fossils from the Emyaksin Formation, northern Siberia. *Acta Palaeontologica Polonica*, **60**, 421–512.

—— —— FENG, W., KUTYGIN, R. and VAL'KOV, A. 2009. The Lower Cambrian fossil anabaritids: affinities, occurrences and systematics. *Journal of Systematic Palaeontology*, **7**, 241–298.

—— —— RUNNEGAR, B., SKOVSTED, C. B., STEINER, M. and VENDRASCO, M. 2012. Chronology of early Cambrian biomineralisation. *Geological Magazine*, **149**, 221–251.

—— —— LANDING, E., STEINER, M., VENDRASCO, M. and ZIEGLER, K. 2017. Terreneuvian stratigraphy and faunas from the Anabar Uplift, Siberia. *Acta Palaeontologica Polonica*, **62**, 311–440.

LANDING, E., MYROW, P., BENUS, A. P. and NARBONNE, G. M. 1989. The Placentian Series: appearance of the oldest skeletalized faunas in southeastern Newfoundland. *Journal of Paleontology*, **63**, 739–769.

LASEMI, Y. 2001. *Facies analysis, depositional environments and sequence stratigraphy of the upper Precambrian and Palaeozoic rocks of Iran*. Geological Survey of Iran, Tehran, 180 pp. [in Persian]

—— and AMIN-RASOULI, H. 2007. Archaeocyathan build-ups within an entirely siliciclastic succession: new discovery in the Toyonian Lalun formation of northern Iran, the proto-Paleotethys passive margin of northern Gondwana. *Sedimentary Geology*, **201**, 302–320.

—— —— 2017. The lower–middle Cambrian transition and the Sauk I–II unconformable boundary in Iran, a record of late early Cambrian global Hawke Bay regression. 343–366. *In* SORKHABI, R. (ed.) *Tectonic evolution, collision, and seismicity of Southwest Asia: In honor of Manuel Berberian's forty-five years of research contributions*. The Geological Society of America Special Paper, **525**.

LEUCKART, R. 1854. Salpen und Verwandte. *Zoologische Untersuchungen*, **2**, 47–63.

LI, G., STEINER, M., ZHU, M., ZHU, X. and ERDTMANN, B. D. 2007. Early Cambrian fossil record of metazoans in South China: generic diversity and radiation patterns. *Palaeogeography, Palaeoclimatology, Palaeoecology*, **254**, 226–246.

LU, Y. 1979. *Cambrian mineral deposits in China and the bio-environmental control hypothesis*. The Geological Publishing House, Beijing. [in Chinese]

LUO, H., JIANG, Z. and TANG, L. 1994. *Stratotype section for Lower Cambrian stages in China*. Yunnan Science and Technology Press, Kunming. [in Chinese]

—— —— XU, Z., SONG, X. and XUE, X. 1980. On the Sinian–Cambrian boundary of Meishucun and Wangjiawan, Jinning county, Yunnan. *Acta Geologica Sinica*, **54**, 95–111. [in Chinese, English summary]

—— —— —— WU, X., SONG, X. and OUYANG, L. 1982. *The Sinian–Cambrian boundary in eastern Yunnan, China*. Yunnan Institute of Geological Sciences, The People's Publishing House, Yunnan. [in Chinese, English summary]

—— —— —— —— —— XING, Y., LIU, G., ZHANG, S. and TAO, Y. 1984. *Sinian–Cambrian boundary stratotype section at Meishucun, Jinning, Yunnan*. China People's Publishing House, Yunnan. [in Chinese, English summary]

MADANIPOUR, S., EHLERS, T. A., YASSAGHI, A. and ENKELMANN, E. 2017. Accelerated middle Miocene exhumation of the Talesh Mountains constrained by U-Th/He thermochronometry: evidence for the Arabia–Eurasia collision in the NW Iranian Plateau. *Tectonics*, **36**, 1538–1561.

MALEK-MAHMOUDI, F., DAVOUDIAN, A. R., SHABANIAN, N., AZIZI, H., ASAHARA, Y., NEUBAUER, F. and DONG, Y. 2017. Geochemistry of metabasites from the North Shahrekord metamorphic complex, Sanandaj–Sirjan Zone: geodynamic implications for the Pan-African basement in Iran. *Precambrian Research*, **293**, 56–72.

MALOOF, A. C., PORTER, S. M., MOORE, J. L., DUDÁS, F. Ö., BOWRING, S. A., HIGGINS, J. A., FIKE, D. A. and EDDY, M. P. 2010. The earliest Cambrian record of animals and ocean geochemical change. *Bulletin of the Geological Society of America*, **122**, 1731–1774.

MAMBETOV, A. M. 1988. New representatives of Mollusks and Conodontomorphs from the lower and middle Cambrian of the Tien Shan and the Lesser Karatau Range. 148–154. *In*

ZHURAVLEVA, I. T. and REPINA, L. N. (eds) *Cambrian of Siberia and Central Asia. Proceedings of the Institute of Geology and Geophysics of the Siberian Division of the Academy of Sciences of the USSR*, 720. Nauka, Moscow. [in Russian]

MATTHEWS, S. C. and MISSARZHEVSKY, V. V. 1975. Small shelly fossils of late Precambrian and early Cambrian age: a review of recent work. *Journal of the Geological Society*, **131**, 289–303.

MISSARZHEVSKY, V. V. 1967. *Zonal stratigraphy of the oldest Cambrian deposits of the Siberian Platform*. Unpublished PhD thesis, University of Moscow, Moscow, Russia, 23 pp.

—— 1973. Conodontomorph organisms from the Precambrian–Cambrian boundary beds of the Siberian Platform and Kazakhstan. 53–58. *In* ZURAVLEVA, I. T. (ed.) *Problems of palaeontology and biostratigraphy in the Lower Cambrian of Siberia and the Far-East*. Nauka, Novosibirsk. [in Russian]

—— 1974. New data on the oldest fossils of the Early Cambrian of the Siberian Platform. 179–189. *In* ZURAVLEVA, I. T. and ROZANOV, A. Y. (eds) *Biostratigraphy and palaeontology of the Lower Cambrian of Europe and northern Asia*. Nauka, Novosibirsk. [in Russian]

—— 1977. Conodonts (?) and phosphatic problematica from the Cambrian of Mongolia and Siberia. 10–19. *In* TATARINOV, L. P. (ed.) *Palaeozoic invertebrates of Mongolia*. Nauka, Moscow. [in Russian]

—— 1980. Early Cambrian Mongolian Hyolitha and Gastropoda. *Paleontological Journal*, **15**, 18–25.

—— 1989. *Oldest skeletal fossils and stratigraphy of Precambrian and Cambrian boundary beds*. Proceedings of the Geological Institute, USSR Academy of Science, **443**, 1–237. [in Russian]

—— and MAMBETOV, A. M. 1981. *Stratigraphy and fauna of the Cambrian and Precambrian boundary beds of the Maly Karatau Range*. Proceedings of the Geological Institute of the USSR Academy of Sciences, AN USSR, **326**, 1–92. [in Russian]

MOGHADAM, H. S., LI, X. H., STERN, R. J., GHORBANI, G. and BAKHSHIZAD, F. 2016. Zircon U–Pb ages and Hf–O isotopic composition of migmatites from the Zanjan–Takab complex, NW Iran: constraints on partial melting of metasediments. *Lithos*, **240–243**, 34–48.

—— KHADEMI, M., HU, Z., STERN, R. J., SANTOS, J. F. and WU, Y. 2015. Cadomian (Ediacaran–Cambrian) arc magmatism in the ChahJam–Biarjmand metamorphic complex (Iran): magmatism along the northern active margin of Gondwana. *Gondwana Research*, **27**, 439–452.

—— LI, X. H., GRIFFIN, W. L., STERN, R. J., THOMSEN, T. B., MEINHOLD, G., AHARIPOUR, R. and O'REILLY, S. Y. 2017. Early Paleozoic tectonic reconstruction of Iran: tales from detrital zircon geochronology. *Lithos*, **268–271**, 87–101.

NOWLAN, G. S., NARBONNE, G. M. and FRITZ, W. H. 1985. Small shelly fossils and trace fossils near the Precambrian–Cambrian boundary in the Yukon Territory, Canada. *Lethaia*, **18**, 233–256.

PARKHAEV, P. Y. 2004. New data on the morphology of shell muscles in Cambrian helcionelloid mollusks. *Paleontological Journal*, **38**, 254–256.

—— 2005. Cambrian helcionelloid mollusks as the foundation of evolution in the class Gastropoda. 63–84. *Modern Russian Paleontology: Classical and recent methods*. Paleontological Institute of the Russian Academy of Science, Moscow. [in Russian]

—— 2008. The early Cambrian radiation of Mollusca. 33–69. *In* PONDER, W. and LINDBERG, D. (eds) *Phylogeny and evolution of the Mollusca*. University of California Press.

—— and DEMIDENKO, Y. E. 2010. Zooproblematica and Mollusca from the Lower Cambrian Meishucun section (Yunnan, China) and taxonomy and systematics of the Cambrian small shelly fossils of China. *Paleontological Journal*, **44**, 883–1161.

—— and KARLOVA, G. A. 2011. Taxonomic revision and evolution of Cambrian mollusks of the genus *Aldanella* Vostokova, 1962 (Gastropoda: Archaeobranchia). *Paleontological Journal*, **45**, 1145–1205.

PEEL, J. S. 1988. *Spirellus* and related helically coiled microfossils (cyanobacteria) from the Lower Cambrian of North Greenland. *Rapport Grønlands Geologiske Undersøgelse*, **137**, 5–32.

—— 1991. Functional morphology of the Class *Helcionelloida* nov., and the early evolution of the Mollusca. 157–177. *In* SIMONETTA, A. M. and CONWAY MORRIS, S. (eds) *The early evolution of Metazoa and the significance of problematic taxa*. Cambridge University Press.

PEL'MAN, Y. L., ERMAK, V. V., FEDOROV, A. B., LUCHININA, V. A., ZHURAVLEVA, I. T., REPINA, L. N., BONDAREV, V. I. and BORODAEVSKAYA, Z. V. 1990. New data on stratigraphy and palaeontology of the upper Precambrian and lower Cambrian of River Dzhandy (right tributary of River Aldan). 3–32. *In* REPINA, L. N. (ed.) *Biostratigraphy and palaeontology of the Cambrian of northern Asia*. Nauka, Novosibirsk. [in Russian]

PORTER, S. M. 2010. Calcite and aragonite seas and the de novo acquisition of carbonate skeletons. *Geobiology*, **8**, 256–277.

PRUSS, S. B., TOSCA, N. J. and STARK, C. 2018. Small shelly fossil preservation and the role of early diagenetic redox in the Early Triassic. *Palaios*, **33**, 441–450.

PYLE, L. J., NARBONNE, G. M., NOWLAN, G. S., XIAO, S. and JAMES, N. P. 2006. Early Cambrian metazoan eggs, embryos, and phosphatic microfossils from northwestern Canada. *Journal of Paleontology*, **80**, 811–825.

QIAN, Y. 1977. Hyolitha and some problematica from the Lower Cambrian Meishucun stage in central and S. W. China. *Acta Palaeontologica Sinica*, **16**, 107–130.

—— 1978. The early Cambrian hyolithids in central and southwest China and their stratigraphical significance. *Memoirs of the Nanjing Institute of Geology & Palaeontology*, **11**, 1–43. [in Chinese, English summary]

—— 1989. Early Cambrian small shelly fossils of China with special reference to the Precambrian–Cambrian boundary. 1–340. *In* NANJING INSTITUTE OF GEOLOGY AND PALAEONTOLOGY, ACADEMIA SINICA (ed.) *Stratigraphy and palaeontology of systemic boundaries in China: Precambrian–Cambrian boundary*. Vol. **2**. Nanjing University Publishing House. [in Chinese, English summary]

—— and BENGTSON, S. 1989. Palaeontology and biostratigraphy of the early Cambrian Meishucunian Stage in Yunnan province, south China. *Fossils & Strata*, **24**, 1–156.

—— and YIN, G. 1984. Small shelly fossils from the lowest Cambrian in Guizhou. *Professional Papers of Stratigraphy & Palaeontology*, **13**, 91–124. [in Chinese, English summary]

—— CHEN, M. and CHEN, Y. 1979. Hyolithids and other small shelly fossils from the Lower Cambrian Huangshandong Formation in the eastern part of the Yangtze Gorge. *Acta Palaeontologica Sinica*, **18**, 207–229.

—— ZHU, M., LI, G., JIANG, Z. and VAN ITEN, H. 2002. A supplemental Precambrian–Cambrian boundary global stratotype section in SW China. *Acta Palaeontologica Sinica*, **41**, 19–26.

—— LI, G., ZHU, M., STEINER, M. and ERDTMANN, B. 2004. Early Cambrian protoconodonts and conodont-like fossils from China: taxonomic revisions and stratigraphic implications. *Progress in Natural Science*, **14**, 173–180.

RAMEZANI, J. and TUCKER, R. 2003. The Saghand region, Central Iran: U–Pb geochronology, petrogenesis and implications for Gondwana tectonics. *American Journal of Science*, **303**, 622–665.

REITLINGER, E. A. 1948. Cambrian foraminifera of Yakutsk. *Bulletin of Moscow Society of Naturalists, Geological Series*, **23**, 77–81. [in Russian]

ROZANOV, A. Y., MISSARZHEVSKY, V. V., VOLKOVA, N. A., VORONOVA, L. G., KRYLOV, I. N., KELLER, B. M., KOROLYUK, I. K., LENDZION, K., MICHNIAK, R., PYHOVA, N. G. and SIDOROV, A. D. 1969. The Tommotian stage and the Cambrian lower boundary problem. *Proceedings of the Geological Institute, USSR Academy of Science*, **206**, 1–380. [in Russian]

—— PARKHAEV, P. Y., DEMIDENKO, Y. E., KARLOVA, G. A., KOROVNIKOV, I. V., SHABANOV, Y. Y., IVANTSOV, A. Y., LUCHININA, V. A., MALAKHOVSKAYA, Y. E., MEL'NIKOVA, L. M., NAIMARK, E. B., PONOMARENKO, A. G., SKORLOTOVA, N. A., SUNDUKOV, V. M., TOKAREV, D. A., USHATINSKAYA, G. T. and KIPRIYANOVA, L. D. 2010. *Fossils from the lower Cambrian Stage stratotypes*. Paleontological Institute, Russian Academy of Sciences, Moscow, 228 pp.

SHAHKARAMI, S., MÁNGANO, M. G. and BUATOIS, L. A. 2017*a*. Ichnostratigraphy of the Ediacaran–Cambrian boundary: new insights on lower Cambrian biozonations from the Soltanieh Formation of northern Iran. *Journal of Paleontology*, **91**, 1178–1198.

—— —— —— 2017*b*. Discriminating ecological and evolutionary controls during the Ediacaran–Cambrian transition: trace fossils from the Soltanieh Formation of northern Iran. *Palaeogeography, Palaeoclimatology, Palaeoecology*, **476**, 15–27.

SHU, D., ISOZAKI, Y., ZHANG, X., HAN, J. and MARUYAMA, S. 2014. Birth and early evolution of metazoans. *Gondwana Research*, **25**, 884–895.

SOKOLOV, B. S. and ZHURAVLEVA, I. T. 1983. *Stage subdivision of the Lower Cambrian of Siberia. Atlas of fossils*. Proceedings of the Institute of Geology and Geophysics, Siberian Branch of the USSR Academy of Sciences, **558**, 216 pp.

STAMPFLI, G. M. and BOREL, G. D. 2002. A plate tectonic model for the Paleozoic and Mesozoic constrained by dynamic plate boundaries and restored synthetic oceanic isochrons. *Earth & Planetary Science Letters*, **196**, 17–33.

STEINER, M., LI, G., QIAN, Y. and ZHU, M. 2004. Lower Cambrian small shelly fossils of northern Sichuan and southern Shaanxi (China), and their biostratigraphic importance. *Geobios*, **37**, 259–275.

—— —— —— —— and ERDTMANN, B. D. 2007. Neoproterozoic to early Cambrian small shelly fossil assemblages and a revised biostratigraphic correlation of the Yangtze platform (China). *Palaeogeography, Palaeoclimatology, Palaeoecology*, **254**, 67–99.

STÖCKLIN, J. 1968. Structural history and tectonics of Iran: a review. *AAPG Bulletin*, **52**, 1229–1258.

—— and EFTEKHARNEZHAD, J. 1969. *Geological map of Zanjan, 1:100000 scale*. Geological Survey of Iran, Tehran.

—— RUTTNER, A. and NABAVI, M. 1964. On the lower Paleozoic and Precambrian of North Iran. *Geological Survey of Iran, Report*, **1**, 1–13.

—— NABAVI, M. and SAMIMI, M. 1965. Geology and mineral resources of the Soltanieh Mountains (Northwest Iran). *Geological Survey of Iran, Report*, **2**, 1–44.

SYSOEV, V. A. 1965. Main features of evolution of hyoliths. 5–20. *In* VOZIN, V. F. (ed.) *Paleontology and biostratigraphy of the Paleozoic and Triassic sediments of Yakutia*. Nauka, Moscow. [in Russian]

TALBOT, C. J. and ALAVI, M. 1996. The past of a future syntaxis across the Zagros. 89–109. *In* ALSOP, G. I., BLUNDELL, D. J. and DAVISON, I. (eds) *Salt tectonics*. Geological Society of London Special Publication, **100**.

TASHAYOEE, R., HAMDI, B., VAZIRI, H. and YOUSOFZADEH, E. 2012. *Biostratigraphy of the Soltanieh Formation in the Garmab–Sorkhdar section based on the small shelly fossils*. *In* 31st Geoscience Congress, Geological Survey of Iran, Tehran. [in Persian]

TOPPER, T. P., BROCK, G. A., SKOVSTED, C. B. and PATERSON, J. R. 2009. Shelly fossils from the lower Cambrian *Pararaia bunyerooensis* Zone, Flinders Ranges, South Australia. *Memoirs of the Association of Australasian Palaeontologists*, **37**, 199–246.

VAHDATI DANESHMAND, F. and NADIM, H. 1999. *Geological map of Marzan Abad, 1:100000 scale*. Geological Survey of Iran, Tehran.

VAL'KOV, A. K. 1968. To the fauna of the Kessyusa Formation of the Lower Cambrian of the Olenyok uplift. 115–119. *In* MOKSHANCEV, K. B. (ed.) *Tectonic, stratigraphy and lithology of sedimentary formations of Yakutia*. Yakutsk Publishing House. [in Russian]

—— 1975. *Biostratigraphy and hyoliths of the Cambrian of the northeastern Siberian Platform*. Nauka, Moscow, 140 pp. [in Russian]

—— 1982. *Biostratigraphy of the Lower Cambrian of the Eastern Siberian Platform (Uchur–Maya Region)*. Nauka, Moscow, 91 pp. [in Russian]

—— 1987. *Biostratigraphy of the Lower Cambrian of the Eastern Siberian Platform (Yudoma–Olenek Region)*. Nauka, Moscow, 136 pp.

—— and SYSOEV, V. A. 1970. Cambrian angustiochreids of Siberia. 94–100. *In* BOBROV, A. K. (ed.) *Stratigraphy and*

paleontology of the Proterozoic and Cambrian of the East Siberian Platform. Yakutsk Publishing House. [in Russian]

VASIL'EVA, N. I. 1998. Small shelly fauna and biostratigraphy of the Lower Cambrian of the Siberian platform. *Transactions of the Scientific Research Institute of Geology*. All Russia Petroleum Research Exploration Institute, St Petersburg, 139 pp. [in Russian]

VORONIN, Y. I., VORONOVA, L. G., GRIGORIEVA, N. V., DROZDOVA, N. A., ZHEGALLO, E. A., ZHURAVLEV, A. Y., RAGOZINA, A. L., ROZANOV, A. Y., SAYUTINA, T. A., SYSOEV, V. A. and FONIN, V. D. 1982. The Precambrian–Cambrian boundary in the geosynclinal regions (reference section Salany-Gol, MNR). *Proceedings of the Joint Soviet–Mongolian Paleontological Expedition*, **18**, 1–150. [in Russian]

VORONOVA, L. G. and MISSARZHEVSKY, V. V. 1969. Finds of algae and worm tubes in the Precambrian–Cambrian boundary beds of the northern part of the Siberian Platform. *Proceedings of the USSR Academy of Sciences*, **184**, 207–210. [in Russian]

VOSTOKOVA, V. A. 1962. The Cambrian gastropods from Siberia and Tajmyr. *Proceedings of the Research Institute of Arctic Geology*, **28**, 51–74. [in Russian]

WALCOTT, C. D. 1899. Pre-Cambrian fossiliferous formations. *Bulletin of the Geological Society of America*, **10**, 199–244.

WANG, Y., YIN, G., ZHENG, S. and QIAN, Y. 1984. Stratigraphy of the Sinian–Cambrian boundary in the Yangze area of Guizhou. 1–31. *In The Upper Precambrian and Sinian–Cambrian boundary in Guizhou*. People's Publishing House, Guizhou. [in Chinese, English summary]

WENZ, W. 1938. Gastropoda. Teil 1: Allgemeiner Teil und Prosobranchia. *In* Schindewolf, O. H. (ed.) *Handbuch der Paläozoologie, band 6*. Bornträger, Berlin.

WRONA, R. 2004. Cambrian microfossils from glacial erratics of King George Island, Antarctica. *Acta Palaeontologica Polonica*, **49**, 13–56.

XING, Y., DING, Q., LUO, H., HE, T. and WANG, Y. 1984. The Sinian–Cambrian boundary of China and its related problems. *Geological Magazine*, **121**, 155–170.

YANG, X. and HE, T. 1984. New small shelly fossils from Lower Cambrian Meishucun stage of Nanjiang area, northern Sichuan. *Professional Papers of Stratigraphy & Palaeontology*, **13**, 35–48.

—— HE, Y. and DENG, S. 1983. On the Sinian–Cambrian boundary and the small shelly fossil assemblages in Nanjiang area, Sichuan. *Bulletin of the Chengdu Institute of Geology & Mineral Resources*, **4**, 91–10. [in Chinese, English summary]

YANG, B., STEINER, M. and KEUPP, H. 2015. Early Cambrian palaeobiogeography of the Zhenba–Fangxian Block (South China): independent terrane or part of the Yangtze Platform. *Gondwana Research*, **28**, 1543–1565.

—— —— LI, G. and KEUPP, H. 2014*a*. Terreneuvian small shelly faunas of east Yunnan (South China) and their biostratigraphic implications. *Palaeogeography, Palaeoclimatology, Palaeoecology*, **398**, 28–58.

—— ZHANG, L., DANELIAN, T., FENG, Q. and STEINER, M. 2014*b*. Chert-hosted small shelly fossils: expanded tool of biostratigraphy in the Early Cambrian. *GFF*, **136**, 303–308.

—— STEINER, M., ZHU, M., LI, G., LIU, J. and LIU, P. 2016. Transitional Ediacaran–Cambrian small skeletal fossil assemblages from South China and Kazakhstan: implications for chronostratigraphy and metazoan evolution. *Precambrian Research*, **285**, 202–215.

YIN, J., DING, L., HE, T., LI, S. and SHEN, L. 1980. *The palaeontology and sedimentary environment of the Sinian System in Emei-Ganluo area, Sichuan*. People's Publishing House, Sichuan, 268 pp. [in Chinese, English summary]

YU, W. 1979. Earliest Cambrian monoplacophorans and gastropods from western Hubei with their biostratigraphical significance. *Acta Palaeontologica Sinica*, **18**, 233–270. [in Chinese, English summary]

—— 1981. New earliest Cambrian monoplacophorans and gastropods from W. Hubei and E. Yunnan. *Acta Palaeontologica Sinica*, **20**, 552–556. [in Chinese, English summary]

—— 1984. Early Cambrian molluscan faunas of Meishucun Stage with special reference to Precambrian–Cambrian boundary. 21–33. *In Academia Sinica Developments in Geoscience. Contribution to 27th International Geological Congress, Moscow*. Science Press, Beijing. [in Chinese]

—— 1987*a*. New molluscan materials of the Tethys. 51–59. *In* McKenzie, K. G. (ed.) *International symposium on Shallow Tethys 2, Wagga Wagga, 15–17 September 1986*. Balkema, Rotterdam.

—— 1987*b*. Yangtze micromolluscan fauna in Yangtze region of China with notes on the Precambrian–Cambrian boundary. 19–344. *In* NANJING INSTITUTE OF GEOLOGY AND PALAEONTOLOGY, ACADEMIA SINICA (ed.) *Stratigraphy and palaeontology of systemic boundaries in China: Precambrian–Cambrian boundary*. Vol. **1**. Nanjing University Publishing House. [in Chinese, English summary]

—— 1988. New advances in the study of earliest Cambrian molluscan fauna of China. *Chinese Science Bulletin*, **33**, 1555–1557. [in Chinese, English summary]

—— 1990. The first radiation of shelled mollusks. *Palaeontologica Cathayana*, **5**, 139–170.

ZANCHI, A., BERRA, F., MATTEI, M., GHASSEMI, M. and SABOURI, J. 2006. Inversion tectonics in Central Alborz, Iran. *Journal of Structural Geology*, **28**, 2023–2037.

—— ZANCHETTA, S., BERRA, F., MATTEI, M., GARZANTI, E., MOLYNEUX, S., NAWAB, A. and SABOURI, J. 2009. The Eo-Cimmerian (Late? Triassic) orogeny in North Iran. 31–55. *In* BRUNET, M. F., WILMSEN, M. and GRANATH, J. W. (eds) *South Caspian to Central Iran Basins*. Geological Society of London Special Publication 312.

ZANDKARIMI, K., NAJAFIAN, B., VACHARD, D., BAHRAMMANESH, M. and VAZIRI, S. H. 2016. Latest Tournaisian–late Viséan foraminiferal biozonation (MFZ8–MFZ14) of the Valiabad area, northwestern Alborz (Iran): geological implications. *Geological Journal*, **51**, 125–142.

ZHANG, X., AHLBERG, P., BABCOCK, L. E., CHOI, D. K., GEYER, G., GOZALO, R., HOLLINGSWORTH, J. S., LI, G., NAIMARK, E., PEGEL, T., STEINER, M., WOTTE, T. and ZHANG, Z. 2017. Challenges in defining the base of Cambrian Series 2 and Stage 3. *Earth-Science Reviews*, **172**, 124–139.

ZHAO, Z., XING, Y., MA, G., YU, W. and WANG, Z. 1980. The Sinian System of eastern Yangtze Gorges, Hubei. 31–55. *In Research on Precambrian Geology: Sinian Suberathem in China*. Tianjin Science & Technology Press.

ZHU, M. Y., ZHURAVLEV, A. Y., WOOD, R. A., ZHAO, F. and SUKHOV, S. S. 2017. A deep root for the Cambrian explosion: implications of new bio and chemostratigraphy from the Siberian Platform. *Geology*, **45**, 459–462.

ZHURAVLEV, A. Y., HAMDI, B. and KRUSE, P. D. 1996. IGCP 366: ecological aspects of the Cambrian radiation – field meeting. *Episodes*, **19**, 136–137.